Loughborough University

SkyRide

Final Report - 18TTD009 Group Design Project

Department of Aeronautical and Automotive Engineering,

Loughborough University, Leicestershire LE11 3T U, UK

Project SkyRide – S270

DESIGN TEAM

Harry Hay
Group Leader and Propulsion Design

Darshan Balasingam
Batteries and Systems Design

Ryan Beecroft
Design and Modelling

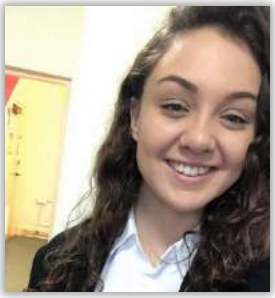

Georgia Gregory
Risk and Reliability

Ewa Mikinka
Structural Design

Erandika Mohanathasan
Business and Sales

Simran Panesar
Stability and Systems

Vandan Patel
Parachute and Landing Gear Design

George Smith
Aerodynamics Design

Edmund Tong
Aircraft Performance

Executive Summary

In this report, Project SkyRide design a 5 seat general aviation aircraft named the S270 (the SkyRide 270kW engine aircraft). The aim of the S270 is to increase regional mobility and reduce congestion of roads in the US by providing a low cost, fast alternative for commuters that frequently travel by car or public transport. This aircraft will make use of the existing infrastructure of small airports in the US, the majority of which are currently underutilised. This S270 follows the thin haul transport model (THT), serving as a scheduled service or on-demand "Air-Taxi". The aircraft will carry out a standard 135 nmi mission in 45 minutes, with the capability of performing an extended sizing mission of 250 nmi in 2 hours. This is a significant time saving when compared to the equivalent car, train or bus journey. The cost of this standard 45-minute flight will be approximately $45 per person, which gives a total profit of 15%.

In order to outperform and outsell competitors, the S270 aircraft will incorporate a number of advanced technologies to reduce operating costs and environmental impact. The most important of which is a series-parallel hybrid powertrain, which consists of a Siemens SP260D electric motor, a dual planetary gearset power split device and a 6 cylinder, horizontally opposed, avgas burning internal combustion engine (ICE). Lithium sulphur batteries, with an energy density of 520 Wh/kg, will be used to power the electric motor. The wing structure consists of a single spar and reinforced composite skin; this skin reduces the required number of structural ribs to 2 per wing, and thus reduces weight of the aircraft. A parachute system is installed in the aircraft which adds redundancy in the case of a loss of power or control and can be activated by passengers if the pilot were to become incapacitated. The S270 is a more electric aircraft (MEA), with increased electrification across all systems. Hydrostatic actuation across many control surfaces is an MEA concept that has improved the performance of the S270 by reducing mass and improving reliability, completely removing the requirement for hydraulics onboard the aircraft. A fly-by-light system is another innovation incorporated into the design and is shown to be ten times lighter than the equivalent fly-by-wire system. The entry to service date of the S270 is 2025 therefore all technologies incorporated in the design have a technology readiness level (TRL) of 7+. However, the design of the aircraft will allow for technologies to be continually upgraded throughout its operational lifetime, which will keep Project SkyRide ahead of competitors by continually reducing operating costs and environmental impact.

The S270 uses a V-tail configuration to reduce mass of the aircraft. The ruddervators control pitch and yaw which can often lead to control issues, however the S270 has been found to be stable in lateral and longitudinal directions, and hence the need for stability augmentation is mitigated.

Cost analysis has shown a 43% reduction in operating costs and a 37% reduction in unit costs compared to competitor aircraft. Cost of production will be further reduced as production of the S270 expands to a larger scale.

Public perception of the S270 will be vital to its success, therefore the propeller and powertrain have been designed to minimise noise which will significantly reduce disturbances to people living near the small regional airports. In addition, taxi, take-off and climb phases are all powered by mostly electric propulsion with minimal contribution from the ICE, which reduces noise in these close-to-ground phases of the mission.

Part 1 of this report outlines a brief technical description of the aircraft. Part 2 outlines a detailed design of all aspects of the aircraft, including propulsion, structures, onboard systems, aerodynamics, and stability and control. Detailed cost and risk analysis are also conducted to assess the viability of the overall project. Finally, Part 3 shows the public engagement activities carried out by the Project SkyRide team. This main aim of this public engagement was to increases the public's awareness of environmental issues associated with air travel and show people how Project SkyRide is tackling these issues.

Contents

Nomenclature

Symbol	Definition
a	Wing lift-curve slope
a_{1t}	Tail lift-curve slope
ADSB	Automatic dependent surveillance-broadcast
AR	Aspect Ratio
b_1	Span location of aileron inner chord
b_2	Span location of aileron outer chord
$\bar{\bar{c}}$	Mean aerodynamic chord
C_D	Drag coefficient
C_{D0}	Parasitic drag coefficient
C_{Di}	Induced drag coefficient
C_{ff}	Turbulent flat plate friction coefficient of fuselage
C_{ft}	Turbulent flat plate friction coefficient of tail
C_{fw}	Turbulent flat plate friction coefficient of wing
CG	Fuselage centre of gravity
C_L	lift coefficient
cld0	Wing section drag coefficient
$C_{L\delta a}$	Roll authority
$c_{L\delta a}$	Incremental increase of lift coefficient with respect to deflection
C_{lp}	Roll damping
CPI	Consumer price index
CPU	Control protection unit
C_r	Root chord
C_{rRV}	Ruddervator root chord
C_t	Tip chord
d	Blade diameter
D_2/D_1	Blade diameter ratio
DEP	Distributed electric propulsion
d_f	Fuselage diameter
e	Oswald's efficiency factor
ECS	Environmental control system

ECU	Engine control unit
EFIS	Electronic flight instrument system
EHA	Electro-hydrostatic actuator
EMA	Electro-mechanical actuator
EMEDS	Expulsion de-icing system
FBL	Fly-by-light
FCC	Flight control computer
Fexp	Increasing labour experience
FLIR	Forward looking infrared
FMS	Flight management system
h	Centre of gravity
h_n	Neutral point
ICE	Internal combustion engine
i_t	Tailplane setting angle
I_y	Pitch moment of inertia
j	Advance Ratio
K_1	Factor accounting for relative flap chord for chord lengths other than 25%
K_2	Flap deflection factor
K_3	Flap kinematics factor
K_Λ	Empirical correction factor for wing sweep
K_W	Surface area factor
L/D	Lift to drag ratio
L’	Aerofoil thickness location parameter
l_f	Fuselage length
L_f/d_f	Fuselage fineness ratio
LIDAR	Laser imaging detection and ranging
LT	Tail moment arm
M	Mach number
MEA	More electric aircraft
MFD	Multi-function display
n	Rotational speed of propeller
N	Number of units produced

N_2/N_1	Blade quantity ratio
p	Roll rate
pb/2v	Roll helix angle
PFD	Primary flight display
$\bar{q}$	Dynamic pressure
QDF	Quantity discount factor
QFD	Quality functional deployment
RADAR	Radio detection and ranging
RFP	Request for proposal
R_{Ls}	Lifting surface correction factor
R_{Nf}	Fuselage Reynolds number
R_{Nt}	Tail Reynolds number
R_{Nw}	Wing Reynolds number
R_{Wf}	Wing fuselage interference factor
SHP_{rated}	Maximum rated shaft horsepower of the engine
S_T	Tail area
S_w	Wing planform area
S_{wetf}	Fuselage wetted area
S_{wetW}	Wing wetted area
S_{wf}/S_w	Area ratio for flaps
T_2	Time to double bank angle
TAA	Technologically advanced aircraft
t/c	Thickness to chord ratio
T_p	Phugoid time period
T_r	Roll subsidence time period
TRL	Technology readiness level
U_1	Steady state flight speed
V	Airspeed
V_H	Tail volume coefficient
VTOL	Vertical take-off and landing
W_B	Weight of fuselage including nose landing gear
W_W	Weight of wing including main landing gear

X_B	Distance from datum line to fuselage centre of gravity
X_{LE}	Distance from nose to leading edge of wing
X_{OEM}	Operational empty centre of gravity
X_W	Distance from datum line to wing centre of gravity
Γ	Dihedral angle
λ	Taper ratio
$\Delta C_{L,max,f}$	Increase in wing max lift coefficient by flaps
$\Delta c_{L,max,f}$	Increase in aerofoil max lift coefficient by flaps
(ΔC_{Lmax})	Maximum increase in lift for a flap with 25% chord
Λ_{LE}	Leading edge sweep
δ_a	Aileron deflection
ζ_{DR}	Dutch roll damping ratio
ζ_{SP}	Short period mode damping ratio
ζ_{Phug}	Phugoid mode damping ratio
ω_{nSP}	Short period mode natural frequency
ω_{nPhug}	Phugoid mode natural frequency
$\eta_{gearbox}$	Gearbox efficiency
$\eta_{power\ split\ device}$	Power split device efficiency
η_T	Tail efficiency
δ_{flap}	Flap deflection
$\Delta C_{Dwindshield}$	Incremental drag coefficient due to windshield
$d\varepsilon/d\alpha$	Downwash gradient

Part 1. Technical Description

1.1. Introduction

The road transportation system in the US has been under increasing pressure over the last decade; this is mainly due to unreliable bus and rail networks forcing commuters to travel using their own vehicles, resulting in widespread congestion [1]–[4]. One possible solution to this problem is to utilise regional air travel; however, existing short regional flights only operate out of a limited number of hubs, which leads to frequent delays and overall passenger dissatisfaction [5]. In addition, funding cuts to the Essential Air Service (EAS) [6] mean that people living in remote locations will need to find alternative methods of travel to increase their regional mobility. Project SkyRide proposes to solve these transport issues by operating frequent scheduled and on-demand flights out of many of the underutilised regional airports in the US, a concept known as the Thin Haul Transport (THT) model [7]. The service will have low operating costs due the design and manufacture of highly efficient 5-seater aircraft that benefits from electric taxi, take-off, climb and cruise, as well as increased electrification across all systems. Modern manufacturing methods will be utilised to ensure that the large-scale manufacture of these small taxi aircraft is low-cost and efficient; this will help to maximise market share by the service entry date of 2025, with the possibility of significant expansion in the following years. The Cirrus SR22 is the main competitor aircraft for the SkyRide S270 in performance and mission profile; therefore, the success of this project will be highly dependent on the operating and unit costs of the S270 being lower than the SR22. Minimising door to door time for passengers will also be vital in the success of the project, hence a standard mission of 135 nm should not exceed 45 minutes from the start of taxi to passenger egress. In order for the aircraft to serve more than just short commuting trips, a 250 nm sizing mission will also be achievable. This report will outline a detailed breakdown of the aircraft design along with design optimisation and trade-off studies. A detailed cost breakdown will also support the design, thus validating the viability of the SkyRide S270 aircraft.

1.2. Requirements

Design of the air taxi was preceded by research on the specifics of air taxi operation profile. This led to generation of requirements that must be met by the design. The aircraft needs to match or exceed the existing general aviation aircraft available on the market, especially aircraft that are suited for air taxi applications. These include the need to minimise operating costs and optimise the design mission profile of the air taxi. All problematic issues relevant to the air travels were also considered. The requirements served as a basis for detailed calculations, particularly for aircraft performance, as

described and presented in Section 2.4. A list of design requirements with their justification is presented in Table 1 [8].

Table 1 Design requirements.

Requirement	Justification	Compliance
Standard passenger capacity of four	This is standard capacity of a taxi. It is also suitable for average US family.	Met. Cabin accommodates four seats for passengers.
Single pilot	This minimises operating costs and it is general practice in general aviation.	Met. Cabin and avionics designed to be used and operated by a single pilot.
Aircraft cruise speed of 180 knots	This is the speed attained by most general aviation aircraft of similar capacity.	Met. Aircraft designed to cruise at 180 kts.
Standard mission at distance of 135 nm covered in 45 minutes	Average commuting distance should not exceed 135 nm as there are many small airports in US with distances between them smaller than 135 nm.	Met. Design mission is specified for 135 nm, travelled in 45 minutes with average speed of 180 kts.
Ability to perform 250 nm mission with full loading	This gives flexibility to meet customers need for extended distance and carrying capability.	Met. Sizing mission designed to be performed with four passengers for 250 nm.
Entry into service date 2025	Quickly developing air taxi market with potentially high demand.	Met. The implemented technologies are already existing or close to be certified.
Multiple propulsion units or single engine with aircraft parachute	This gives extra safety and redundancy in case of engine failure.	Met. Aircraft is equipped with full parachute.
Special considerations for passenger comfort, egress and boarding	These are problematic issues for low cost air travels.	Met. Internal cabin layout designed to give maximum comfort to passengers; large doors allow for easy access.

1.3. Market Research

The general aviation market in the US is very well developed. In order to make the new design feasible and competitive with aircraft already in use, extensive market research has been carried out. Initial research concentrated on performance features, such as cruise speed and range, which are regarded as important parameters potential customers would look at. Data for main competitor aircraft of similar roles and passenger capacity have been plotted in Fig.1, together with imposed speed and range requirements. Out of all the competitors considered, Cirrus SR22 is by far the most popular aircraft. For that reason, key parameters of the S270 are compared to those of the SR22 to ensure the design has potential to compete with the most successful small aircraft on the market.

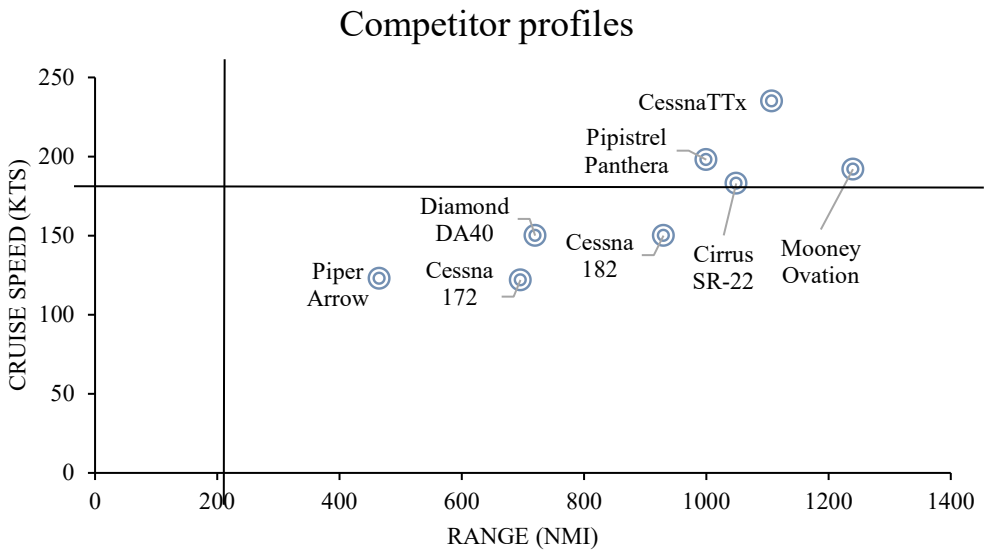

Fig. 1 Competitor profiles for cruise speed and range in GA market.

It directly follows from the research that the required range is tremendously exceeded by all the considered aircraft, while the speed requirement is met only by a few. Although currently the general aviation market is dominated by piston-engine aircraft, governmental restrictions on noise and carbon footprint for the near future [9] entail the need for greener aircraft, which can be satisfied by either hybrid or fully electric aircraft. The industry has been looking for a feasible solution of electrifying the aircraft; so far, most concepts proposed by various companies including Rolls-Royce, Siemens and Airbus are limited to flying demonstrators, such as DA36 E-Star, a single seat motor glider built by Diamond Aircraft in cooperation with Siemens or all-electric E-Fan 2.0 developed by Airbus. This was abandoned at the cost of developing an electric airliner [10]. Pipistrel company developed an all-electric light sport aircraft called Pipistrel Alpha Electro. Instead of a regular passenger transport aircraft it meets the needs of flight school aircraft, with a two-person capacity, 1-hour endurance and cruise speed of 105 knots. Passenger capability of 4 is met by another aircraft manufactured by Pipistrel, a hybrid twin-fuselage aero-taxi HY-4. However, its cruise speed is far below the desired 180kts. The speed is met by electric aerobatic Extra 330LE aircraft, however it can only carry one passenger for 20 minutes [11]. It can therefore be concluded that at present, no hybrid aircraft of the characteristics described by requirements exists; this justifies the need for developing a green, fast and efficient aircraft, the niche the S270 aims to fill.

1.4. Key Parameters

The S270 aims to provide thin-haul flights for a maximum of 4 passengers, the key parameters of the aircraft are given below in Table 2.

Table 2 Key aircraft parameters.

Parameter	Value	Parameter	Value
Wing Span (m)	10.32	Maximum Continuous Power (kW)	230
Wing Area (m^2)	14.32	ICE Engine Output (kW)	270
Cruise Speed (m/s)	92.6	Electric Motor Output (kW)	240
Cruise Altitude (ft)	12,000	Fuel Consumption at Cruise (kg/hr)	47.4
Stall Speed at sea level (flaps extended) (m/s)	28	Range at typical cruising speed (nmi)	137
Maximum Take Off Weight (kg)	1679	Maximum range at Normal Mission Conditions (nmi)	263
Maximum Climb Rate (ft/min)	1605	Time to Cruising Altitude (min)	10
Take Off Ground Roll (ft)	522	Landing Ground Roll (ft)	912

The S270 aims to deliver 4 passengers with a 135 nautical mile range in a mission time of 65 minutes. Using hybrid propulsion and a larger wing area, the climb rate of the aircraft outstands major competitors such as the Cirrus SR22. In order to achieve higher fuel efficiency, the S270 also utilises hybrid propulsion in the climb and descent phases to accommodate the aims of greener propulsion. The flight profile and the relevant degree of electric propulsion is shown in Fig 2.

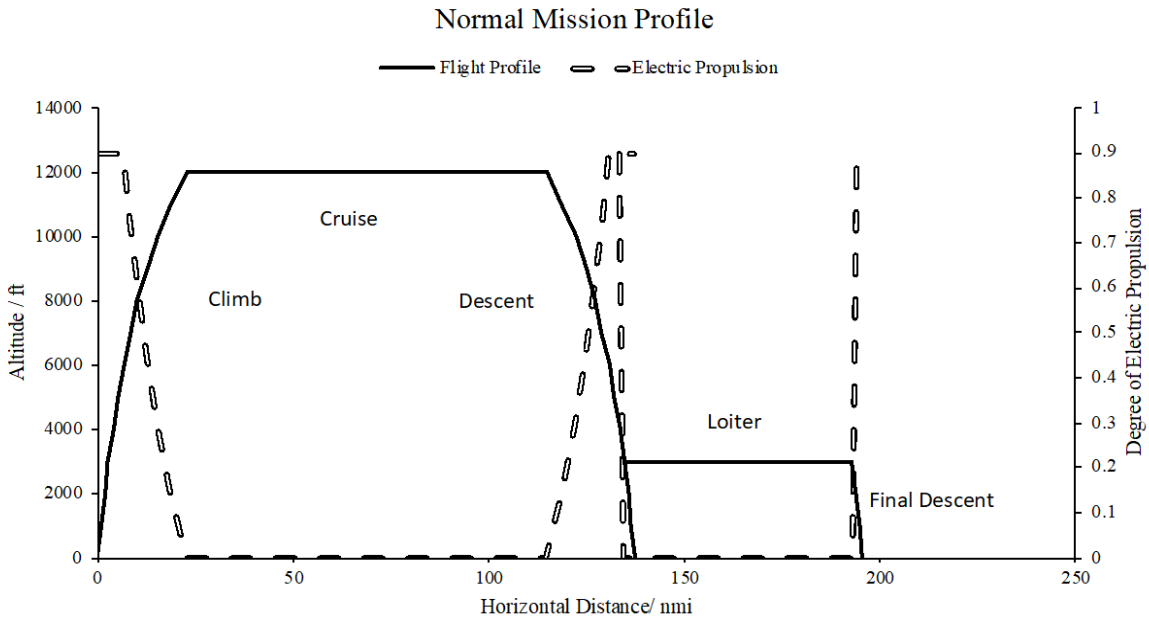

Fig. 2 Mission profile.

1.5. S270 3D Renders and General Arrangement Drawing

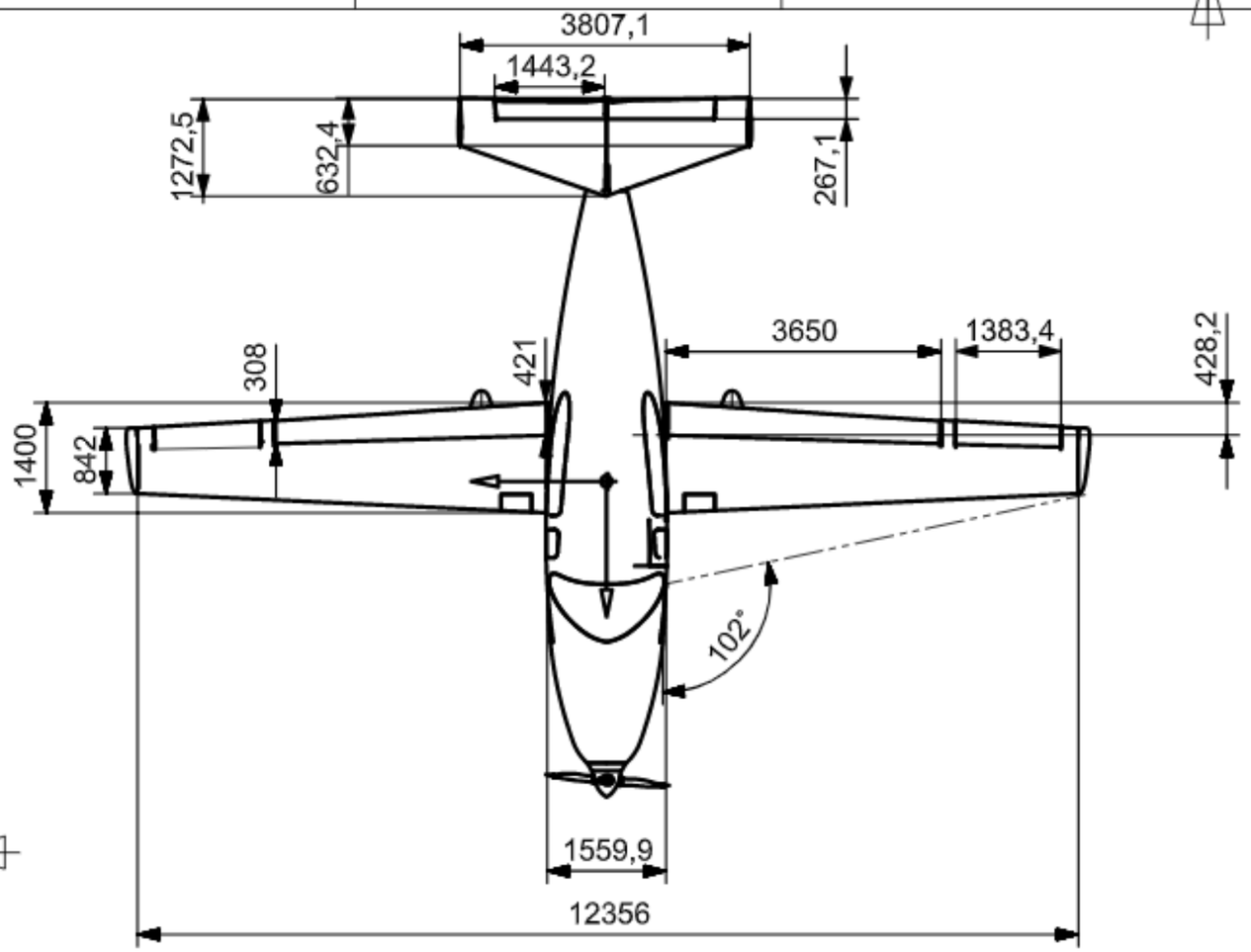

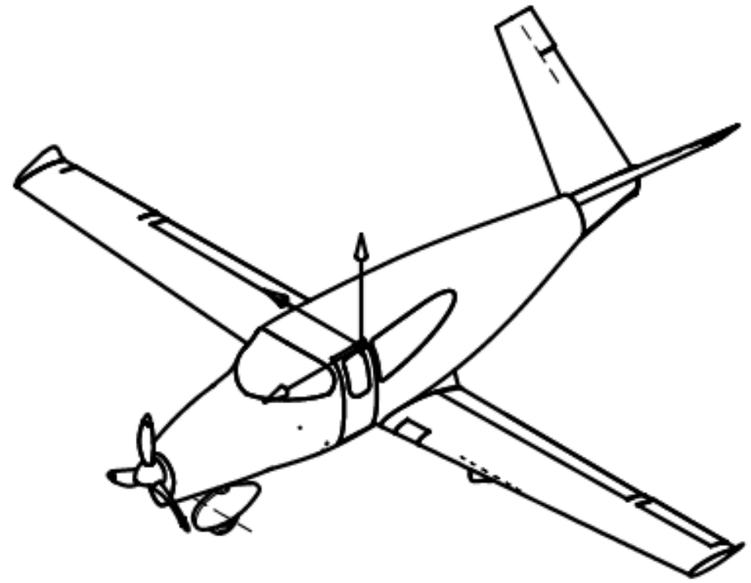

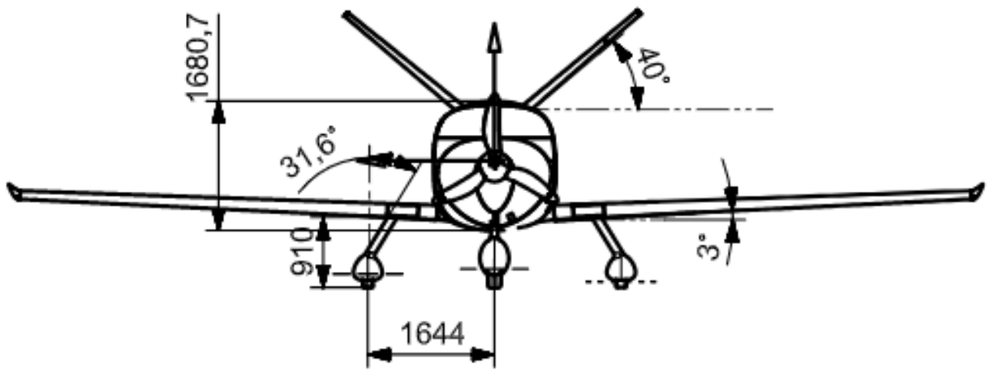

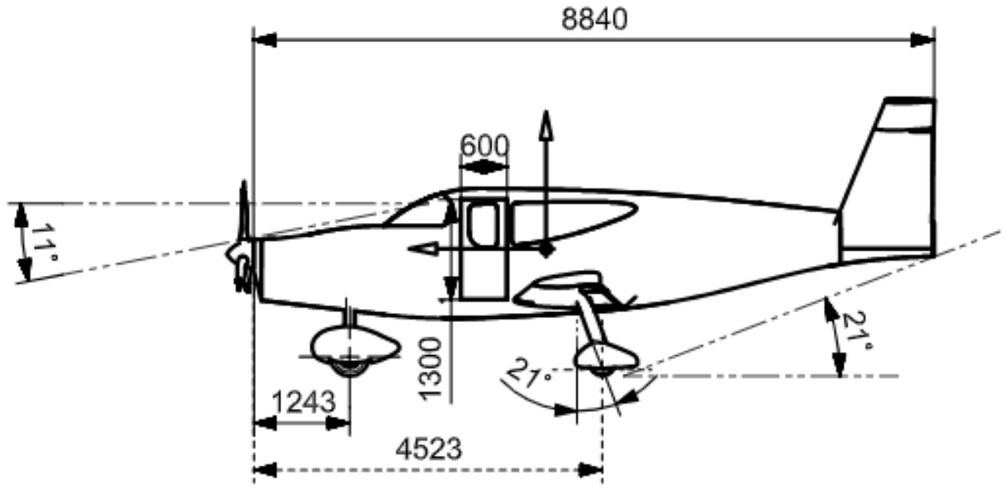

SIZE	A3	SCALE	1:80	MATERIAL	ENTER MATERIAL
LINEAR TOL UOS	±0.2	DRAWING TO BS8888		FINISH	CLEAN AND SCRATCH FREE
ANGULAR TOL UOS	±0.5°	ALL DIMENSIONS MM		DRAWN BY	RYAN BEECROFT
Loughborough University				PROJECT GROUP	THIN HAUL AIR TAXI
				TITLE	PROJECT SKYRIDE S-270
				DRAWING NO.	1
				MODULE NO.	DATE 02/05/2019
				GROUP DESIGN PROJECT	SHEET 1 OF 1

CAD PART: AircraftAssembly2

1.6. Aerodynamics Summary

Optimisation of the aircraft aerodynamics was carried out to compliment the electric take-off phase through selection of an accommodating aerofoil. Levels of twist and taper ratio were analysed to trade-off the induced drag of the aircraft against its tip stall probability, this allowed an appropriate wing planform geometry to be chosen. Final values of drag will also be presented.

1.6.1. Aerofoil

The selected aerofoil is the NASA/Langley LS(1)-0413 (GA(W)-2) pictured by Fig. 3 was determined by a vigorous down selection process presented in Section 2.3.3. For the given take-off flight phases, the GA(W)-2 postulates a 2-D L/D of 111.6, approximately twice that produced by the Roncz/Marske7 aerofoil which is used by the Cirrus SR22 competitor aircraft (63.3). In addition, its inherent thickness provides suitable housing volume for wing contained elements at the expense of a relatively low drag. Table 3 presents a summary of the aerofoil characteristics [12].

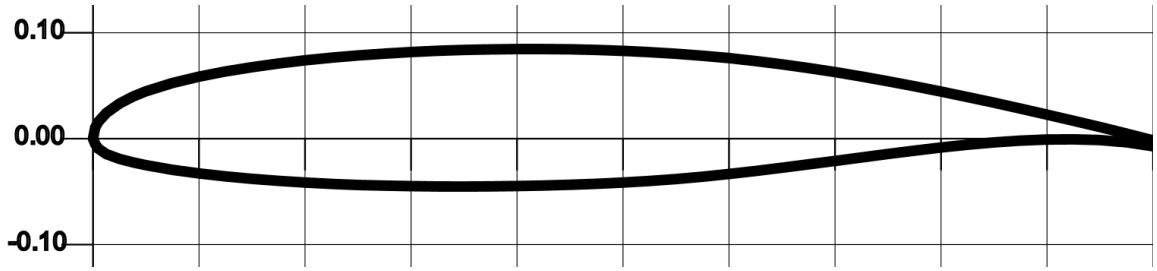

Fig. 3 NASA/Langley LS(1)-0413 (GA(W)-2).

Table 3 Aerofoil characteristics (cruise).

Max C_L	Stall Angle (deg)	Max C_L/C_D	Max Thickness (%)	t/c Max (%)
1.98	15	123.92	12.9	37.5

1.6.2. Wing Planform

The planform geometry is governed by the dimensions presented within Table 5. Following a 1.06% increase in the preliminary wing area to reduce the stall speeds, a trade-off study is presented by Section 2.3.2 to optimise the spanwise stalling location against the induced drag reduction dependent on the tip chord. As a comparison to the SR22 competitor, the S270 delivers lifting capability with a larger aspect ratio hence promoting a 3.1% theoretical base reduction in the induced drag produced in cruise for a given lift requirement, thus improving efficiency. Resulting incidence angles to meet design requirements pertaining to the wing planform are presented by Table 4.

Table 4 Angle of attack requirements.

	Take-off	Cruise	Landing
Angle of Attack (deg)	7.15	0.17	9.23

Table 5 S270 Wing planform dimensions.

Parameter	Value
Planform Area (m^2)	14.32
Span (m)	12.38
Aspect Ratio	10.7
Taper Ratio	0.6
Root Chord (m)	1.40
Tip Chord (m)	0.842
Mean Aerodynamic Chord (m)	1.15
Dihedral (deg)	3
Outboard Twist (deg)	-3

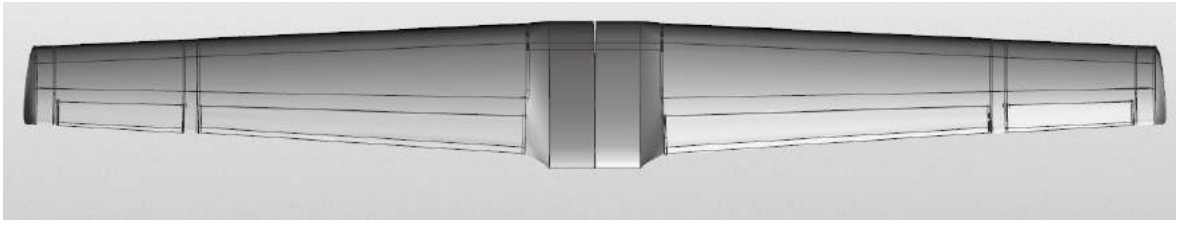

Fig. 4 Wing planform geometry.

1.6.3. Drag Breakdown

Table 6 presents the completed drag parameters for the S270 aircraft at 4 key flight conditions; namely the take-off, cruise, loiter and landing. The S270 observes a reasonable value of parasitic drag in cruise and acknowledges a slightly larger C_D than that of the Cirrus SR22 competitor (0.018). This is justified by the optimisation carried out through the take-off and climb phase, whereby a larger wing area was incorporated to improve the lifting performance and part contributes to a 200ft/min increase in the climb rate.

Table 6 Full drag breakdown of the 4 key flight phases.

Mission Leg	Lift, C_L	Parasitic, C_{D0}	Induced, C_{Di}	Total, C_D
Take-off	1.33	0.0500	0.0714	0.121
Cruise	0.316	0.0254	0.00402	0.0294
Loiter	1.33	0.0347	0.0708	0.106
Landing	1.71	0.0796	0.118	0.197

1.7. Propulsion Summary

Low operating costs and a positive public perception will be vital for the success of Project SkyRide, this can be partly achieved through implementation of a Hybrid Electric Propulsion (HEP) system. HEP will reduce emissions and fuel burn, while offering performance benefits and added redundancy [13]–[19]. The S270 will use a series-parallel hybrid architecture, based on the engine design of the Toyota Prius third generation engine [20]. A series-parallel configuration offers added redundancy when compared to series or parallel architectures because the aircraft can operate using full Internal Combustion Engine (ICE) power, full electric power, or a combination of both. A detailed trade-off study for the HEP architecture is outlined in Section 2.6.1.

1.7.1. Powertrain Design

The S270's engine is shown in Fig. 5. The largest and heaviest component in the powertrain is the ICE; a 6 cylinder, horizontally opposed, avgas burning engine. The ICE design is similar to the continental I0550 engine, with increased efficiency and reduced weight due to the incorporation of modern components and technologies. A discussion of the ICE selection process is outlined in Section 2.6.2. Unlike the Prius, the S270 powertrain has only one motor-generator (MG), which reduces weight of the system by approximately 50 kg. The second MG in road vehicles is primarily responsible for energy generation via the regenerative braking system, something that cannot be implemented into small aircraft. A detailed motor selection process is outlined in Section 2.6.3. The power split device is a key component in the S270's engine; this multi-geared device allows the ICE and MG to power the propeller independently or in-tandem [21]–[24]. A detailed description of the operation of the power split device is outlined in Section 2.6.5.

Figure 6 shows a dimensioned drawing of the powertrain; to minimise mechanical losses through excess gearing, the ICE and motor have been placed one in front of the other. This allows for the frontal area of the powertrain to be minimised and in turn, reduces the frontal area of the nose, which furthermore reduces drag of the aircraft.

1.8. Mass Breakdown

A detailed mass and balance breakdown of components is summarised in Table 7 and visually represented in Fig. 7. Finding an optimum centre of gravity along with a reduced weight is important when designing an aircraft. Lower weights mean the aircraft can be operationally cheaper and optimum centre of gravity allows the aircraft to be stable and balanced. The S270 has an empty weight of 1005kg. This is lighter than the Cirrus SR22, however due to extra weight from batteries, the maximum take-off weight of the S270 is slightly higher. A detailed explanation into the methods used to find component masses can be found in Section 2.9.

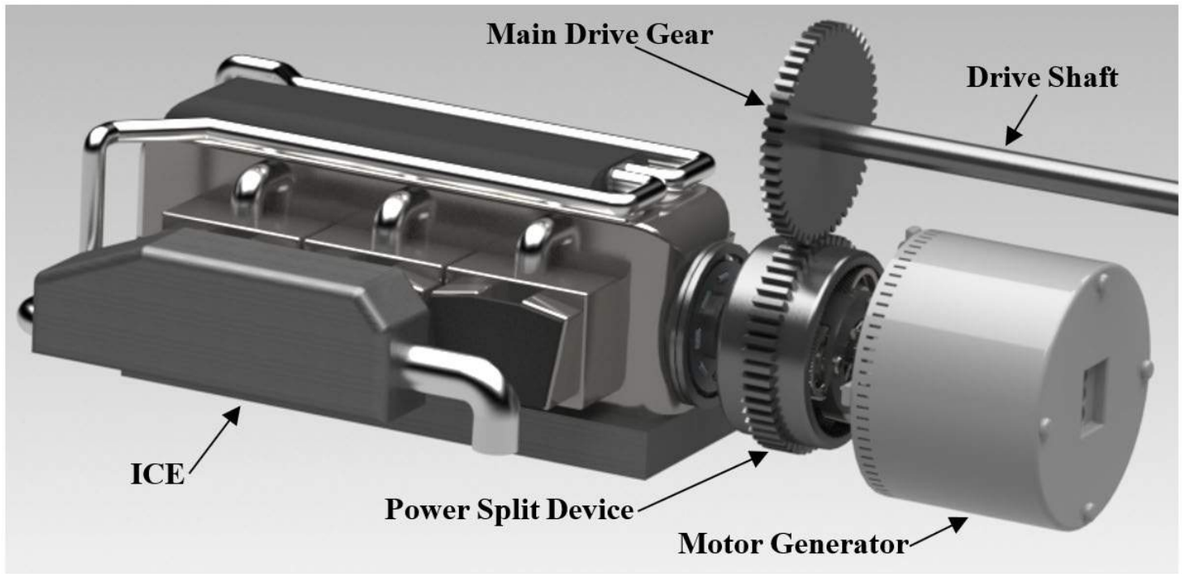

Fig. 5 Powertrain of the S270 aircraft; consisting of ICE, power split device and electric motor.

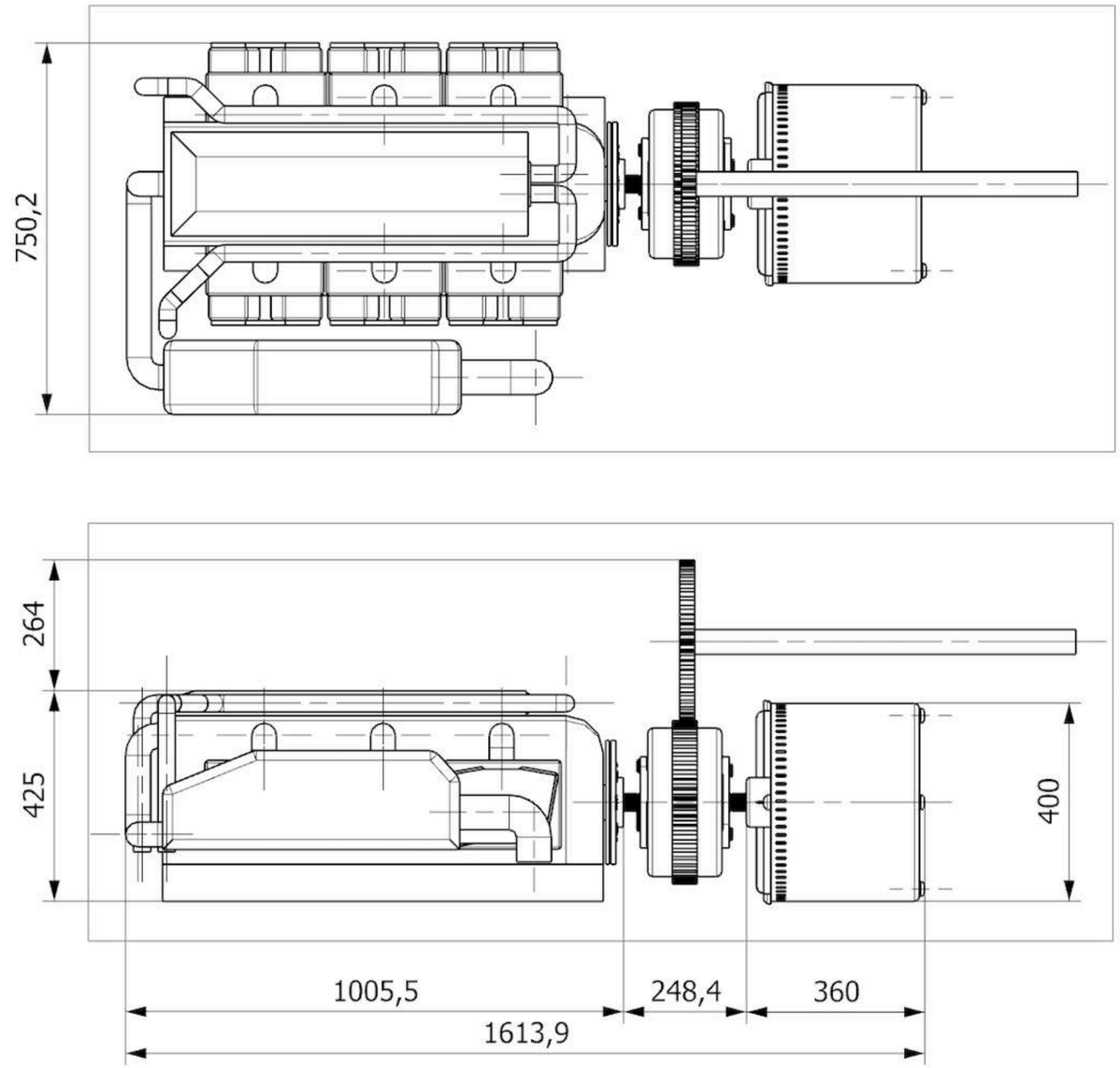

Fig. 6 Dimensioned drawing of the S270 powertrain.

Table 7 Mass breakdown.

Group	Weight Item	Method	Mass (kg)	X (m)	Y (m)	Z (m)
Group I - Structural Parts	Wing	Class I	120	4.11	0	-0.05
	Empennage	Class I	27	8.2	0	0.7
	Fuselage	Class I	107	3.4	0	0.2
	Nacelle	Class I	16	0.4	0	0
	Main LG	Class I	44	4.5	0	-0.85
	Nose LG	Class I	22	1.24	0	-1
Group II - Powertrain Parts	Engine	Known	180	1.1	0	-0.1
	Engine Install	Class I	3	1.1	0	-0.1
	Controller	Class I	25	1.3	0	0.25
	Power split device	Known	20	0.5	0	0.2
	Motor speed reduction unit	Known	20	0.5	0	0.2
	Cables	Estimate	25	4.5	0	-0.03
	Motor	Known	50	0.2	0	0.4
	Propeller	Class I	37	0	0	0
Group III - Fixed Equipment	Avionics	Known	37	4	0	-0.3
	Controls	Class I	49	4.7	0.03	-0.05
	Electrical	Class I	62	7	0	-0.02
	Air Conditioning	Class I	24	4.8	-0.03	-0.15
	Oxygen	Class I	12	6	0	-0.1
	Parachute	Known	49	5.3	0	0.35
	Furnishings	Class I	76	4.7	0	0.2
Group IV - Variable Payload	Passenger/Pilot	Known	445	4.7	0	0.2
	Batteries	Known	146	7	0	-0.1
	Fuel	Estimate	75	3.2	0	-0.05
Totals	Total Empty Weight			1005kg		
	Max Take-off Weight			1671kg		
	X-Location Centre of Gravity			4.06m		
	Y-Location Centre of Gravity			0m		
	Z-Location Centre of Gravity			0.15m		

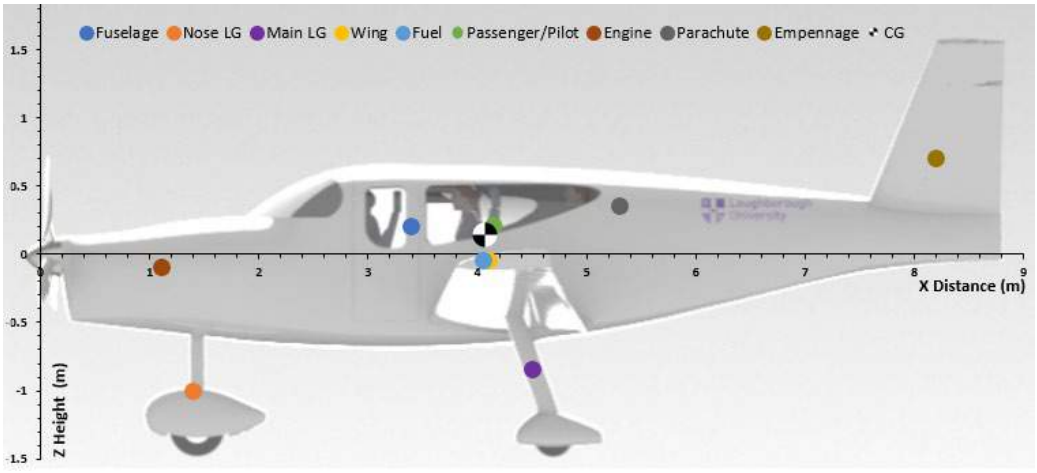

Fig. 7 Centre of gravity location.

1.9. Batteries Summary

The innovation of battery technology has been slow since the commercial release of Lithium-Ion cells in 1991 by Sony [25]. This new revolutionary cell improved the gravimetric energy densities by 530% from earlier lead acid technology, thus allowed greater scope for new applications. However, lithium-ion has now matured over the years and is close to reaching its theoretical (energy density) maximum of 390Wh/kg on a cell level [26]. This limits its use on a larger scale without increasing the number of cells and therefore increasing weight. Tesla's implementation of these cells in electric vehicles has proven its feasibility in high current draw operations, but significant specific energy improvements are limited.

Table 8 Battery research.

Battery Type	Specific Energy (Wh/kg)	TRL	Projected TRL (2021)
Li-Ion	100-260	9	9
Zinc-Air	470	9	9
Solid State	400	5	7
Lithium-Sulphur	400	6	8

Technology Readiness Level (TRL) is an important factor to determine whether technology can be certified by a certain date. Therefore, a 2021 projected TRL was considered to allow 4 years for the certification process. Table 8 displays the research conducted on the different types of batteries. A TRL level of at least 8 must be used as it demonstrates tested technology ready for implementation [27]. Specific Energy is also an important parameter as it determines the total battery weight, which contrary to fuel, does not reduce during a flight mission; therefore, it is crucial to maximise this value. Zinc-Air satisfies both the specific energy and TRL requirements as it has been implemented in many smaller scale applications; however, this technology has not been proven in electric vehicles. Solid state batteries' lower TRL level had also led to a disregard of the technology [28].

Lithium-Sulphur batteries, however, have been tested in flight by the Zephyr 7 [29]. It was found to be a desirable option due to its high theoretical ceiling of 2600Wh/kg [30]; therefore, research was conducted to find current developers of this technology. OXIS Energy have developed cells with a current energy density of 400Wh/kg and a target of 500Wh/kg by the end of 2019 [30]. As proposed in the design freeze report [8], the S270 will use projected figures from current capabilities. The high-power cell variant offered by OXIS Energy was used for preliminary calculations, along with a conservative projected energy density of 520 Wh/kg [31]. An optimisation and arrangement of cells was also studied, which is evident in Section 2.7.

1.10. Parachute Design

As the S270 is designed as a single engine aircraft, it is a requirement that a parachute system is added as a redundancy measure. The Cirrus SR20 and SR22 were the first general aviation aircraft that had a 'whole-airframe' parachute system designed and implemented. This system was verified and accepted by the FAA, hence a parachute system for the S270 is certifiable.

The parachute system is located at the back of the aircraft cabin and can be deployed by the pilot or passengers in emergencies. The parachute was sized to have a diameter of 20.5m when fully open and weighed in at 49kg. This allowed the aircraft to fall to the ground at a rate of 1600 feet per minute [32]. On impact with the ground, it was estimated the loading would be equivalent of a straight drop from a height of four meters. This was a major factor in landing gear selection between fixed and retractable design. Disregarding cost and manufacturing complexities, the retractable gear did not favour well when a parachute deployment sequence experienced a loss of power or actuation. Impact on the ground with a retracted gear would cause incomprehensible damage to the fuselage and passengers inside. The parachute deployment sequence and design can be seen fully in Section 2.11.

Fig. 8 Parachute deployment.

1.11. Stability and Control Summary

To define the stability of the S270, an in-depth analysis was conducted of various tail configurations. Tail moment arm, area and dihedral angle could be adjusted as we adopted a V-tail configuration. This was chosen to reduce the induced drag from the empennage section and reduce manufacturing time with fewer parts and a simpler configuration.

In general, it was found that increasing the tail moment arm or tail area were both stabilising characteristics. The dihedral angle is a destabilising characteristic with smaller angles contributing more to longitudinal stability but reducing lateral control. The ruddervators are responsible for both yaw and pitch moments meaning fewer control surfaces. A preliminary design was produced by converting the conventional tail on the Cirrus SR22 to a V-tail. Comparing natural pitching moment of the aircraft, the following design was concluded with a larger tail area, shorter moment arm and greater dihedral angle. This was deemed preferable as it had the same performance as the preliminary design and had less structural weight due to reduced fuselage length.

Table 9 Tail dimensions.

Parameter	Value
Planform Area (m^2)	4.5
Dihedral Angle, **Γ** (deg)	40
Aspect Ratio	5
Span (m)	4.743
Root Chord, Cr (m)	1.266
Tip Chord, Ct (m)	0.631
MAC, $\bar{\mathbf{c}}$ (m)	0.984
Moment Arm, l_t (m)	4 (from main wing quarter chord)
Elevation above Wing (m)	0.5

Longitudinal and lateral stability performance were assessed using XFLR5 and AVL with results compared to FAR 23 requirements and design guidelines outlined by Cook [33]. Static stability was used to find the neutral point and a 25% static margin was applied. Whilst remaining stable, this allowed there to be sufficient span for loading, taking into account the tail-heavy condition due to the battery's location. Maximum ruddervator and aileron deflections were also designed to deliver sufficient pitch/yaw/roll rates across the flight envelope as effectiveness is usually reduced in flight.

Table 10 Neutral point, CoG and control surfaces.

Parameter	Value
Neutral Point (%$\bar{\bar{\mathbf{c}}}$ [dist. from wing LE (m)])	0.7455 [0.8543]
Static Margin (%$\bar{\bar{\mathbf{c}}}$ [dist. from wing LE (m)])	0.4955 [0.568] – 0.7455 [0.854]
COG (%$\bar{\bar{\mathbf{c}}}$ [dist. from wing LE (m)])	0.5323 [0.61]
Ruddervator Chord (%$\bar{\bar{\mathbf{c}}}$) / Span (m)	0.2c / 1.9
Ruddervator Maximum Deflection (deg)	± 35
Aileron Chord (%$\bar{\bar{\mathbf{c}}}$) / Span (m)	0.35c / 1.4
Aileron Maximum Deflection (deg)	± 30

Overall, the S270 exhibited good natural stability with both short and long period modes for longitudinal, lateral and directional stability being well damped and stable. Level 1 flying characteristics were achieved in all three modes with short and long period mode frequencies being well separated (see Section 2.5.4) Though these frequencies were calculated to be quite high, this is a function of the flight condition and as such a stability augmentation system should be able to mitigate these instabilities.

1.12. Structures Summary

Light weight and low cost were key design drivers for structure of the S270 leading to the choice of a fully composite aircraft.

The wing structure consists of two spars, which are main load carrying elements. Their webs are made from carbon fabric and foam. Spar caps, whose thickness varies spanwise, are made from unidirectional carbon tape, reinforced with carbon and glass fabric as well as foam. Only two ribs, inboard at wing root and outboard at wing tip are flight loads carrying elements. Four few extra ribs have been incorporated to provide structure for control surface attachment. As non-redundant elements, root and tip ribs are made from carbon fabrics put at different orientations, which means that no direction is privileged in terms of failure. Finally, no stringers are incorporated into the wing structure; instead, the wing skin is reinforced with foam providing local stiffness and preventing buckling. Wing skin has glass fabric layer to improve impact resistance, two load bearing carbon fabric layers, with foam between them. Detailed descriptions with explanations have been provided in Section 2.8. The feasibility of the design has been proven by Finite Element Method (FEM) analysis for maximum loading conditions; all the loads can be carried with decent reserve factor. FEM results have been shown and discussed in Section 2.8.5.

Skin of S270 fuselage is made from carbon fibres tape produced from low cost polyacrylonitrile yarn and reinforced with aramid honeycomb core to reduce material costs. The skin is put on the fuselage mandrel using filament winding technique, speeding up manufacturing process ad allowing for

accuracy. Main load bearing structures are hollow frames, which are filled with foam for reinforcement at structurally weakest points. The skin and frames are cured as one piece, which allows for significant savings in time and labour costs. Finally, V-tail incorporates 8 ribs placed along two spars, with an extra stub spar incorporated for reinforcement, as V-tails usually carry higher loads than other tail configurations. Internal structure of S270 can be seen in Fig. 9.

Fig. 9 Internal structure layout of the S270.

1.13. Systems Summary

The aircraft systems are set of processes that must exist within an aircraft to ensure its operational success. They are broken down to a number of sub-systems which include flight control systems; avionic systems; fuel and power system; environmental control system and the electrical system. Figure 10 illustrates the location of these systems on the aircraft.

The flight control system incorporates the control surfaces of the aircraft and the linkages made in between allowing the aircraft to fly. The S270 utilises a Fly-By-Light (FBL) system for these surfaces which are divided between primary and secondary controls. More modern actuation techniques, currently uncommon in small light aircraft, are employed to promote the S270 as an MEA.

The avionics systems consist of all the electronic components in the aircraft. These include the main PFD/MFD displays, navigation/communication, ADS-B, Autopilot as well as the multitude of underlying components which allow them to run, such as the FMS.

Since the S270 is hybrid-electric aircraft, some systems can be regarded as quite conventional. The fuel delivery is one such system as it is stored, much like other aircraft, in the wing. The batteries,

however, reveal a more interesting design. The power from these are fed directly to a parallel-hybrid system, isolating one from the other and introducing redundancy.

A comfortable cabin is essential for the success of the S270; this is primarily controlled by the Environmental Control System (ECS) by promoting air circulation and regulating the temperature within the cabin. Furthermore, it is also responsible for assisting the battery cooling system during peak loads.

The electrical system illustrates the power delivery to all sub-systems; however, this system is kept separate from the propulsive batteries network. Redundancies have been integrated to ensure the safe operation of the aircraft, including prioritising power supply to essential components and isolation mechanisms to prevent ‘run-away’ failures.

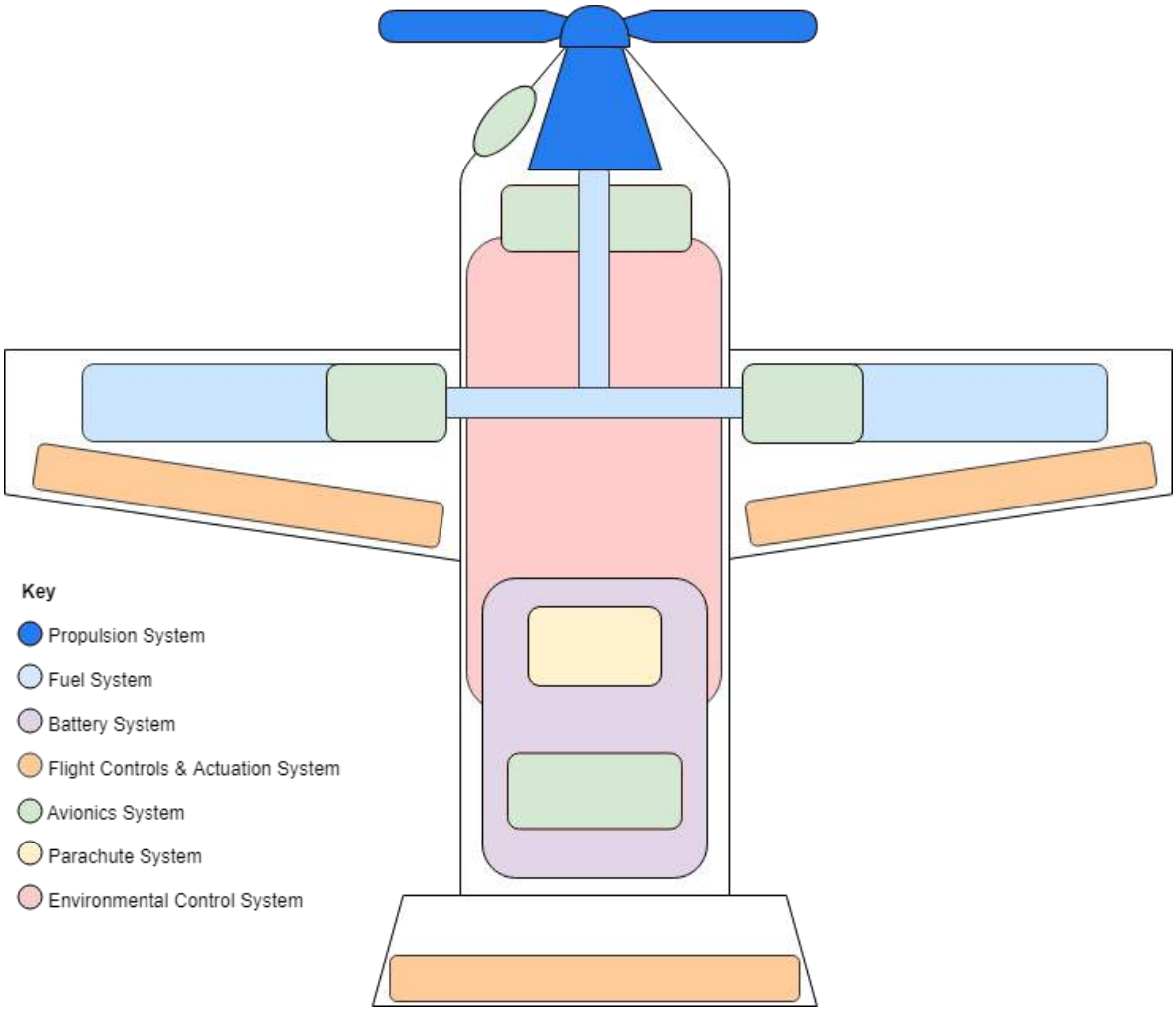

Fig. 10 All aircraft systems.

1.14. Risk and Reliability

Safety is a priority for the S270 and there are numerous safety measures implemented to increase the reliability of the aircraft and safety of the passengers and pilot. A full risk assessment is presented in the Section 2.14 comprising the pilot, aircraft, environment and external risks. Each of these risks are categorised according to their severity and probability. Safety measures and solutions to the risks associated to the aircraft are highlighted; with the battery cooling system providing the most concern. The battery cooling system is critical for the safety of the aircraft; therefore, there is an option to disconnect the batteries from propulsion, as well as vents to increase air flow. The engine will go through extensive testing before being certified for use on the aircraft, proving the reliability of the system.

1.14.1. Certification

The aircraft is designed to regulation stated in FAA 14 CFR Part 23 under the category of "normal" aircraft. The S270 is a level 2, low speed aircraft carrying 4 passengers. The most important aspect of aircraft certification will be the hybrid electric propulsion system. The engine will be classified as an ICE with power augmentation provided by the batteries and once coupled with an Engine Control Unit (ECU), complies with 14 CFR Part 23 regulations.

1.15. Cost Analysis

Cost of the S270 was analysed using The Eastlake Model [34] and a breakdown is given by Table 11.

Table 11 Cost breakdown overview.

Parameter	Cost ($)
Total cost to produce	710,582.23
Minimum selling price	726,710.23
Selling Price with 15% profit	835,716.76
Total Flyaway Cost	443,276.20
Cost per flight hour	206.73
Per Person (without profit)	51.68
Per Person (with 15% profit)	59.43

Table 12 below presents a cost comparison of the S270 with competitor aircraft. As is presented, the S270 forecasts financial saving in both unit cost and operating cost.

Table 12 Cost comparison between competitors.

Aircraft	Unit Cost ($)	Operating Cost per hour ($)
S270	726,710	206.73
Cirrus SR22	765,450 [35]	245 [36]
Cirrus SR22T	889,000 [37]	210 [38]
Piper PA34	1,050,000 [39]	360 [40]
Beechcraft G36	855,750 [41]	225 [42]

1.16. Business Case Summary

Fig. 11 An example of the booking system application.

The design of the S270 is for frequent short haul flights from small regional airports. This design brief is perfect for a company, such as Surf Air, that could run an air taxi service providing both scheduled and on-demand flights. The customer will be able to view and book seats weeks' in advance with scheduled flights or request a flight for as soon as possible at the nearest airport location. Booking can be made easier by basing the booking system online and within an app. An example can be seen in Fig. 11. With sufficient training of aircraft refuelling and pre-flight checks, there is no additional staff required apart from the pilot.

1.17. Evaluation and Feasibility

The S270 is a new innovative aircraft optimised and tailored for a thin haul transport model. The design features original hybrid electric propulsion technology factoring in a 2025 entry to service date consideration. This outlines a major selling point in comparison to existing general aviation aircraft currently operating similar mission profiles. Throughout the design procedure, competitors such as the Cirrus SR22, Piper and Beechcraft Bonanza series aircraft have been used to benchmark the design and offer comparison to evaluate Skyride's new aircraft. Consumers opting to purchase the S270 for air taxi operation can expect up to a 37% saving with respect to unit cost in addition to a maximum operating cost saving of 43%. The design however could benefit from further extensive work into the infrastructure governing operation of the air taxi concept. Work has been done to outline preliminary feasibility such as the possible staff requirement, airport facilities and a mobile application for use in a business context. Further efforts would extend to prototype generation and testing within an operational environment to gauge the feasibility in a practical context.

Part 2. Supporting Information

2.1. Design Problem and Requirements

Currently, there are very few aircraft fit for a thin haul application. This is largely attributed to the high operating costs which have caused several past businesses to fail. The wide number of underutilised airports across the US provide the infrastructure, but there is little in place to make short haul, high frequency flights a viable transportation alternative. This is the primary aim of Project Skyride.

2.1.1. Air Taxi Business

The concept of air taxiing has been trialled in numerous companies, with varying degrees of success. Surf Air is a successful company based in California that operates by members paying monthly subscription fees. They operate using a larger Pilatus PC-12 aircraft and run only scheduled flights, rather than on demand. For frequent flyers this is a good set up, however the monthly fees and lack of on demand flying makes it not suitable for other users. BlackBird Air is a company that controls numerous flights a day where customers can book a seat on a flight easily through an app. The app is very simple to use with a wide variety of flight times, aircraft and locations. This company also does not offer any on demand flights, so flyers have no flexibility to travel times. ImagineAir is an example of an unsuccessful company which operated by customers renting the entire aircraft instead of singular seats on a flight. They lacked the funding in order to scale the business into a profitable company. DayJet was a company that attempted to run on demand flights, however they suffered in the financial crisis in 2008 and suspended all flights [43].

Fig. 12 US airport system

Uber Elevate is a new concept, where VTOL aircraft are operating from rooftop to rooftop in very densely populated cities. They propose to work purely from on demand flights, with cheap tickets making the travel service more desirable than other modes of transport, such as driving. The VTOL

concept requires a long certification process, as well as safety regulations and costing regarding the rooftop to rooftop concept. The locations of this service are also limited to the most populated cities. Therefore, there are advantages flying from small, unused airports in a variety of locations, as the S270 was designed to do.

2.2. Design Evolution

The design evolution segment describes the procedure exercised to navigate from initial conceptual design to a final concept. Various stages were implemented to guide a suitable refinement process to eliminate concepts deemed not viable in the context of the design requirements. In addition, customer influence was gauged through the initial QFD analysis to feed a down selection matrix, to determine a final concept presented Fig. 19.

2.2.1. Initial Concepts

Making use of the specification provided by the AIAA, several designs were generated. A QFD analysis of minimum design requirements served as an initial basis for the designs. The broad initial approach taken yielded conventional configurations much like the S270's potential competitors to more unique designs incorporating DEP and tilt rotors. High importance was attributed to satisfying a low operating cost with secondary focus being placed upon producing a low environmental impact. These two aspects were held at the highest regard in tailoring the concept selection since previous companies operating a similar transport model attribute their failures to high operating costs and high emissions, particularly noise. It was decided early on that all designs must make use of hybrid propulsion and designed with the passenger's comfort and ease of boarding/egress in mind. As an initial filter, those that used VTOL were eliminated as the requirement specifies the use of airports and runways.

2.2.2. Down Selection Matrix

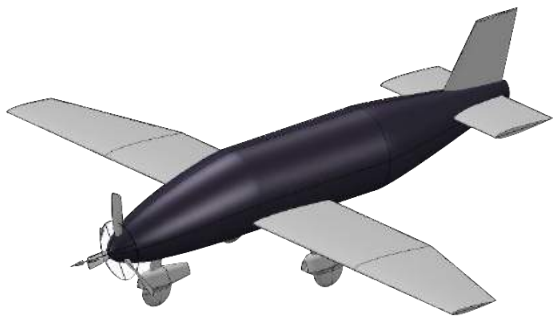

Fig. 13 Concept I (Low wing, single hybrid engine, fixed gear).

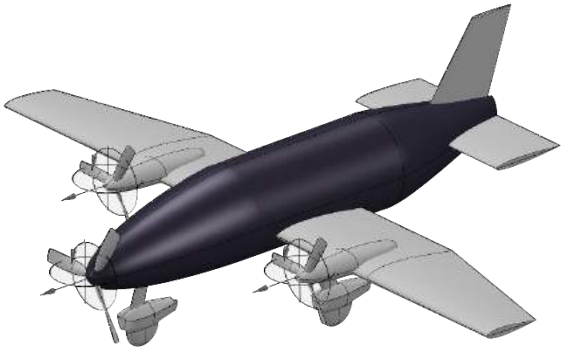

Fig. 14 Concept II (Low wing, 1 ICE, 2 electric fans, fixed gear).

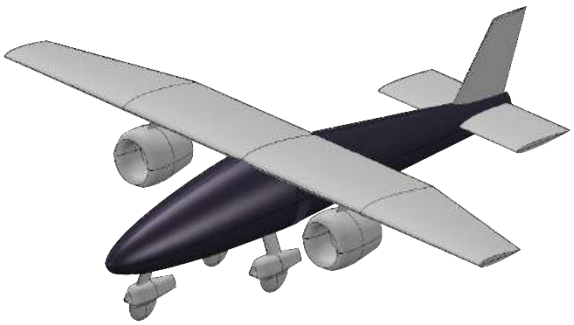

Fig. 15 Concept III (High wing, 2 under-wing ducted electric fans, fixed gear).

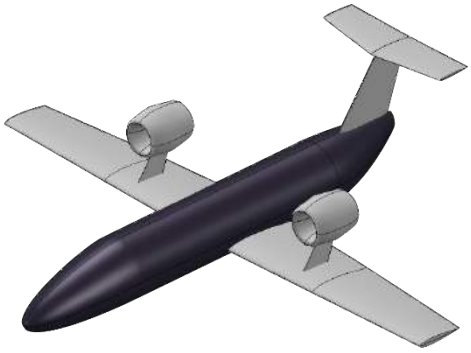

Fig. 16 IV (Mid wing, 2 over-wing ducted electric fans, retractable gear).

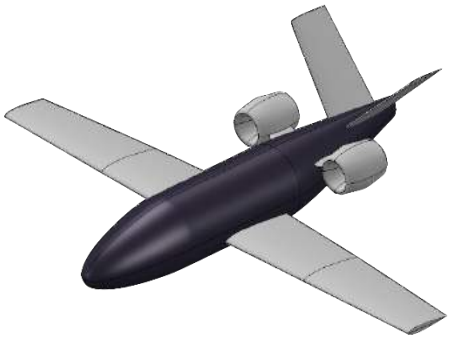

Fig. 17 Concept V (Low wing, 2 rear mounted ducted fans, retractable gear).

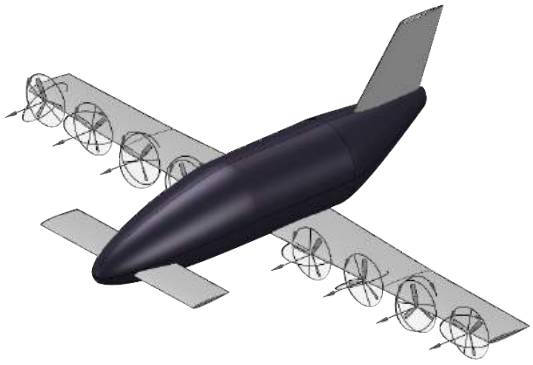

Fig. 18 Concept VI (Low wing, DEP, canard configuration, retractable gear).

From the remaining designs, these 6 were chosen (Fig. 13-18) to be compared using a down selection matrix. Operating cost with respect to fuel burn and maintenance are the most important factors for customers of the Project Skyride aircraft as they directly impact the competitiveness. Unit cost was deemed less important as cost over service life could compensate for this. Passenger comfort and environmental factors were considered of equal importance. Passenger experience directly affects customer perception, hence the success of the aircraft. In being environmentally friendly, the aircraft can reduce the impact on those in surrounding areas by reducing noise and carbon emissions. Moreover, they can conform to strict governmental regulations.

Table 13 Down selection matrix.

Level 1	Parameter	Operating Cost (Fuel)		Operating Cost (Maintenance)			Unit Cost	Passenger		Environment		Score
	Weight	0.3			0.1			0.25		0.25		
Level 2	Parameter	Engine Configuration	Aerodynamics	Service	Access	Components	0.1	Noise	Egress	Emissions	Noise	
	Weight	0.18	0.12	0.05	0.025	0.025		0.1	0.15	0.05	0.2	
Concept I	Weighting (1-5)	3	4	2	5	2	5	2	4	3	4	**3.545**
	Score	0.54	0.48	0.1	0.125	0.05	0.5	0.2	0.6	0.15	0.8	
Concept II	Weighting (1-5)	2	3	1	4	1	3	3	2	2	3	**2.495**
	Score	0.36	0.36	0.05	0.1	0.025	0.3	0.3	0.3	0.1	0.6	
Concept III	Weighting (1-5)	4	3	4	3	3	2	3	3	4	4	**3.38**
	Score	0.72	0.36	0.2	0.075	0.075	0.2	0.3	0.45	0.2	0.8	
Concept IV	Weighting (1-5)	4	3	2.5	4	2.5	3	2	2	4	4	**3.1675**
	Score	0.72	0.36	0.125	0.1	0.0625	0.3	0.2	0.3	0.2	0.8	
Concept V	Weighting (1-5)	4	3	3	2	2.5	3	4	3	4	3	**3.2925**
	Score	0.72	0.36	0.15	0.05	0.0625	0.3	0.4	0.45	0.2	0.6	
Concept VI	Weighting (1-5)	5	4	4	4	3.5	1	4	4	5	5	**4.1175**
	Score	0.9	0.48	0.2	0.1	0.0875	0.1	0.4	0.6	0.25	1	

2.2.3. Concept Selection

Concepts I and VI came out as the designs best fitting to the design requirements, with the DEP performing better than conventional configuration with single-hybrid engine. Concept I is largely similar to the Skyride aircraft's main competitor, the Cirrus SR22 but adopting more innovative propulsion methods. Hybrid methods have several benefits such as reduced fuel burn, noise and redundancy. These benefits are amplified with the DEP concept, though it suffers from high wing loading at least twice as high as traditional ICE aircraft [44] due to batteries and propulsion components stored in the wing. This concept was to be fully electric which would mean high battery weight as there is significant room for improvement in terms of battery technology and energy density. Stresses in structures are consequently greater hence requiring additional reinforcements increasing the weight. Moreover, technology readiness level poses a threat to concept VI not being certified by the entry to service date, which was considered too great a risk to the project and therefore this design was eliminated. As a result, concept 1 was deemed the most feasible and served as the basis for further detailed design.

2.2.4. Design Changes

Further developments were made to concept I to improve the efficiency and incorporate more innovative design. Considering the use of hybrid propulsion, any further efficiencies were to be derived from aerodynamic improvements. The first alteration was to adopt a V-tail configuration to help reduce the induced drag between the tail junctures by 33%. In addition, this reduces the manufacturing time which would significantly help the business to meet demand and keep costs at a minimum. This configuration also benefits from fewer moving parts as the ruddervator control surface is used for both yaw and pitch control. However, this does result in roll-yaw coupling which could pose a complication for an inexperienced pilot. This will be overcome with a roll damper stability system which will help to reduce the Dutch roll excitation and provide a counteracting roll moment to overcome any inherent instability.

2.2.5. Final Concept

The final concept remained largely the same but with minor changes which arose across the project. This was a low wing, V-tail with fixed landing gear and a hybrid engine. Climb and landing were decided as the phases to be made electric. Passenger boarding was chosen to be from the rear of the aircraft, though the location of the batteries was moved to the empennage. To speed up turnaround time, the battery swaps can be conducted whilst the passengers board at the front of the aircraft. Not only this, but also the pilot can board and divert straight to the cockpit and passengers to the right. The final concept is shown in Fig. 19.

Fig. 19 Final concept.

2.3. Aerodynamics

The following segment supports the aerodynamics section presented within the technical description. Documented through Sections 2.3.1 – 3 is the aerofoil derivation for the main wing alongside the wing planform justification itself. In addition, an updated drag analysis is presented with supporting flow visualisation by means of Star CCM+ computational fluid dynamics.

2.3.1. Wing Planform Geometry

The wing planform geometry was optimised following an increase in the preliminary wing area to 14.32m^2. The consideration for swept and tapered wing types tailored the geometry to satisfy its function. Swept wings are generally favoured on high speed aircraft whereby their primary purpose is to delay the onset of shockwaves and its associated drag when approaching the speed of sound. Given the operating cruise Mach number of approximately 0.3 utilised by the S270, the use of a large wing sweep was not necessary. Despite this, taper was highly regarded for implementation to reduce the induced drag produced by the wing tips. Further optimisation of taper considered the structural implications of adopting a larger aspect ratio; the ability to increase the root chord lends itself to structurally reinforcing the wing in instances of high bending loads. Despite this concept offering beneficial aspects, consideration for the enhanced probability of tip stall when implementing taper ratio is considered in Fig. 20.

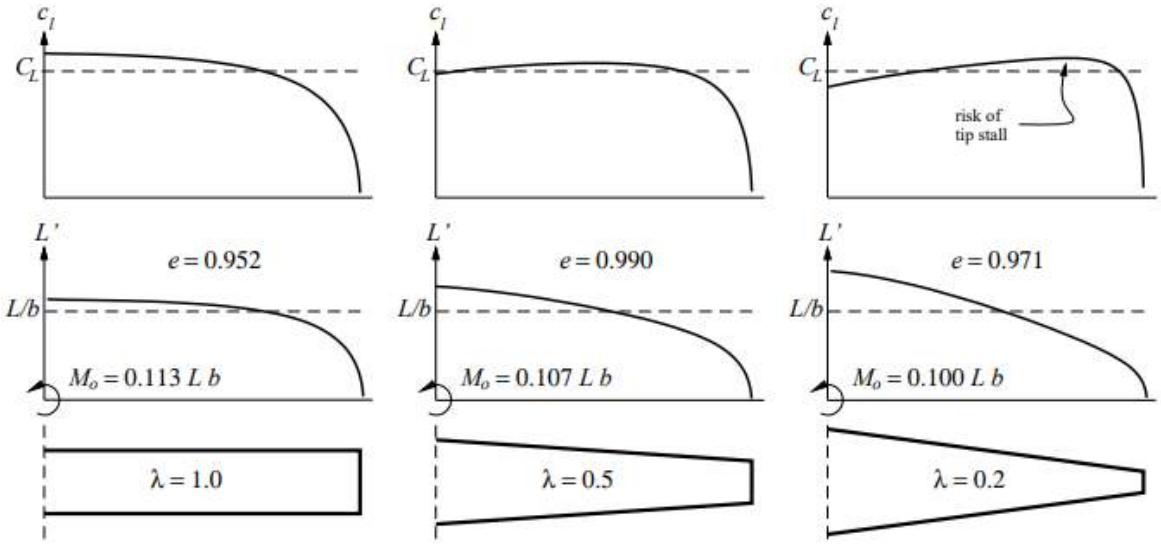

Fig. 20 Lift effect of taper ratio variation.

For taper ratios approaching 50 – 60%, there is a tendency for the maximum lift location to move further outboard. Minimising the taper ratio offers a more efficient wing by reducing the induced drag. However, this presents a potential stability issue as the risk of losing aileron control in a tip stall must be navigated. The S270 opts for a taper value of 0.6 as it is the optimal trade-off point for drag reduction and stability. The location of stall on the wing is greatly influenced by the wing twist; it is desirable to achieve a stall location as far inboard as possible to reduce the risk of losing aileron control. An optimisation study is shown in Fig. 21, where the spanwise lift distribution is compared for different twist values. Twist enables a reduction in the local incidence of the tip with respect to the root chord and provides a natural reduction in the lift. Outboard twist values in the range -1 to -3 degrees were selected for evaluation at the maximum cruise range and take-off stall conditions.

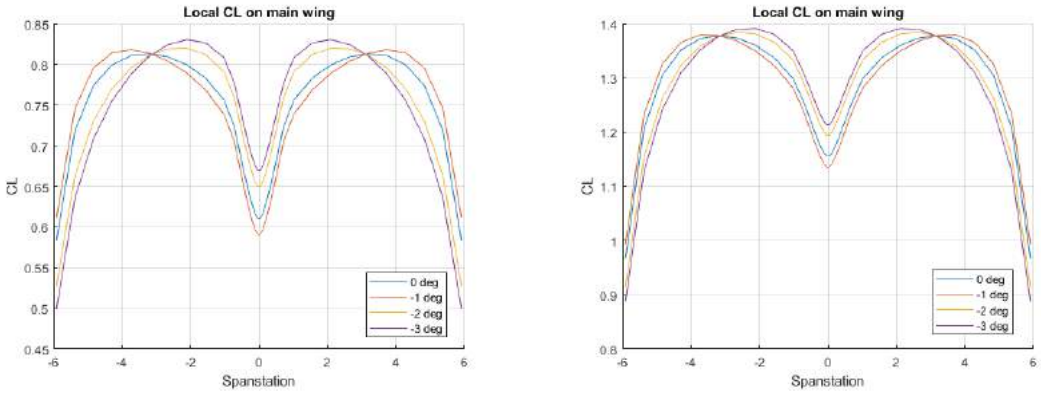

Fig. 21 Lift distribution for varying outboard twist.

The plots clearly demonstrate that the for the twist values approaching -3 degrees, there is a significant inboard translation of the maximum lift location. This thereby reduces the risk of losing aileron control in the event of a stall. The plots also demonstrate a convergence whereby the change

in lift distribution is minimal for the -2 to -3 degree twist values. Therefore, further investigation into larger twists was deemed unnecessary and a final value of -3 degrees was selected for implementation.

2.3.2. Flaps

The next consideration was flap design. Initial trade-offs between different flap configurations were evaluated through the down selection matrix presented by Table 14. The weightings as provided within the "Importance" column of the table were derived based upon the QFD generated during the early stages of this project. Keeping the operational cost down has been of paramount importance throughout the design process and hence minimising weight was deemed vital. Table 14 outputs plain flaps as being the most suitable option for implementation with the Fowler flap being a close competitor. Whilst more intricate designs such as the Fowler and Double-slotted flap offer enhanced lifting performance, the plain flap provides easier maintenance and manufacture with a reduction in the wing structure complexity and overall weight.

Table 14 Flap configuration down selection (higher values represent greater importance).

	Importance	Plain	Fowler	Double-slotted
Lifting Performance	2	1	2	2
Weight	3	3	2	1
Complexity	1	3	2	1
Total		14	12	8

As tested within Tornado VLM, the S270 wing planform was designed to achieve a C_L of 1.68 and 1.70 in the take-off and landing stalling conditions respectively. Therefore, in order to meet the total lifting requirement for the stall conditions (2.080 and 2.297 respectively), a thorough flap design was carried out by utilising the techniques outlined by HAW Hamburg [45]. Two primary equations were utilised:

$$\Delta C_{L,maxf} = \Delta c_{L,maxf} \frac{S_{W,f}}{S_W} K_\Lambda \quad (1)$$

$$\Delta c_{L,maxf} = k_1 k_2 k_3 (\Delta c_{L_{max}})_{base} \quad (2)$$

The k_n coefficients as defined in the nomenclature were obtained using the graphs outlined in the sizing document and were primarily dependent on the flap type, flap deflection and flap chord. The area ratio was minimised (within the constraints of the sizing plots) in order to reduce the drag and structural implications on the wing. The sizing document took elements from reports published in the 1970s and hence there is an understood limitation preventing a complete optimisation of the flap area. Further work is recommended to optimise deflection against the flap dimensions. Final

dimensions and relevant flap deflections are shown in Table 15. The final planform geometry and corresponding dimensions are provided in Section 1.6.2.

Table 15 S270 flap properties.

Property	Value
Inboard Flap Chord (m)	0.421
Outboard Flap Chord (m)	0.308
Single Flap Span (m)	3.65
Takeoff Deflection (deg)	22.5
Landing Deflection (deg)	60
Cruise Deflection (deg)	0

2.3.3. Aerofoil Selection

The following outlines the procedure conducted to derive a suitable aerofoil. Three initial flight phases, (the parameters for which are presented in Table 16) were evaluated within Tornado VLM to produce a series of spanwise lift distributions for the derived wing planform in Section 2.3.1. Firstly, the maximum range flight condition is considered. This was a particularly important condition to satisfy given that the additional weight imposed by the propulsion system makes the S270 a heavier aircraft than most competitors and hence operating cost could be reduced through optimising aerodynamics. In addition, the high lift phases were utilised to investigate the performance at stall to ensure that the final aerofoil can satisfy all aspects of the design mission safely.

To set an input lift requirement within the solver, the total lift requirements for each phase were obtained from performance analysis, and reductions were made to factor in the lift contribution from the flaps. These were notably a C_L of 0.4 and 0.6 (as earlier mentioned) in the take-off and landing phases respectively such that only the intended wing lift contribution would be analysed within Tornado VLM. Upon simulation, the output spanwise lift distributions were analysed to identify the largest 2D lift coefficients for which the selected aerofoil must achieve within its lift-curve slope. These output requirements are presented within Table 16.

Table 16 Flight phases computed through Tornado VLM.

Flight Condition	M	Altitude (ft)	Total Lift Requirement	Input Wing C_L (No Flaps)	Required 2D C_L
Max. Range	0.18	12000	0.753	0.753	0.834
Take-off (Stall)	0.09	0	2.08	1.68	1.84
Landing (Stall)	0.08	0	2.30	1.70	1.86

Upon generating a range of 2D lift requirements, 8 aerofoils commonly associated with low speed aerodynamics applications, namely the NACA 2412, 2415, 23012, 23015, 23018, Marske-7, GA(W)-1 and GA(W)-2, were analysed using Xfoil at the 3 previously mentioned flight conditions in order to generate a series of lift-curve slopes. Using the plots presented by Figs 22-24 the aerofoils which could achieve the required 2D lift coefficients were then kept for a L/D optimisation study.

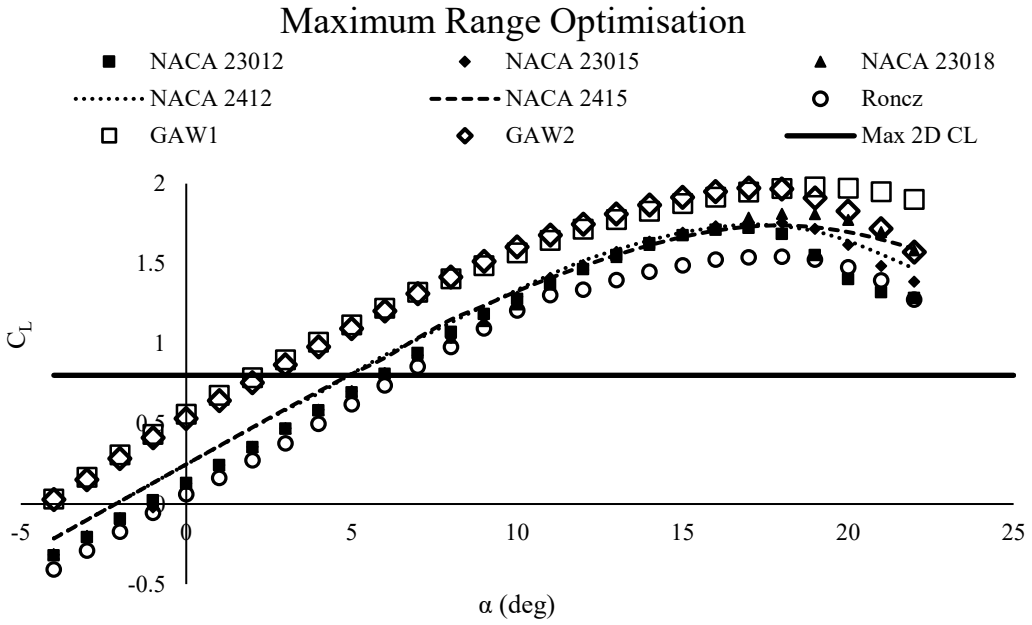

Fig. 22 Aerofoil lift-curve sloped for maximum range optimisation.

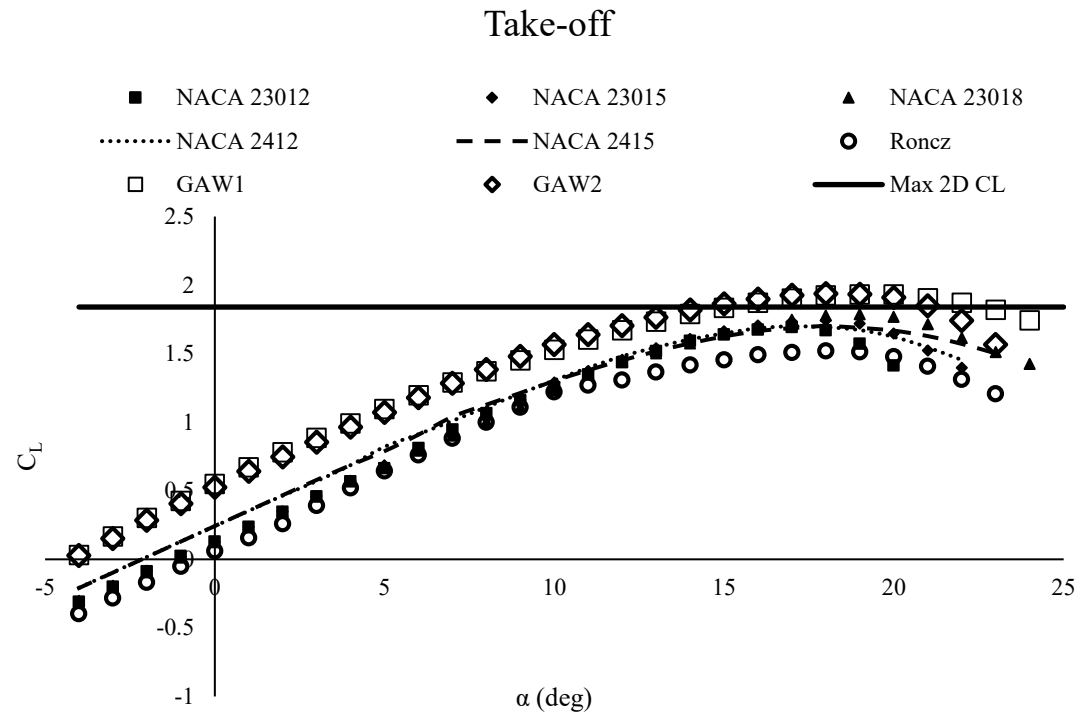

Fig. 23Aerofoil lift-curve slopes at take-off

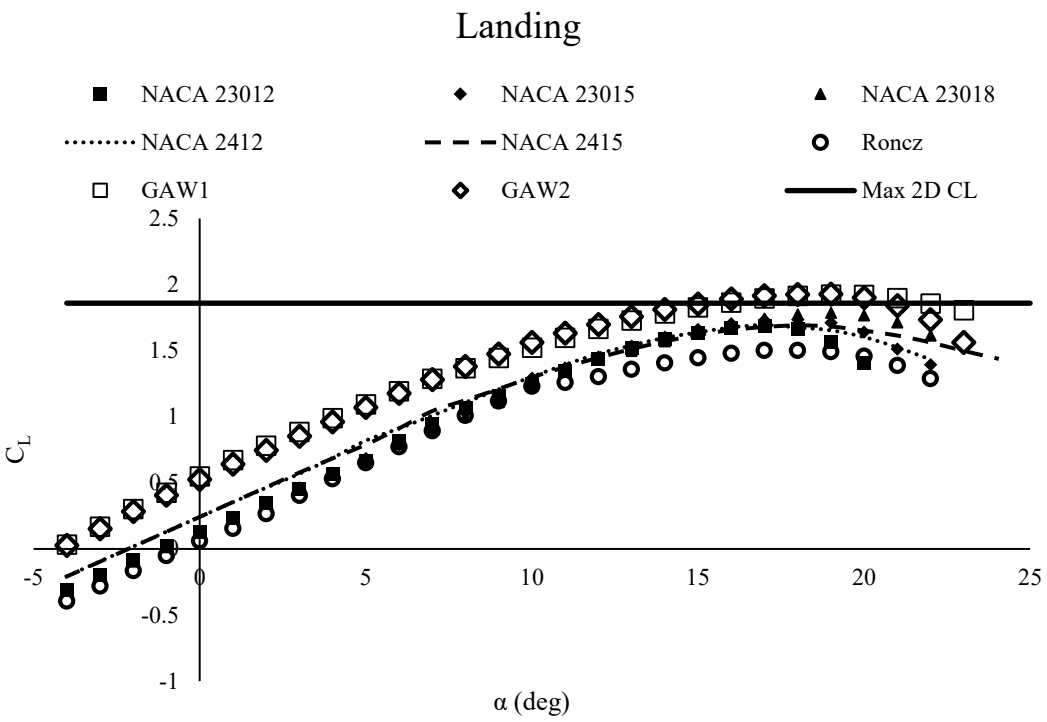

Fig. 24 Aerofoil lift-curve slopes at landing

Initial observations indicate that all aerofoils can accommodate the maximum range requirement. However, for the high lifting take-off and landing phase, the NACA aerofoils failed to facilitate the lifting requirement. Two aerofoils that performed well were the GA(W)-1 and GA(W)-2. They were able to achieve all 2D lifting requirements in excess of their maximum achievable lift coefficient before stall and were hence chosen for further refinement. In addition, the NACA 23018 was kept for further evaluation given this aerofoil could just about accommodate the lifting requirement. A study investigating L/D for the design take-off and cruise conditions (the landing phase was neglected since maximising lift is not beneficial for this flight condition) was then conducted to select a final aerofoil. Tornado VLM was further utilised to determine the largest 2D lift requirement for these design phases. Xfoil was then incorporated to output the required aerofoil incidence and its corresponding value of L/D at the Tornado VLM specified lift requirements.

Table 17 Lift to drag optimisation for design take-off and cruise phases.

Aerofoil	Take-off (design)		Cruise (design)	
	Incidence (deg)	L/D	Incidence (deg)	L/D
NACA 23018	14.9	100.46	3.27	78.05
GA(W)-1	11.4	83.03	-0.170	117.7
GA(W)-2	11.8	92.55	0.166	106.39

As demonstrated by Table 17, the NASA/Langley GA(W) aerofoils achieve superior drag performance in the design cruise phase despite being outperformed by the NACA 23018 during take-off. This is because the GA(W) series aerofoils have a large inherent thickness which can accommodate a given lift coefficient at a lower than average angle of incidence. In addition, the thickness lends itself to supporting the wing contained elements of the S270 aircraft through providing a large internal volume for fuel storage.

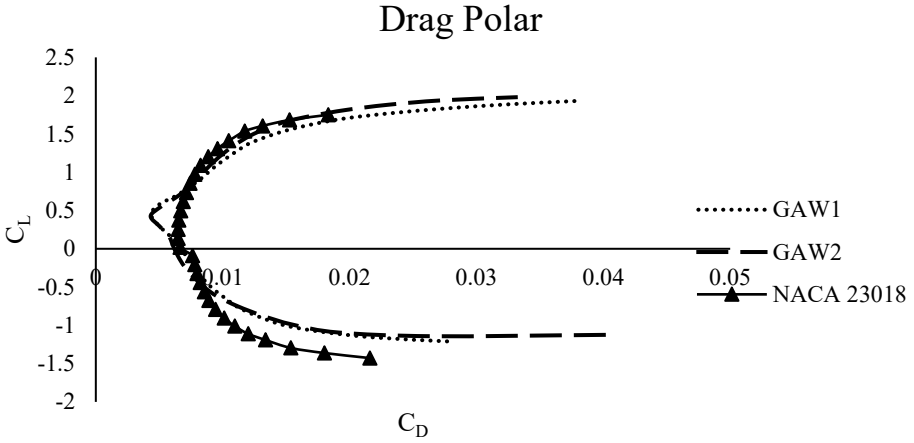

Fig. 25 Cruise drag polar for the 3 candidate aerofoils.

Further analysis considered the drag polar plots pertaining to the three aerofoils at cruise. As shown by Fig. 25, the GA(W) series aerofoils achieve vastly higher coefficients of lift at the cruise phase than those produced by the NACA 23018. In addition, the NACA 23018 produces a noticeably high $C_{Dmin,}$ when compared with both GA(W) series aerofoils. Consolidation of these outcomes result in the NASA/Langley LS(1)-0413 (GA(W)-2) being selected for all sections of the wing planform. This aerofoil offers a substantially high stall angle for all flight conditions accompanied by a high maximum lift. The maximum range condition is extensively satisfied as demonstrated by the lift requirement plot on the lift curve slope; an element of vast importance given the additional weight imposed by the propulsion system.

2.3.4. Drag Analysis

A method of calculating the aircraft drag coefficient is offered by Roskam [46] in combination with the works of Lan [47]. Equations (3) – (5) form an initial basis for determining the updated component drag values compared to those obtained in the Design Freeze Report [8].

$$C_D = C_{D0} + C_{Di} \tag{3}$$

$$C_{D0} = C_{D_{wing}} + C_{D_{fuselage}} + C_{D_{propeller}} + C_{D_{flaps}} + C_{D_{gear}} + C_{D_{windshield}} \tag{4}$$

$$C_{Di} = \frac{{C_L}^2}{\pi e AR} \tag{5}$$

Table 18 presents a breakdown of the component contribution to the total zero-lift drag coefficient including a percentage breakdown of the cruise drag.

Table 18 Component zero-lift drag contributions.

Component	Zero-Lift Drag Coefficient, CD0				% of Total (Cruise)
	Take-off	Cruise	Loiter	Landing	
Wing	0.00964	0.00816	0.00965	0.00984	32.1
Fuselage	0.00968	0.00830	0.00970	0.00986	32.7
Empennage	0.00254	0.00215	0.00253	0.00259	8.44
Propeller	0.00668	0.000603	0.00664	0.0105	2.37
Flaps	0.0153	0	0	0.0407	0
Landing Gear	0.00589	0.00589	0.00589	0.00589	23.2
Windshield	0.000311	0.00031	0.00031	0.00031	1.22
Total	0.0500	0.0254	0.0347	0.0797	100

2.3.5. Wing Drag Contribution

The zero-lift wing drag contribution is governed by Equation (6), and comprises elements assumed from the books written by Roskam and Lan [47], [48] such as the wing-fuselage interference factor, R_{wf}, and the lifting surface correction factor, R_{LS}.

$$C_{D_{wing}} = R_{w_f} R_{l_s} C_{f_w} \left\{1 + L'\left(t/c\right) + 100\left(t/c\right)^4\right\} \frac{S_{wet_w}}{S} \tag{6}$$

$R_{l_s} \approx 1.07$, $R_{w_f} = 1$ for Cruise, 1.06 for remaining mission phases.

$$C_{f_w} = \frac{0.455}{\left(\log_{10}[\![R_{N_w}]\!]\right)^{2.58}(1 + 0.144M^2)^{0.58}} \tag{7}$$

For the NASA/Langley LS(1)-0413 (GA(W)-2) aerofoil, the following parameters were used:

$\left(\frac{t}{c}\right)_{max} = 0.129$ at 0.375c. For $\left(\frac{t}{c}\right)_{max}$ locations ≥ 0.3c, $L' = 2$.

$S_{wet_w} = S_{exposed} \times k_w$, where $S_{exposed}$ = 12.58m^2 and $k = 1.9767 + 0.5333\left(\frac{t}{c}\right) = 2.045$ for $\left(\frac{t}{c}\right)_{max}$.05. S = 14.32m^2.

Table 19 Wing drag contribution.

Mission Phase	R_{Nw}	M	C_{fw}	$C_{D_{wing}}$
Take-off	2.95E+06	0.110	0.00367	0.00964
Cruise	5.39E +06	0.284	0.00330	0.00816
Loiter	2.92E +06	0.119	0.00368	0.00965
Landing	2.62E +06	0.0982	0.00375	0.00984

2.3.6. Fuselage Drag Contribution

The fuselage drag contribution is determined in the following development, outlined in [47]:

$$C_{D_{wing}} = R_{w_f} C_{f_f} \left\{ 1 + \frac{60}{\left(l_f / d_f\right)^3} + 0.0025 \left(l_f / d_f\right) \right\} \frac{S_{wet_f}}{S} \tag{8}$$

$$C_{f_f} = \frac{0.455}{\left(\log_{10} [\![R_{N_f}]\!]\right)^{2.58} (1 + 0.144M^2)^{0.58}} \tag{9}$$

$\left(l_f / d_f\right)$ = fuselage fineness ratio. As used through the Design Freeze Report [8], this value was estimated at 5 based on competitor assumptions. Having undergone extensive progress in the design of the S270, this value is now calculated using $l_f = 8.8m$ and $d_f = 1.7m$.

$\left(l_f / d_f\right) = 5.17 \cdot \frac{S_{wet_f}}{S}$ was initially estimated as 2 based on competitor assumptions. The newly developed S270 now exhibits $S_{wet_f} = 34.26$ and $S = 14.32$, thereby increasing the ratio to 2.39.

Table 20 Fuselage drag contribution.

Mission Phase	R_{Nf}	M	C_{ff}	$C_{D_{fuselage}}$
Take-off	2.26E+07	0.110	0.00264	0.00968
Cruise	4.14E+07	0.284	0.00240	0.00830
Loiter	2.24E+07	0.119	0.00264	0.00970
Landing	2.01E+07	0.0982	0.00269	0.00986

2.3.7. Empennage Drag Contribution

The empennage drag contribution models the V-Tail as a wing section and employs the same assumptions and methods from the wing drag contribution.

Table 21 V-Tail drag contribution.

Mission Phase	R_{NT}	M	C_{fT}	$C_{D_{Tail}}$
Take-off	2.21E+06	0.110	0.00387	0.00254
Cruise	4.04E +06	0.284	0.00346	0.00215
Loiter	2.19E +06	0.119	0.00385	0.00253
Landing	1.97E +06	0.0982	0.00395	0.00259

2.3.8. Propeller Drag Contribution

The S270 aircraft uses a fuselage contained engine and hence the consideration for nacelle and pylon drag is negated as any engine components are accounted for within the fuselage dimensions. The sole external geometry contributing to the drag as part of the engine is the wind-milling propeller. Equation (10) estimates the wind-milling propeller drag for the 4 key mission phases.

$$C_{D_{wmprop}} = \frac{33SHP_{rated}}{\bar{q}SU_1} \tag{10}$$

SHP_{rated}= maximum rated shaft horsepower of the engine for the required mission phase, $\bar{q}$= dynamic pressure, and U_1=steady state flight speed in ft/sec.

Table 22 Wind-milling propeller zero-lift drag.

Mission Phase	SHP_{rated}	U_1	$\bar{q}$	$C_{D_{wmprop}}$
Take-off	304.8	123.21	863.81	0.00668
Cruise	289.66	303.81	3641.85	0.000603
Loiter	339.28	109.53	682.67	0.00664
Landing	339.28	131.23	896.95	0.0105

2.3.9. Flap Drag Contribution

The flap zero-lift drag coefficient was calculated through adoption of Equation (11) provided by Roskam[47]

$$C_{D_{wing}} \approx 0.0023\left(\frac{flap\ span}{wing\ span}\right) \times \delta_{flap} \tag{11}$$

Flap span = 3.65m, wing span = 12.38m, δ_{flap} = flap deflection in degrees, which varies for the different flight phases.

Table 23 Flap drag contribution.

Mission Phase	δ_{flap} (deg)	$C_{D_{flaps}}$
Take-off	22.5	0.00153
Cruise	0	0
Loiter	0	0
Landing	60	0.0407

2.3.10. Landing Gear Drag Contribution

Fig. 26 Candidate landing gear geometries; with and without aerodynamic fairing.

The landing gear drag comprises assumptions made available within the works of Roskam [48] in conjunction with the conclusions made of the HT-Series [49] aircraft which provides a retractable landing gear estimate of 0.0122. However, considerations are made for a fixed landing gear with the implementation of fairings, which predictably permit 50% reduction in profile drag for a given gear configuration as described by Roskam. To validate this drag saving, simulations within Star CCM+ were undertaken on the nose gear with and without fairings. Figure 26 above presents the two candidate geometries.

To generate the solution grid, a meshing limit of 3,000,000 cells was set in order to limit the computational cost of the simulations. Volume refinement was focused within wake regions of the flow domain with complimenting surface controls offering local refinement to the landing gear geometries. The final flow domain is given by Fig. 27.

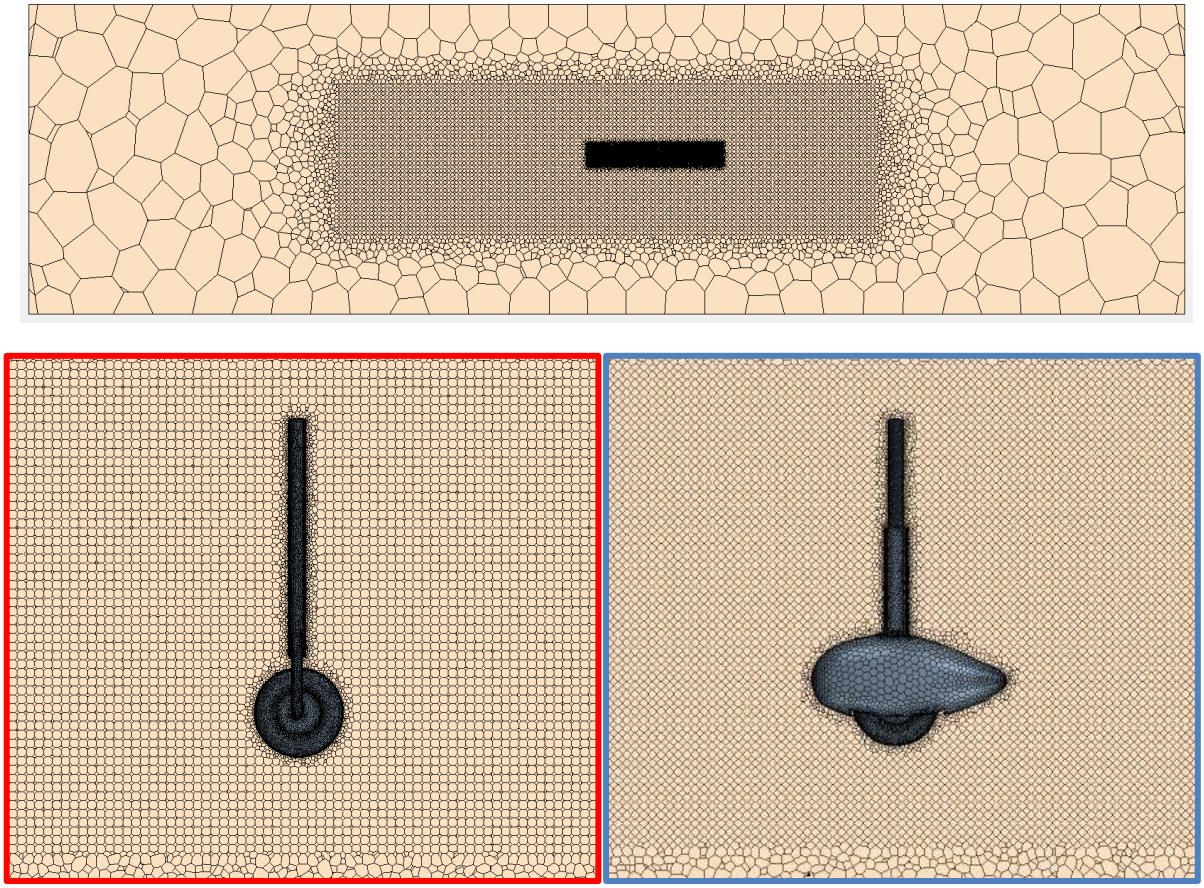

Fig. 27 Top: Global mesh. Bottom left: Landing gear mesh, no fairing. Bottom right: Landing gear mesh, with fairing.

The K-Epsilon turbulence model was implemented due to its stability performance and competence in resolving conventional flows [50]. A complete list of solver properties is given by Table 24.

Table 24 Solver properties.

Category	Selection
Space	Three Dimensional
Time	Steady
Material	Gas
Flow	Coupled Flow
Equation of State	Ideal Gas
Viscous Regime	Turbulent
Reynolds-Average Turbulence	K-Epsilon Turbulence

Two avenues of evaluation were navigated to assess the drag saving through utilisation of the fairing. Firstly, the drag coefficients, presented in Table 25, are compared. As previously stated, the predicted drag saving postulated by Roskam and Lan [47] stands at approximately 50%. As previously stated, the predicted drag saving postulated by Roskam and Lan [47] stands at approximately 50%. Whilst the fairing simulation demonstrates sound compatibility with the value predicted by the research, a larger drag saving of 66% is identified stemming from the larger simulated drag for the gear without fairing.

Table 25 Drag characteristics.

C_{D0}	Without Fairing	With Fairing	Drag Reduction (%)
Predicted	0.0122	0.00610	50
CFD	0.0174	0.00589	66

Supporting evidence for the drag saving is offered by flow visualisation. Presented by Fig. 28-29 is a scalar comparison of the velocity field acting through the domain. It is shown that for the gear without fairing, a larger wake is generated, indicated by the blue regions of stagnant, detached flow. The more streamlined geometry promotes reduced probability of flow detachment, thus reducing the effects of pressure drag and hence will be implemented on the final aircraft design.

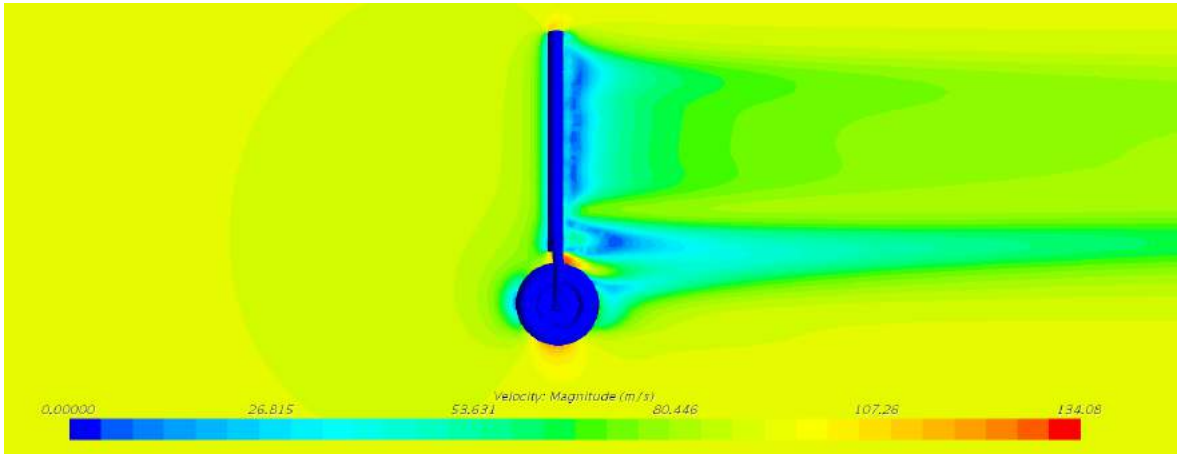

Fig. 28 Landing gear (without fairing) velocity magnitude scalar scene.

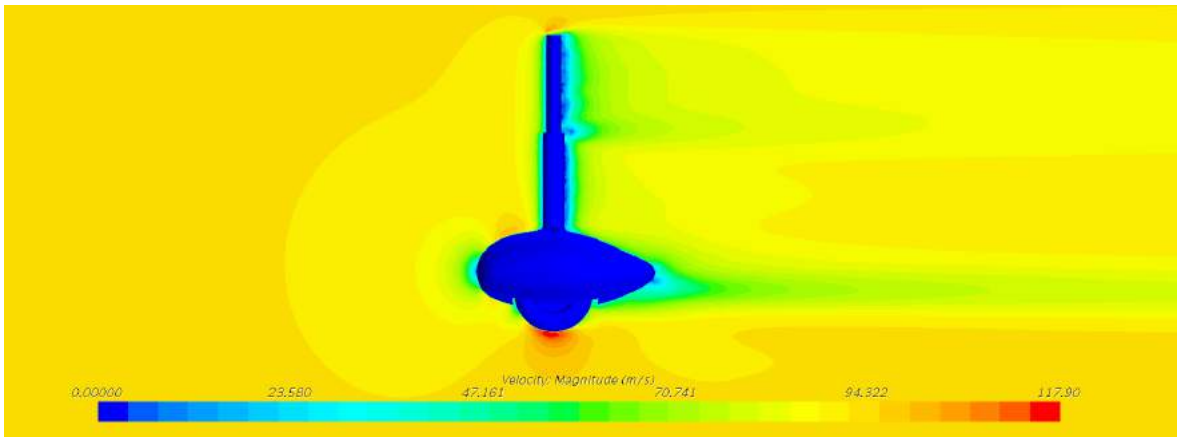

Fig. 29 Landing gear (with fairing) velocity magnitude scalar scene.

$C_{D_{gear}}$ **= 0.00589** for all mission phases.

2.3.11. Windshield Drag Contribution

$$C_{D_{windshield}} = \left(\Delta C_{D_{windshield}}\right)\frac{S_{fuselage}}{S} \tag{12}$$

$\Delta C_{D_{windshield}}$ = incremental drag coefficient due to windshield, which, for single curvature window, flush with surface = 0.002

$S_{fuselage}$ = frontal area of fuselage = 2.23m^2

$C_{D_{windshield}} = 0.000311$ for all mission phases.

2.3.12. Induced Drag Contribution

Equation (5) for each mission phase was utilised in computing the induced drag[47].

e = Oswald's efficiency factor = $1.78(1 - 0.045AR^{0.68}) - 0.64$ for straight/moderately swept wing at transonic flight conditions.

AR = 10.7, e = $1.78(1 - 0.045 \times 10.7^{0.68}) - 0.64$ = **0.739**.

Table 26 Induced drag breakdown.

Mission Phase	C_L	C_{Di}
Take-off	1.33	0.0714
Cruise	0.316	0.00402
Loiter	1.33	0.0708
Landing	1.71	0.118

2.4. Performance

This section of the report focuses on the performances of the S270. The section will first talk about the designed airspeeds and characteristic speeds that follows the FAA Part 14 CFR 23 requirements. A normal operating flight profile with a range of 135 nautical miles will be presented. A more in-depth performance analysis of different flight phases where shown in the following sections. A performance analysis on extended range mission of 250 nm is presented in the end of this section.

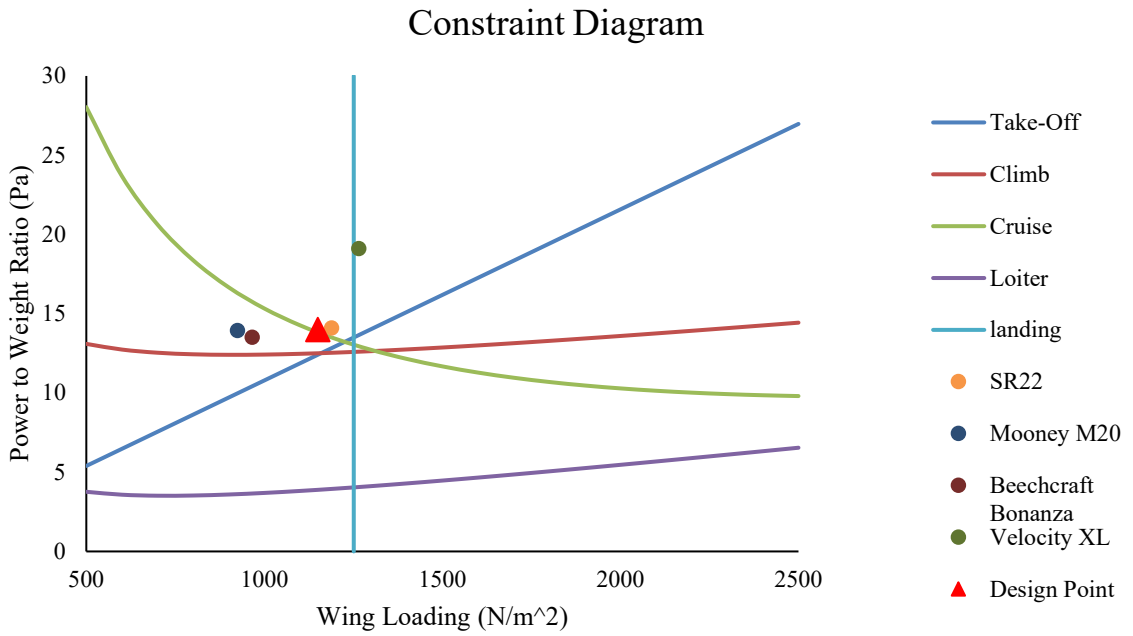

Fig. 30 Constraint Diagram

The following section reveals the aircraft performance and normal mission design based on the constraint diagram shown in Fig. 30 in order to meet the needs of the requirements.

2.4.1. Characteristic Speeds

According to the FAA Part 14 CFR 23 requirements, several characteristic speeds are required to meet the regulations as a design requirement. A list of definitions of FAA Part 14 CFR 23 characteristic speeds are shown in Table 27.

Table 27 Characteristic speeds.

V Speeds	FAA Requirement [51]	Value for S270 (m/s)
Stall Speed (Flaps Extended)	Part 23.49: V_{so} cannot exceed 61 knots (31m/s) for single engine aircraft	28
Manoeuvre Speed	Minimum operating manoeuvring speed is limited to a maximum of $\boldsymbol{V_{s1}\sqrt{n_1}}$ (72.6 m/s)	80
Cruise Speed	The minimum cruising speed cannot be less than $\mathbf{33}\sqrt{\frac{WS}{g}}$ (82.8 m/s)	92.6
Design Dive Speed	Design dive speed cannot be less than 1.4 of V_{cmin} (115.92 m/s)	116
Never Exceed Speed	The never exceed speed should be greater than 0.9 of the minimum requirement of design dive speed.	128

The flight envelope of the aircraft at normal mission and a gust envelope with gust speeds of 7.5, 15.25 and 20 m/s is shown in the figure below.

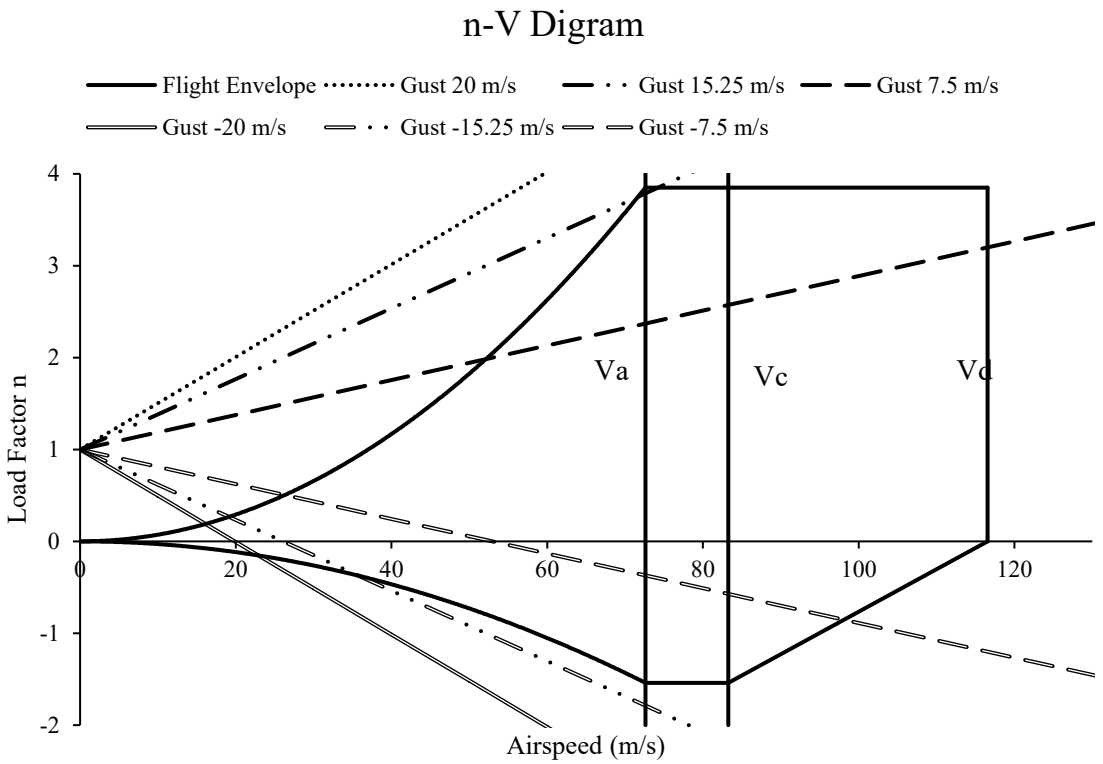

Fig. 31 Flight and Gust Envelope

2.4.2. Flight Profile

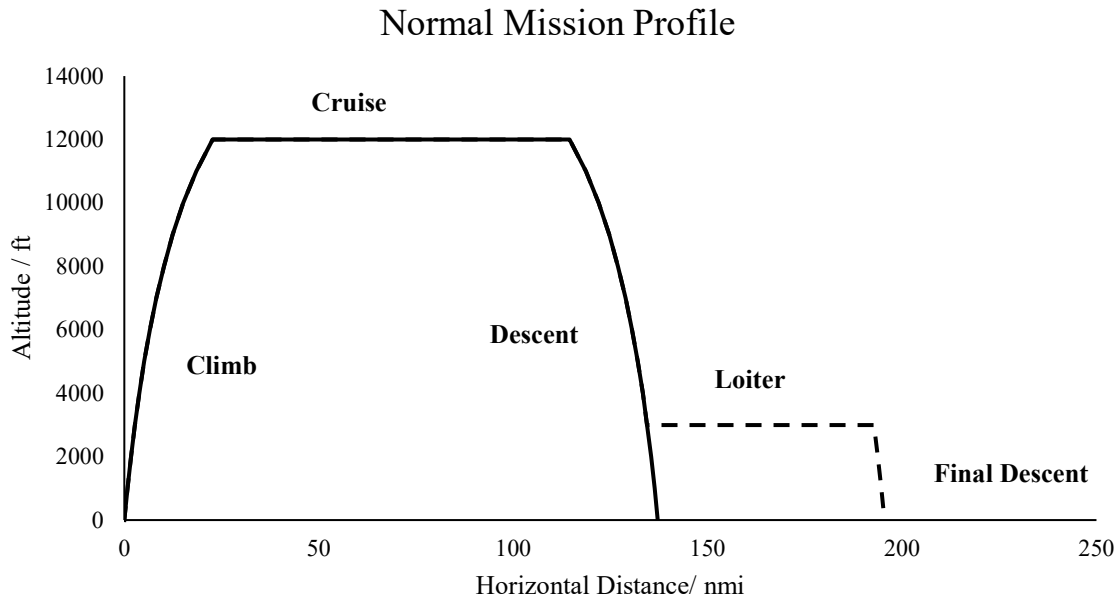

Fig. 32 Flight Profile of Normal Mission

A graph of the flight profile of the normal mission of the S270 is shown in the Fig. 32. The normal mission of the S270 aims to complete a flight of a range of 135 nautical miles in 65 minutes time. This includes time in taxiing in both the destination and the port of departure as well as warming up the engine. The time of different phases of the normal mission profile is shown in the table below.

Table 28. Flight time for normal mission.

Flight Phase	Cumulative Time (min)	Cumulative Distance (nmi)
Taxi and warm up	7.5	0
Take off and Climb	22.5	23
Cruise	47.5	113
Descent	55.5	133
Final Descent and Landing	57.5	135
Taxi and Parking	65	135
Loiter	100.5	191
Final Descent and Landing (with loiter)	102.5	193
Taxi and Parking (with loiter)	110	193

The initial requirement states that the taxi and warm up time should be completed in 10 minutes during the start and end of the mission while the total airborne time of the aircraft should be less than 45 minutes. The initial mission sizing indicates that to meet total mission with 10 minutes taxi, it requires significant increase in cruise speed as well as battery and propellant mass, as compared to

the case with the extra time airborne and reduced time on ground. The decision was therefore made to decrease the taxi and warm up time by 2.5 minutes during the start and end of mission. This is regarded as feasible solution as the airports and airfields being used in the system are meant to be small air fields, meaning that the taxi and warm up time can be reduced as the waiting time for take-off as well as the taxi time from apron to the runway is insignificant. The warm up time of the engine is also significantly reduced due to the electric propulsion contributed in the hybrid system.

2.4.3. Take-off Performance

The S270 is set to take-off at full throttle with a continuous output power of 230kW. The take-off ground roll distance is relatively short compared to the main competitor, the Cirrus SR22, in normal operations. The design velocity of lift off is set to be 37 m/s whereas the maximum lift coefficient in take-off is 1.9, hence giving a stall speed of 32 m/s in take-off conditions. The take-off performance with various lift off speeds at sea level conditions and maximum take-off weight is shown in Fig. 33.

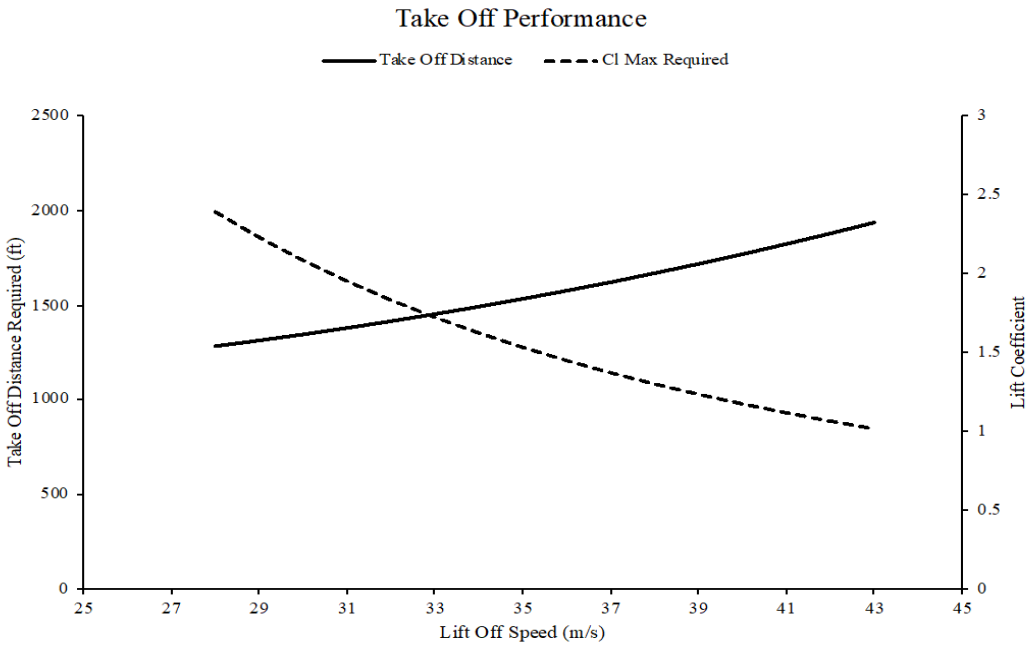

Fig. 33 Take-off performance

With the designed lift off speed to be set at 37 m/s, a detailed take off performance of normal mission can be shown in Table 29.

Table 29 Take-off performance of the S270 aircraft at sea level conditions.

Parameter	Value
Power Output	230 kW
Degree of Electric Propulsion	90%
Lift Off Speed	37 m/s
Stall Speed	32.2 m/s
Friction Coefficient [52]	0.02
Take-Off Distance (Ground Roll) (ft)	522
Take-Off Distance (50 ft Obstacle) (ft)	1619

2.4.4. Climb Performance

The S270 takes off at the maximum continuous output power of the hybrid engine at 230 kW and continues to produce the same amount of output power until the top of climb. The acceleration of airspeed is affected by the angle of attack of the aircraft as well as the climb gradient, therefore the airspeed of the climb was assumed to increase linearly from V_2 to the cruising speed in normal flight mission. The climb gradient of the normal climb phase is shown in Fig. 34.

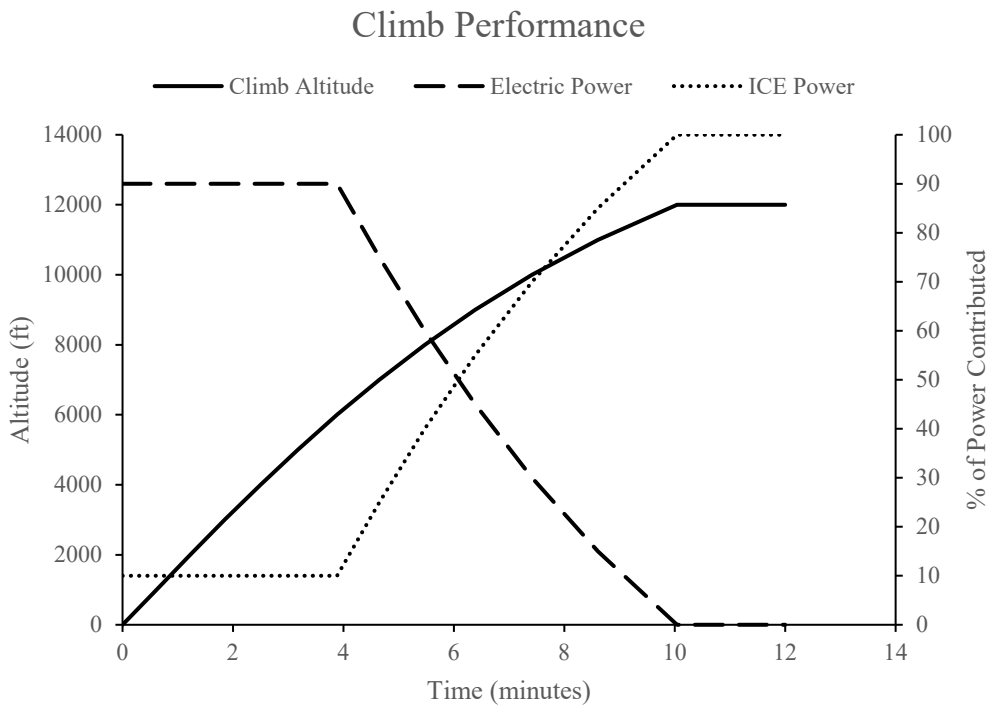

Fig. 34 Climb Performance and Engine Power Distribution

As shown in Fig. 34, the climb gradient of the flattens at the top of climb during normal mission. In the first four minutes of the climb, the internal combustion engine is put into idle as it is easier to warm up the engine at sea level. During the later parts of the climb, the internal combustion energy power contribution increases until the electric motor is being turned off at cruise. The maximum

contribution of the electric motor in climb was determined by varying the motor contribution until an optimal battery mass vs fuel burn point was reached. The maximum motor contribution in climb was determined to be 232.6 kW, which is 90% of total power required.

2.4.5. Approach and Landing Performance

The landing requirement of the S270 is to be able to completely stop within 2500 ft while clearing an obstacle of 50 ft height at the start of the approach. The total landing distance required is separated into three phases, the approach distance, the flare distance and the ground roll distance. The velocities of each of these phases are also set based on the stall speed of the aircraft. The speed at start of the approach, flare and ground roll is 1.3, 1.23 and 1.15 times of the stall speed of the aircraft [52].

A comparison of different design approach speeds has been carried out to find the suitable design approach performance regarding the maximum lift coefficient with flaps extended and the landing distance required. Landing performances of S270 in various touchdown speeds is shown in Fig. 35.

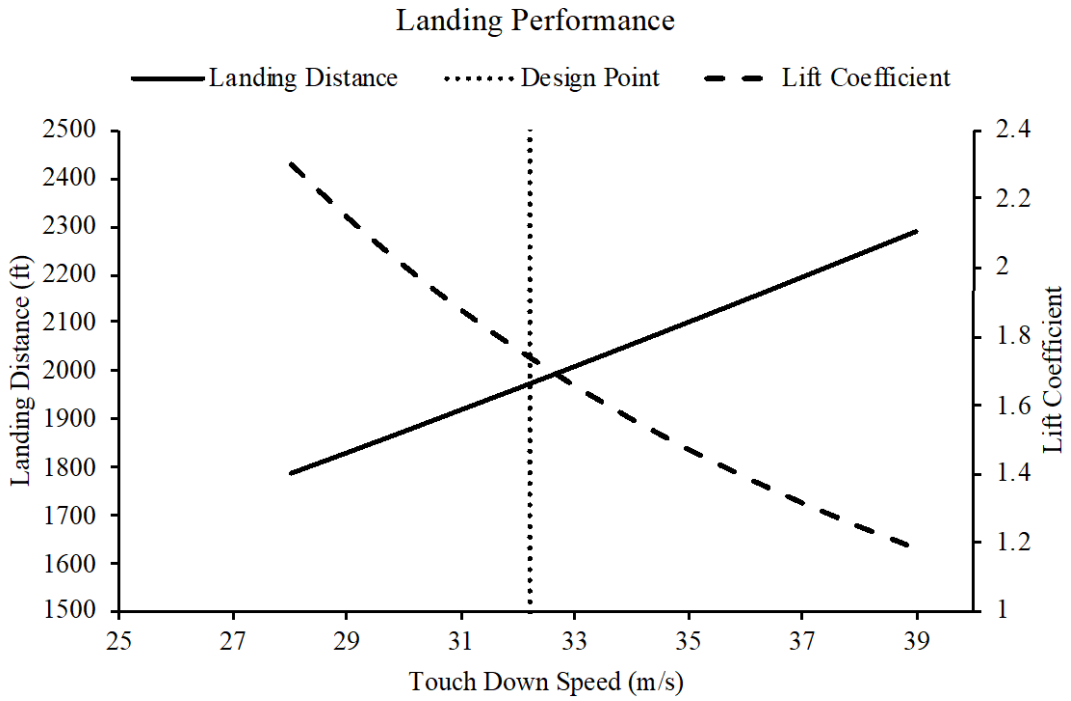

Fig. 35 Landing distance and touch down speed.

As proposed by Roskam [53], the maximum lift coefficient during landing for a single propeller driven engine set between 1.6 to 2.3. Hence, despite the short landing distances, touch down speeds below 32 m/s are considered to be unfavourable as the lift coefficient required are too high. The finalized landing and approach profile at sea level is shown in the Table 30 below.

Table 30 Approach and landing profile.

	Dry Conditions	Wet Conditions
Touch Down Speed (m/s)	32.2	32.2
Friction Coefficient [52]	0.5	0.3
Lift Coefficient at Stall	2.2968	2.2968
Stall Speed (m/s)	28	28
Landing Distance (50 ft Obstacle) (ft)	1974	2343
Landing Distance (Ground Roll) (ft)	912	1281

2.4.6. Turn Performance

In Fig. 36, the instantaneous turn performance of S270 regarding to the load factor and the turn radius is shown. The design maneuverer speed of S270 is set as 80 m/s as mentioned in Section 2.4.1. The flight envelope allows a load factor between -1.9 to 3.85 as shown in Section 2.4.1, hence S270 can achieve a turn radius of only 200 m without posing any potential structural damage. Fig. 37 also shows the lift coefficient with the relative turn performance at 30 degrees bank angle. The maximum lift coefficient of the aerofoil used in S270 can provide a lift coefficient of 1.974 at cruise conditions, hence it is suggested that a minimum turn radius of 400 m is required at cruise condition at the design maneuverer speed to prevent the aircraft from stalling.

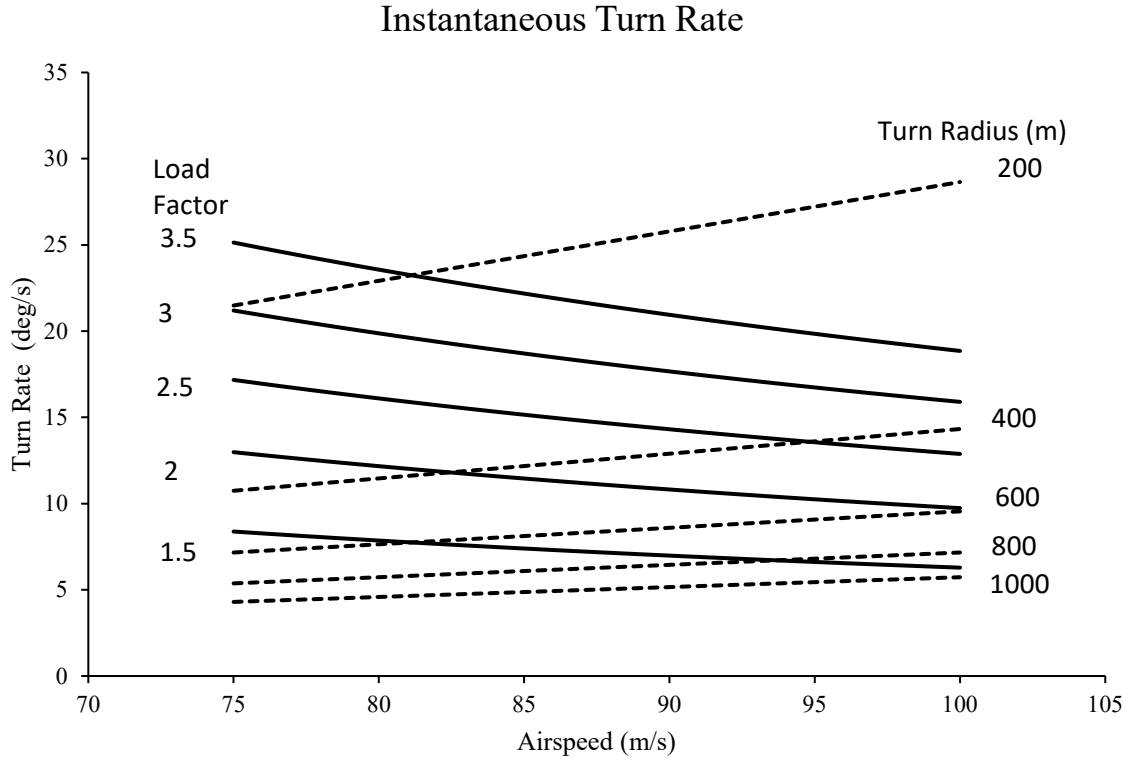

Fig. 36 Instantaneous Turn Performance

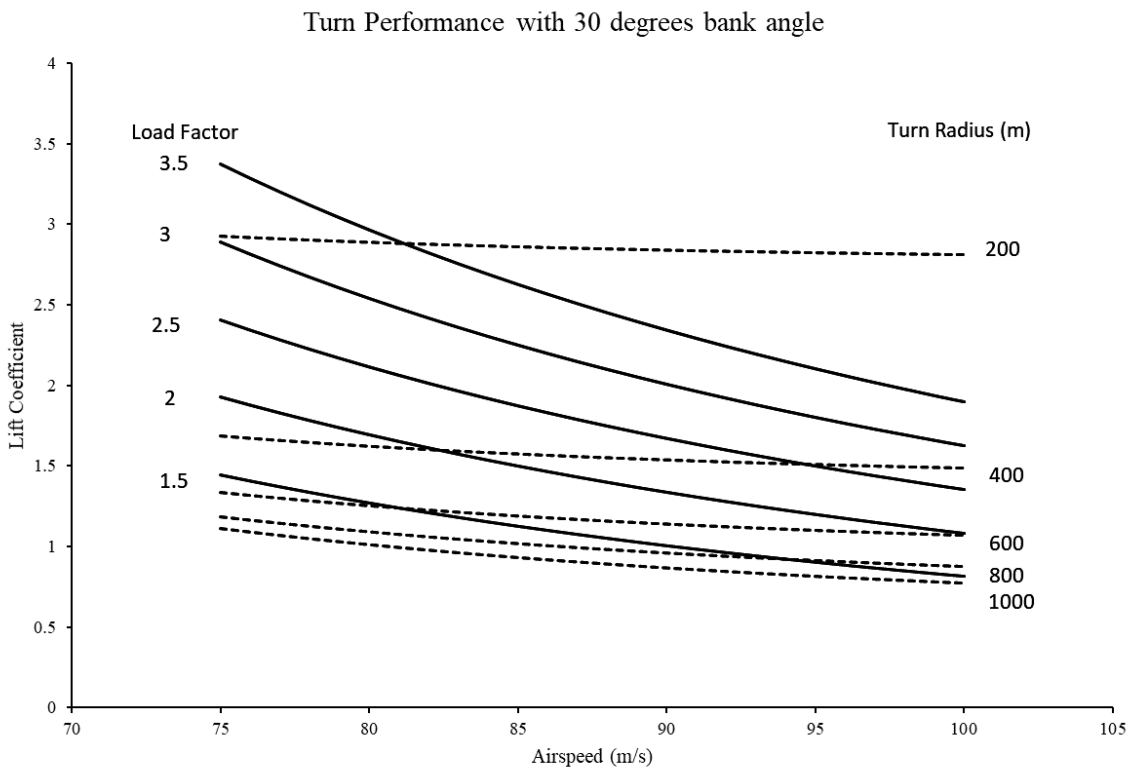

Fig. 37 Turn performance with 30 degrees bank angle.

2.4.7. Range and Fuel Consumption

The normal mission range of the aircraft is 135 nautical miles. According to the specific fuel consumption of the engine described in Section 2.6.6, the specific fuel consumption of the engine is 0.25 kg/kW/hr. The aircraft cruises at 180 knots at a continuous output power of 132 kW at 12000 feet.

Taking in to account the specific fuel consumption and the propulsive efficiencies, the fuel burn for a normal mission of S270 is 47.4 kg/hr. Since the cruising time for the normal mission is set to be 30 minutes, the fuel required in normal cruising mission is 24 kg.

To achieve maximum range, the speed of the aircraft is selected such that the lift to drag ratio is optimised. Fig. 38 shows the lift to drag ratio as well as the power required for the relevant airspeed. The solid line which represents the lift to drag ratio peaks at around 60m/s. After further iteration the speed for maximum range is set to be 60 m/s for the S270 at cruising altitude. At 60 m/s the S270 is able to fly for a range of 482 km (260 nautical miles) with a fuel requirement of 35kg at 12000 ft with the whole cruising phase taking around 2 hours and 15 minutes.

To achieve maximum cruising time, the speed of the aircraft is selected such that the power required for cruising at the equivalent airspeed is at the minimal. Using Fig. 38, the dotted line represents the power to velocity graph and the line is at minimal at around 42 m/s. The maximum endurance

velocity is set to be at 45 m/s after iterations with a total cruising time of 2 hours and 33 minutes while burning 35 kg of fuel and cruising for a distance of 414 km.

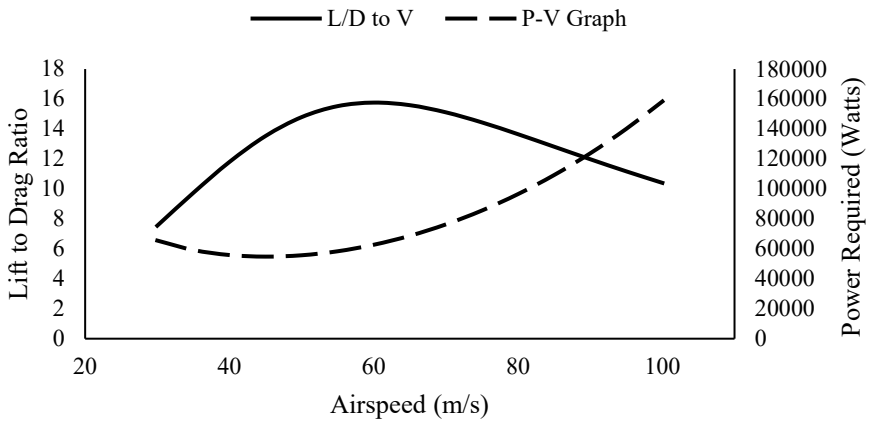

Fig. 38 Airspeed performance graph.

Since the majority of the payload of the aircraft is mainly batteries, the aircraft payload remains unchanged unless there is a reduction in battery mass, hence decrease use in hybridisation. The payload diagram below shows the aircraft range at cruise conditions.

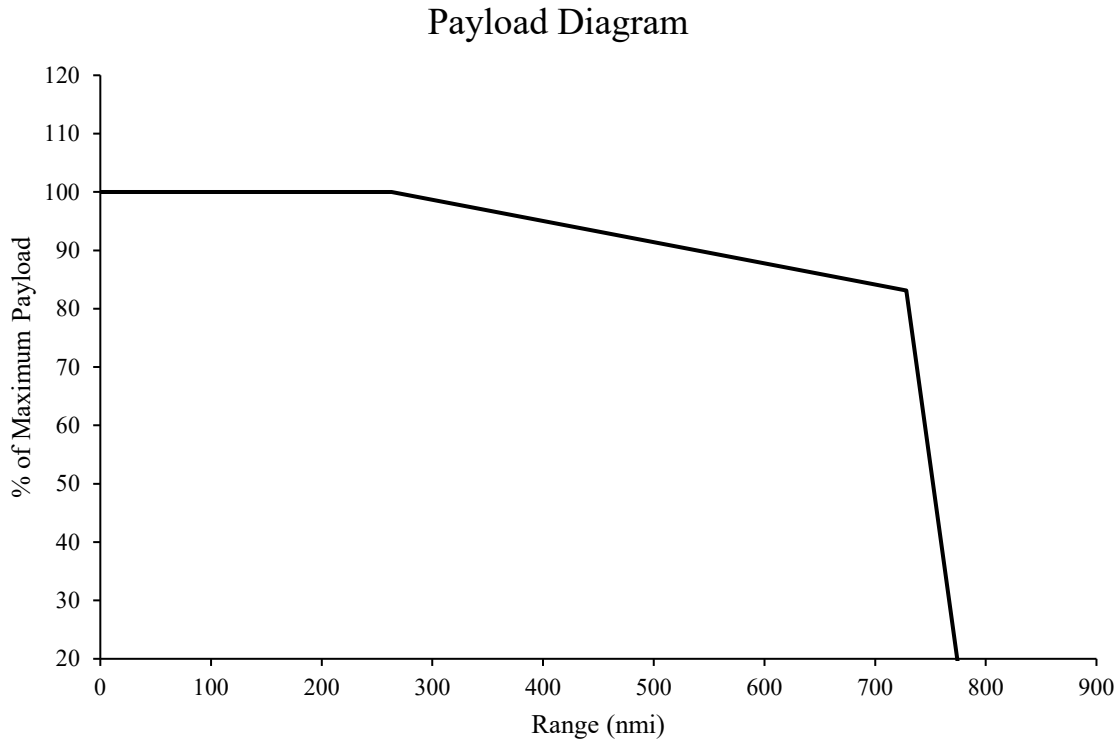

Fig. 39 Payload diagram.

With the high efficiency hybrid propulsion system of S270, the range increases significantly with the increase of fuel mass as shown in the figure above. A detailed mass breakdown of the payload limits are summarized in Table 31.

Table 31 Range and payload performance.

Total Mass (kg)	Fuel Mass (kg)	Payload (kg)	Range (nm)	Flight Time (hr)
1679	75	445	263	1.2
1679	150	370	728	3.8
1230	150	75	776	4.1

2.4.8. Performance Summary

The S270 aims to provide a better performance than other major general aviation aircraft. The table below compares the performance of the S270 to Cirrus SR22, a major competitor in the industry.

Table 32 Performance comparison

	Skyride S270	Cirrus SR22[54][55]
Cruise Speed (knots)	180	170
Maximum Range (nmi)	750	1100
Maximum Take-off Weight (kg)	1679	1545
Never Exceed Speed	116.6	102
Take off Distance (50 ft Obstacle) (ft)	1619	1868
Landing Distance (50 ft Obstacle) (ft)	1974	2343
Fuel Consumption at 75% power (kg/hr)	47.4	48.6
Time to Climb to 10000 ft (min)	7.4	11

2.5. Stability and Control

The V-Tail configuration design of the S270 was based on the need for a new, innovative design as well as one which could contribute to the efficiency of the aircraft. There are multiple benefits to this design when compared to a conventional tail. One of the more significant differences comes from the reduction in parasitic drag due to the reduced number of tail and fuselage junctures[56]. It is important for the drag to be decreased during the cruise phase of the flight to minimise fuel consumption, particularly since this phase is powered by the ICE.

There are several complications associated with this configuration, such as aerodynamic coupling between roll and yaw moments and the increased stresses on the tail surfaces. However, this configuration is common to new aircraft as it is not only aesthetically pleasing, but also has reduced weight due to a reduction in required control devices. By only having two effective tail surfaces,

'ruddervators'[56] are used as a combined rudder and elevator. As a result, only two actuators are required accompanied by a mixer device. This allows the commands to be converted as necessary based on pilot input (yaw/pitch). Another benefit arises from the reduced time to manufacture due to fewer surfaces. This would be beneficial to Project SkyRide, especially during the aircrafts infancy where production will need to be enough to meet demand.

Table 33 Preliminary V-Tail dimensions.

Parameter	Value	Parameter	Value
Area (m^2)	3.45	Root Chord (m)	0.877
Dihedral Angle (deg)	33.4	Tip Chord (m)	0.526
Taper Ratio	0.6	MAC (m)	0.704

Preliminary designs calculations were performed to estimate the tail size. This was achieved by converting the tail surface[57] area of the Cirrus SR22 to the V-Tail configuration of the S270. The dihedral angle was verified by the Beechcraft Bonanza, which has an approximate angle of 35 degrees. These were to be tested by means of stability assessment so that final values for the area size and tail moment arm could be determined.

2.5.1. Preliminary Tail Design Assessment

Initially, the longitudinal performance was assessed by analysing the change in performance when varying tail area, tail moment arm and dihedral angle. These parameters must be balanced appropriately to avoid weight penalties and negative impact on lateral stability.

The dimensions for the SR22 were used as a reference as it is the main competitor. Therefore, the aerodynamic performance of the SR22 is ideal as a basis for comparison. Initial calculations were performed at cruise (max. range) conditions for the S270; 12,000 ft, M = 0.18 (60 m/s) and a CL of 0.753.

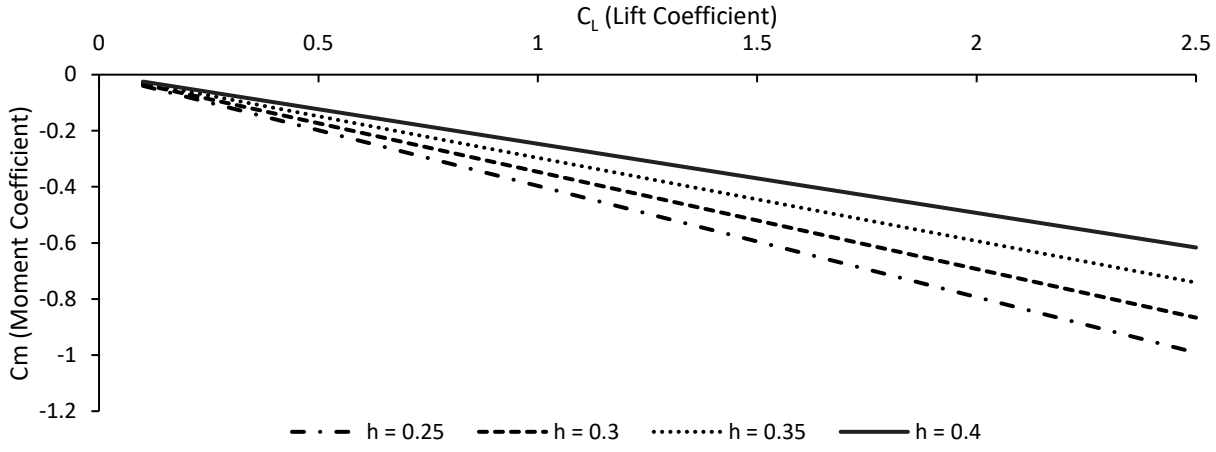

Fig. 40 SR22 (Cm VS CL)

As shown by Fig. 40, the SR22 maintains a negative $\frac{dCm}{dCl_w}$ for a large range of C_L's, with an aft limit of 0.625 of the MAC. The values achieved at h = 0.25 were used, as this coincides with the aerodynamic center for most airfoils. Another benefit of using this value is the additional stability provided by the natural nose down pitch caused by loading closer to the nose. As the batteries are located at the rear of the aircraft, the aft limit for the S270 would need to be generally further back to maintain a stable condition as the aircraft will be at full capacity. To begin, an analysis was done varying the tail area with dihedral angle to assess the stability. The following values were used;

Table 34 Preliminary tail parameters.

Parameter	Value	Parameter	Value
Mass (kg)	1678.5	Tail efficiency (η_t)	0.97
Wing Area, S_w (m^2)	14.32	Cruise C_L (max. range speed)	0.753
Tail Area, S_t (m^2)	3.45	Wing Lift-Curve Slope (a)	6.14
Tail Moment Arm, l_t (m)	4.5	Tail Lift-Curve Slope (a_{1t})	6.43
Wing AR	10.7	Downwash Gradient ($\frac{d\varepsilon}{d\alpha}$)	0.3653
Wing MAC, $\bar{\bar{c}}$ (m)	1.146	Pitch Moment of Inertia (Iy)	13,254

Downwash gradient was found using an assumption of an elliptic wing distribution;

$$\frac{d\varepsilon}{d\alpha} = \frac{2 \times a}{\pi AR} = \frac{2 \times 6.14}{\pi \times 10.7} = 0.3653 \tag{13}$$

This value is likely to be greater than the actual value, as the S270 employs a tapered wing with twist, therefore the induced downwash would be reduced towards the outboard section. To counter this, the tail plane efficiency is assumed to be very high at 0.97.

For the V-Tail configuration, the dihedral angle is a major contributor to the stability. Small angles contribute positively to longitudinal stability and generally have a stabilizing effect. As the angle is increased, the aircraft becomes more unstable. The tail volume coefficient, V_H for a V-Tail varies according to the square of the cosine of dihedral angle[58];

$$V_H = \frac{S_t \times l_t \times cos^2\,\Gamma}{S_w \times \bar{\bar{c}}} \tag{14}$$

An additional assumption made was that the tail plane lift curve slope was reduced by a factor related to the dihedral angle. The following values represented in Table 35 were used for the respective angles;

Table 35 Varied lift-curve slope with dihedal angle.

Dihedral Angle	Tail Lift-Curve Slope	Dihedral Angle	Tail Lift-Curve Slope
30	5.75	35	5.27
40	4.93	45	4.55
50	4.13		

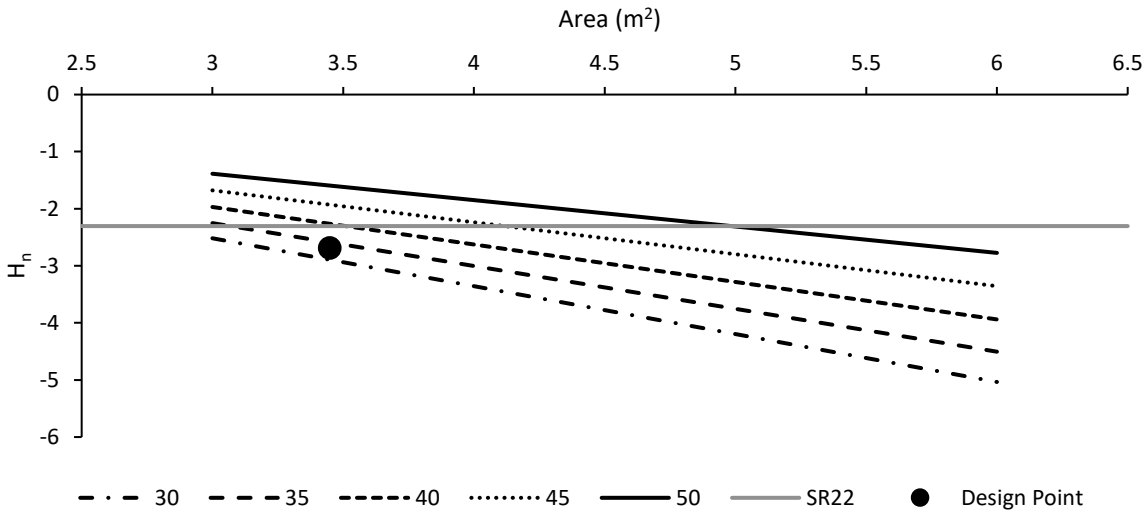

Fig. 41 Varying Tail Area

Figure 41 presents a destabilizing effect of the dihedral angle. This is represented by the shifting effects of lines towards the unstable positive Hn region due to the use of larger angles. The SR22 was determined to have a Hn value of -2.304. As the COG location is moved back, this value becomes increasingly positive. Due to this, it is more desirable to have a steeper negative gradient allowing greater loading to be placed further back. A careful balance must be maintained as this can result in an overly stable aircraft increasing control surface stresses and pilot workload[59].

The design point value of 3.45m^2 at 33.4^o dihedral sits below the SR22 which shows good stability. Though values with a greater area would be more tolerant to aft loading, they come with an increase in weight. These calculations were performed with a tail moment arm of 4.5m; the effect of altering this value was also assessed.

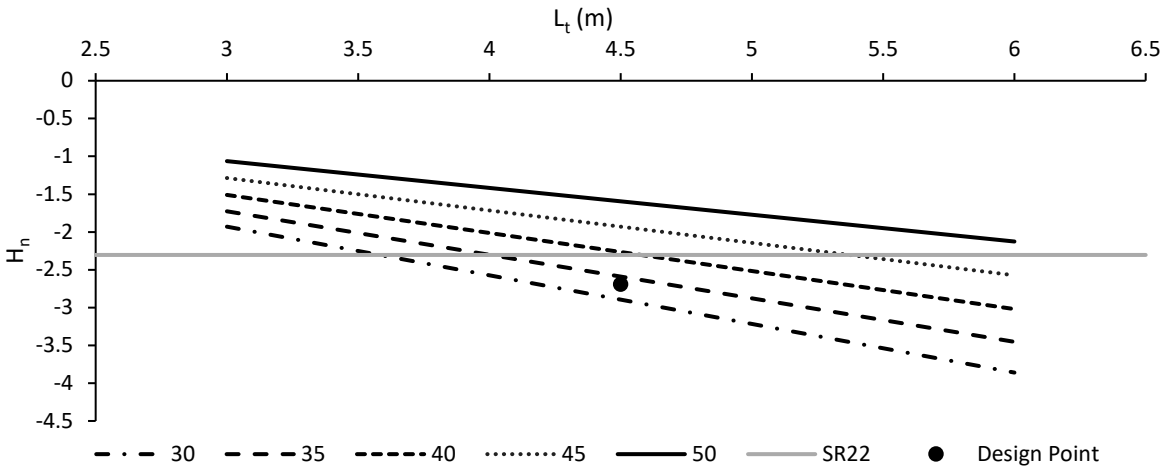

Fig. 42 Varying tail moment arm.

From Figure 42, increasing the tail moment arm is also seen to have a positive effect on the stability. As before, the preliminary design is within the stable region below the SR22. Greater dihedral angles as well as smaller moment arms result in a destabilising effect.

2.5.2. Design Optimisation

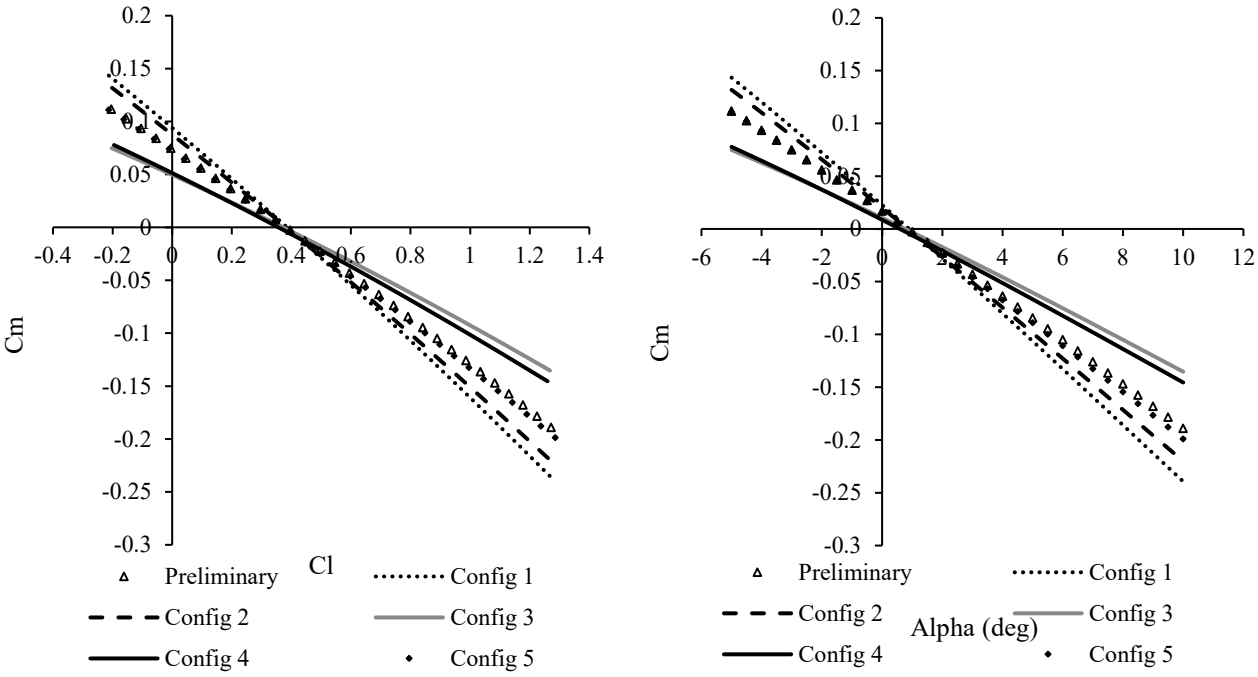

Fig. 43 Pitching moment coefficient (left: with respect to C_L, right: with respect to alpha).

Table 36 Parameters for configuration comparison.

Configuration	St (m^2)	Lt (m)	Dihedral (deg)
Preliminary	3.45	4.5	33.4
1	4	4.5	35
2	3.45	5	35
3	3.45	4	35
4	3.45	4.5	40
5	4.5	4	40

The next step was to assess the performance of a range of configurations and then optimise the preliminary design using XLFR5; this software uses a Vortex Lattice Method and a constant lift condition where the speed is adjusted to maintain flight. The CoG (h) was fixed at $0.565\bar{c}$ for all configurations. This fixed value resulted in a damping ratio of greater than 0.5 for the preliminary design which satisfies the minimum requirement for Level 1 flying characteristics[33].

With a fixed CoG, the effect of each alteration is clear to see in Fig. 43. Config. 1 features a larger tail area and has the strongest gradient $\frac{dC_m}{d\alpha}$ = -1.467 rad^{-1} which implies it is the most stable. This is closely matched by Config. 2 which also features a stabilising characteristic with an increased moment arm. Of these two, it is more desirable to have a greater tail area as increased fuselage length results in far more structural mass. Furthermore, an increase in tail area can also contribute to lateral stability. Reducing the moment arm (Config. 3) and increasing the dihedral angle (Config. 4) both show a destabilising effect with reduced gradients around $\frac{dC_m}{d\alpha}$ = -0.802 rad^{-1}. The preliminary design and Config. 5 are very closely matched, both achieving a gradient around $\frac{dC_m}{d\alpha}$ = -1.203 rad^{-1}. The increased dihedral angle and reduced moment arm in Config. 5 are countered by a favorable larger area. Not only this, but this is closer to the ideal dihedral angle of 47°[60] which permits equal control for yaw and pitch moments ($\cos^2(45) \approx 0.5$). As a result, the parameters of Config. 5 were chosen as the final values.

The neutral point was found by adjusting the CoG location, where $\frac{dC_m}{d\alpha} = 0$; this was done using empirical methods, XFLR5 and AVL.

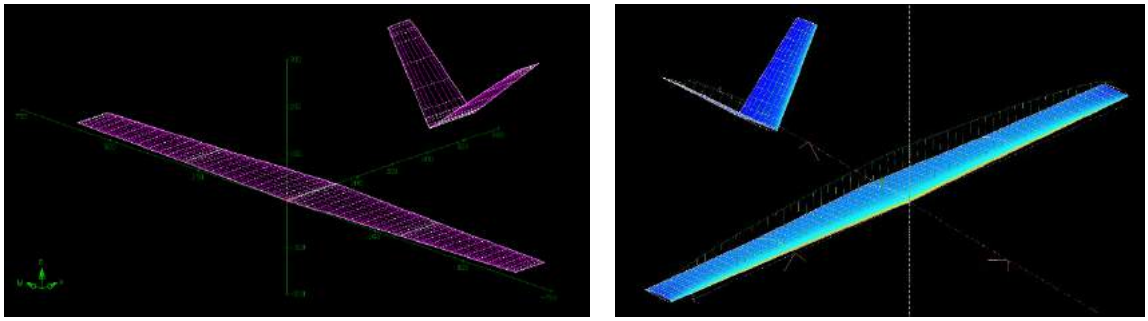

Fig.44 - Simulated Geometries (Left - AVL, Right - XFLR5)

Table 37 Neutral point location comparison between different methods.

Method	Neutral Point Location
Empirical	$0.5678\bar{\mathbf{c}}$
XFLR5	$0.755\bar{\mathbf{c}}$
AVL	$0.736\bar{\mathbf{c}}$
Final Value	$0.7455\bar{\mathbf{c}}$

The inaccuracy in the empirical method can be attributed to the use of 2D airfoil theory, whereas the VLM methods compute a further aft location. In addition, the reduced value can also be linked to the elevated position of the tail at 0.5m. This would reduce the value of $\frac{d\varepsilon}{d\alpha}$ increasing the effectiveness of the tail permitting further aft loading. With a static margin of 25%, there can be a shift of COG between $0.5455\bar{c}$ and $0.7455\bar{c}$. This margin is justified as propeller driven aircraft can be expected to have a 4-10% reduction in static margin[59]. Any further reduction in stability due to flight conditions will be managed by a stability augmentation system. The COG of the aircraft will be

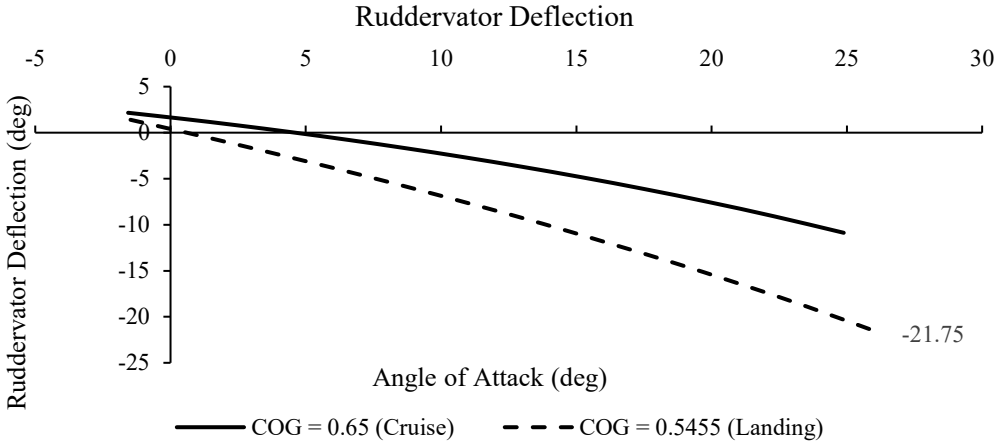

Fig. 45 Ruddervator deflection.

placed at $0.61\bar{c}$ which falls well within this margin.

Using AVL, the ruddervator deflections required for C_L between 0 and 2.6 were determined. Two conditions were used: maximum range condition at cruise (12,000 ft, 60 m/s, COG = $0.61\bar{c}$) and an extreme landing case (sea level, 27.44 m/s, COG = $0.5455\bar{c}$). The second condition yielded a maximum deflection was of -21.75°; further deflection will be required to allow for yaw control as ruddervators control both yaw and pitch. There will be no requirement for trim tabs as the system will be hydraulically actuated therefore eliminating any stick forces[33].

The final dimensions for the tail are as follows;

Table 38 Final tail dimensions.

Parameter	Value	Parameter	Value
Planform Area (m^2)	4.5	MAC, $\bar{\bar{c}}$ (m)	0.9839
Horizontal Projected Area (m^2)	3.45	Taper Ratio	0.4983
Dihedral Angle, Γ (deg)	40	Tailplane Setting Angle, i_t (deg)	0
Leading Edge Sweep, Λ_{LE} (deg)	15	Moment Arm, l_t (m)	4 (from main wing c/4)
Aspect Ratio	5	Elevation above Wing (m)	0.5
Span (m)	4.743	Ruddervator Area (m^2)	0.4804
Root Chord, Cr (m)	1.266	Ruddervator Chord (m)	0.2532 (0.2 x Cr_{RV})
Tip Chord, Ct (m)	0.6309	Ruddervator Deflection	±35 degrees

2.5.3. Aileron Sizing

For directional control, it is important that the ailerons are sized such that sufficient roll response is achieved by the aircraft. According to FAR 23 requirements, an aircraft must be able to perform a 60 degree turn from 30 degree bank angle within 5 seconds at takeoff and 4 seconds at landing[61]. Using these parameters, the roll helix angle (pb/2V) is found using the following method.

$$\frac{pb}{2V} = -\frac{C_{l_{\delta a}}}{C_{l_p}}\delta_a \tag{15}$$

Where $C_{l_{\delta a}}$ is roll authority and C_{l_p} is the roll damping. Using the following formulas and relevant variables, the roll rate was determined. A flap chord length of 0.35c was used.

$$C_{l_{\delta a}} = -\frac{c_{l_{\delta a}} C_R}{Sb}\left[\left({b_2}^2 - {b_1}^2\right) + \frac{4(\lambda - 1)}{3b}\left({b_2}^3 - {b_1}^3\right)\right] \tag{16}$$

$$C_{l_p} = -\frac{\left(a - c_{l_{d0}}\right) + C_R b}{24S}\,[1 + 3\lambda] \tag{17}$$

Where

$$c_{l_{\delta a}} = 1.7253, C_R = 1.403551m, S = 14.32m^2, b = 12.3784, \lambda = 0.6, a = 6.14, c_{l_{d0}} = 0.00816, b_1 = 4.5537m, b_2 = 5.9537m, \delta_{aMAX} = \pm 35^o$$

The span locations were chosen to allow sufficient span for the flaps and 0.15m structural space at the tip. Also, the maximum deflections were chosen as maximum ground deflection is reduced by around 25% in flight[62], therefore ±28° can be expected.

$$C_{l_{\delta a}} = 0.132322 \qquad C_{l_p} = -0.87025 \quad \therefore \quad \frac{pb}{2V} = -\frac{0.132322}{-0.87025} \times \left(28 \times \frac{\pi}{180}\right) = 0.0743$$

Using this value and a range of speeds, the roll rate performance was assessed to see if requirements were met.

Table 39 Roll rate variation with airspeed.

V (m/s)	Roll Rate, p (rad/s)	Takeoff (in 5 sec) (deg)	Landing (in 4 sec) (deg)
25	0.3001	85.99	68.79
50	0.6003	171.9	137.6
75	0.9004	257.9	206.4
100	1.201	343.9	275.2

From Table 39, the roll performance requirement for both conditions is exceeded which ensures the S270's roll control is sufficient.

2.5.4. Longitudinal Stability Assessment

Performing stability analysis using AVL, the following values were obtained for the longitudinal stability.

Table 40 S270 Longitudinal mode performance.

Parameter	Value
Short Period Eigenvalue	-14.36 ± 12.02i
Short Period Mode Damping Ratio, ζ_{SP}	0.767
Short Period Mode Natural Frequency, $\omega_{n_{SP}}$ (Hz)	1.913
Phugoid Eigenvalue	-0.0068 ± 0.6386i
Phugoid Damping Ratio, ζ_{phug}	0.011
Phugoid Natural Frequency, $\omega_{n_{phug}}$ (Hz)	0.102

These values were compared against limits outlined by Cook for short and long period longitudinal modes. It is recommended that the values in Table 40 are met and that the SPPO and phugoid frequencies be well separated[33].

Table 41 Longitudinal design limits.

Flight Mode	Level 1		Level 2	
Short-Period	$\zeta_{SP}min$	$\zeta_{SP}max$	$\zeta_{SP}min$	$\zeta_{SP}max$
	0.50	1.30	0.35	2.00
Phugoid	$\zeta_{phug}min$		$\zeta_{phug}min$	
	0.04		0	

Clearly, the S270 exhibits the ideal stable behavior where both long and short period modes are damped and non-divergent in its natural state. The short period mode values are well within the limits for the most desirable level 1 flight characteristics. The phugoid mode satisfies the level 2 criteria implying a stable aircraft with a positive damping ratio. The period is found to be 9.84s which is well below the requirement for $T_p \leq 55s$. The short mode period is found as 0.336s which means the frequencies of the long and short modes are well separated as recommended by Cook[33].

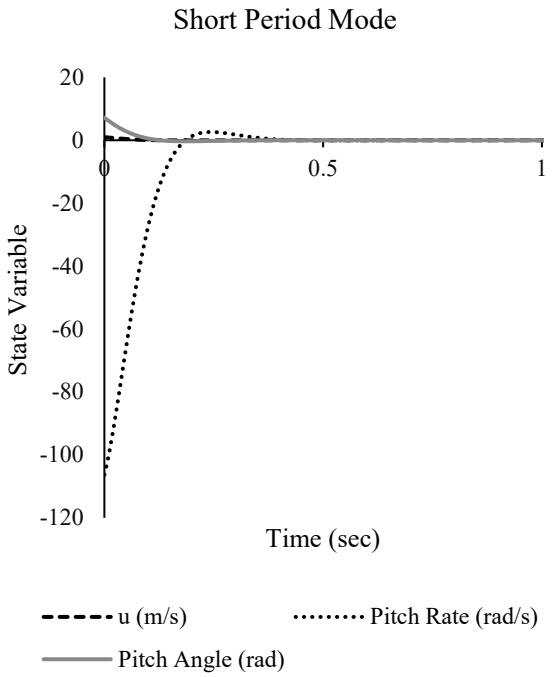

Fig. 46 Short Period Mode

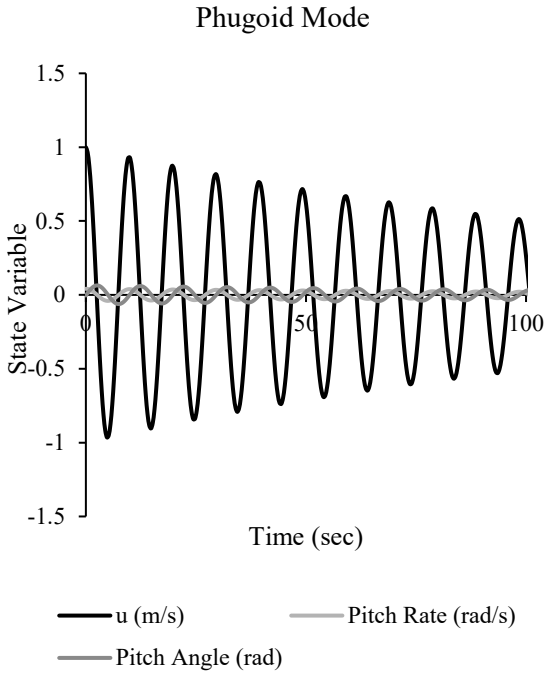

Figure 47 Phugoid Mode

2.5.5. Lateral and Directional Stability Analysis

Using AVL, the lateral stability was also assessed using the modal response for roll subsidence, Dutch roll and spiral modes with values compared to limits set by Cook[33]. The lateral stability of the aircraft is largely determined by the dihedral angle of the main wing to overcome roll disturbances and effective fin area size to overcome yaw disturbances. Roll subsidence is the aircraft's ability to restore the aircraft to wings level following a bank input. The S270 satisfies the limits for Level 1 flight characteristics as outlined in Table 42 and shows a very fast return to stable condition.

Table 42 Roll subsidence.

Flight Phase Category	Maximum Value of T_r (s)			S270 Value (s)
	Level 1	Level 2	Level 3	
A, C	1.0	1.4	-	0.03597
B	1.4	3.0	-	(-27.79 + 0.000i)

Dutch roll is a lateral short period mode excitation between yaw, roll and sideslip angle. Appropriate damping of this mode is crucial to a stable aircraft. This is important for a V-tail aircraft as they feature further inherent instability due to the dihedral angle.

Table 43 Dutch roll.

Flight Phase Category	Minimum Values of ζ_{DR}			S270 Value
	Level 1	Level 2	Level 3	
A	0.19	0.02	0	0.3384 (-4.595 ± 12.78i)
B	0.08	0.02	0	
C	0.08	0.02	0	

From Table 43 the S270 shows a damping ratio that satisfies the limits for all flight phases to Level 1 qualities. This is attributed to the 3 degrees of dihedral applied to the main wing. An original configuration without dihedral was found to have a damping ratio of 0.160 which only satisfied Level 2.

The spiral mode is an unstable mode which develops because of stable flight and the aircrafts tendency to roll towards one side. Since this mode is a long period mode, the time to double bank angle is used to assess the directional stability, this was calculated following Equation (

$$T_2 = T_s \times \ln 2 = \frac{1}{Real\ Part} \times \ln 2 \tag{18}$$

Table 44 Spiral mode.

Flight Phase Category	Minimum Values of T_2 (s)			S270 Value (s)
	Level 1	Level 2	Level 3	
A, C	12	8	5	15.71 (0.0441 + 0.000i)
B	20	8	5	

As shown by Table 44, the S270 takes 15.71 seconds to double the bank angle, which satisfies the criteria for Level 1 flying qualities for phases A and C, but level 2 for phase B. These times are sufficiently large such that the pilot should be able to respond to the disturbance in time before becoming too unstable.

Overall, the S270 is shown to be stable in all 3 modes; longitudinal, lateral and directional. The phugoid and dutch roll modes show the greatest need for a stability augmentation system. Though those that satisfy Level 2 flying qualities are not ideal, the aircraft will be hydraulically actuated therefore the increase in pilot workload should be minimal. Implementation of a closed loop feedback system will help to counter these instabilities.

2.6. Propulsion

The propulsion design of the S270 will be vital in achieving the aim of low-cost operation. In this section, trade-off studies of hybrid architectures, fuel burning engines and electric motors will be carried out. In addition, the engine and electric motor will be optimised to suit the profile of the S270. Finally, an in-depth propeller design will be carried out to maximise efficiency while reducing noise.

2.6.1. HEP Architectures

The first step in designing a HEP system is to determine the hybrid architecture to be implemented; series, parallel or series-parallel. In this section, all three configurations will be compared and contrasted to determine the optimum choice for the S270's powertrain. All configurations are shown in Fig. 48.

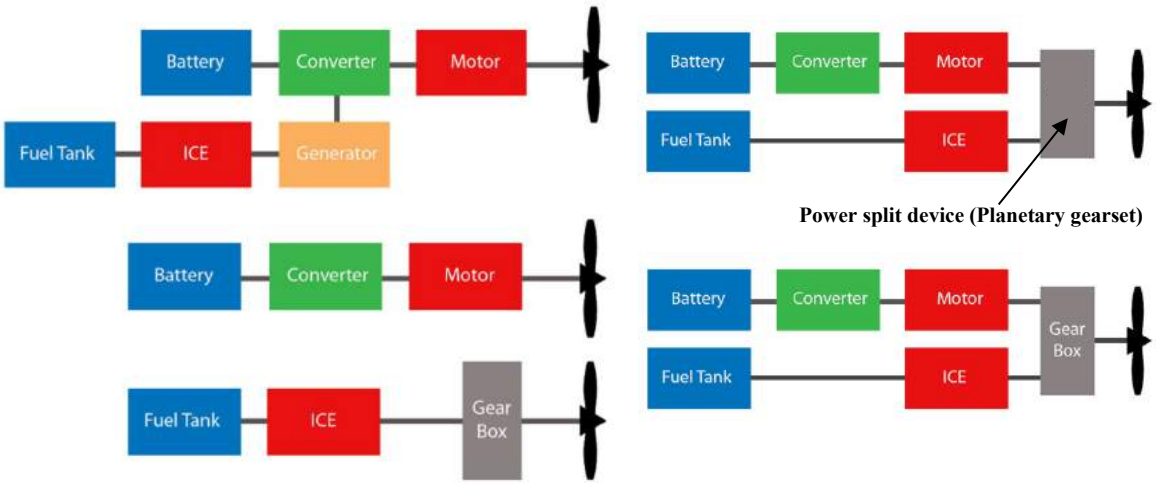

Fig. 48 Hybrid Architectures. Top left: Series. Top right: Series-Parallel. Bottom left: Parallel (DEP configuration). Bottom right: Parallel (mechanically coupled configuration).

A series configuration, often referred to as a range-extender, uses the ICE to power a generator that continually charges the batteries throughout operation. This configuration is particularly useful for high torque applications because of the high torque output of electric motors compared to ICE's. A large amount of energy loss occurs in this configuration due to the energy conversion from ICE mechanical energy into electrical energy in the batteries, then back into mechanical energy by the electric motor [63]. Not utilising the ICE for direct propulsion means that all propulsive output comes from the electric motor which reduces the redundancy of the overall system. In addition, the requirement for a generator adds significant weight to the powertrain [14].

A parallel configuration utilises both the ICE and electric motor to drive the propeller; one option is to use each power source to drive a separate propeller, however this configuration is not suitable for the single propellered S270. A distributed electric propulsion (DEP) aircraft could utilise this arrangement, however, the TRL 7+ requirement is not met by DEP therefore cannot be implemented

into the S270's design. The next parallel configuration utilises a mechanical gearbox to couple the ICE and electric motor to the drive shaft. The main drawback of this configuration is that the ICE cannot operate at optimum efficiency due to its direct connection to the drive shaft [63]. In addition, the mechanical coupling adds a significant level of complexity and mass to the design [13]. A series-parallel configuration combines the benefits of the series and parallel configurations, while eliminating their drawbacks. In this arrangement, the ICE and MG combine their power output through a planetary gearset [22]–[24]. By transferring the ICE power through this planetary gearset, the ICE can operate at closer to its optimum efficiency than it can in a parallel configuration, while reducing the system complexity [14], [63]. This means that the ICE can be smaller than it would need to be in a parallel configuration, without any loss of propulsive output. In addition, the power split device offers approximately 89% efficiency compared to the gearbox required in a parallel configuration, that operates at closer to 85% [64]. Finally, in a similar way to the parallel configuration, the two power sources can operate independently; this adds redundancy to the propulsion system in the event of an engine-out or motor-out scenario.

2.6.2. Fuel Burning Engine Selection

The first step in designing the fuel burning engine is to determine the power requirement for the engine. In order to generate an output power of 230 kW during climb, the engine requires to be sized to account for mechanical losses in the gearbox. The calculation of the maximum power required is shown below.

$$Power_{required} = \frac{230}{\eta_{Gear\ Box}} = \frac{230}{0.89} = 258.4\ kW \tag{19}$$

Hence the power requirement of the engine is set to be 270 kW in order to provide extra power in adverse weather conditions.

There are many types of engine available for general aviation aircraft, however they can be separated into two distinct groups; ICE's and turboprops. Turboprop engines offer a significantly higher power to weight ratio and fuel efficiency. However, the price of turboprop engines is considerably higher than ICE's, therefore turboprops are not suitable for the S270 due to the major importance of low aircraft costs. In addition, the power capability of turboprop engines is much greater than the power requirement for the S270 aircraft, therefore there is no need to have such a powerful engine. Table 45. shows a comparison of prices for a selection of turboprop and ICE engines, clearly ICE engines are drastically cheaper.

Table 45 Engine parameter comparison.

Engine	Type	Unit Cost (£000's)	Max. power (kW)	Dry Weight (kg)	Power/Weight (kW/kg)
Continental IO-550G [65]	ICE (Avgas)	48 [66]	209	195	1.07
Continental IO-580-B1A [67]	ICE (Avgas)	68.7 [68]	235	197	1.19
Lycoming DEL-120 [69]	ICE (Diesel)	-	153	163	0.94
Thielert Centurion 4.0 [70]	ICE (Diesel)	89 [71]	228	286	0.80
RED A03-102 [72]	ICE (Diesel)	130 [73]	368	357	1.03
Arrius 1A1 [74]	Turboshaft	461 [75]	556	223	2.49
Pratt & Whitney PT6A-52 [76]	Turboshaft	400 [77]	634	204	3.11
Lycoming LTS101-600A2 [78]	Turboshaft	415 [79]	459	115	3.99
Rolls Royce M250 [80]	Turboprop	323 [81]	522	133	4.15

The next design consideration is whether to use a spark or compression ignition ICE. Avgas is the main fuel for spark ignition engines and is more readily available at small airports than any alternative. However, it has been reported to have detrimental effects to the environment due to the lead content of the fuel. The price of avgas in the EU has increased significantly in recent years due to extra taxation in a push to reduce its widespread use, however the price of the fuel in the US has remained more stable. Unleaded aviation fuels are being developed, however there are no widely available fuels currently in use. Aviation diesel (for use in compression ignition engines) is an alternative option, which offers a reduction in harmful emissions. In addition, these diesel engines can operate using biodiesel and Jet-A1 with minimal modifications required to the engine. The only certified diesel engine capable of providing sufficient power for the S270 is the Red A03 diesel engine, however, this engine weighs ~1.8 times the IO550 engine and costs 2.7 times as much [72], [73]. There is a large amount of investment going into aviation diesel engine development due to the rising taxation on avgas, however the technology will not be ready by the S270's service entry of 2025.

In the future, Project Skyride will look to remove the ICE altogether and utilise fully electric flight all the time; however, due to the limitations in battery technologies, this may be some way off becoming a reality. The alternative to removing the ICE completely is to implement technologies such as the SMA high power density engine (HPDE), which is quoted as weighing 240 kg and capable of delivering 800 HP (596 kW) of power [82]. This will offer extremely good performance with a considerably lower P/W ratio than existing ICE engines.

After these considerations, the decision has been made to use a spark ignition engine based on the design of the Continental IO-550 engine. An engine will be sized and optimised so that it suits the operation of the S270 and outperforms the 30-year-old Continental engine. Although AVGAS is not the optimum choice, the first iteration of the S270 will use this fuel with a view of moving towards

unleaded gasoline if it becomes more readily available, or diesel when the technology becomes more suitable for higher power applications.

2.6.3. Electric Motor Selection

For the electric motor of the hybrid system, the required power depends on the efficiency of the power split device as well as the generator. However, the maximum power contribution of the electric motor is kept at 90% only as the internal combustion engine contributes around 10% of the power. The required power of the electric power is calculated as shown below.

$$Power_{required} = \frac{230 \times 0.9}{\eta_{power\ split\ device}} = \frac{230 \times 0.9}{0.89} = 232.6\ kW \quad (20)$$

A comparison of electric motors is shown in Table 46. The first point worth noting is that electric motors achieve much higher P/W ratios than ICEs, obviously a very desirable characteristic for aeronautical applications. The Siemens SP260D motor is an electric motor that has been tested and was able to provide a continuous power of 260 kW on a Diamond Extra 330 Aircraft [83]. The SP260D motor weighs only 50 kg and has a power to density ratio of 5.22 kW/kg. The DA36 E-Star uses a serial hybrid configuration and is powered by a Siemens 70 kW electric motor, its first flight was 2011[84]. This motor has been included to show the dramatic improvement in electric motors over the past few years.

With the current available technology, the electric motor of the S270 will be based on the design and performance of the SP260D. Project Skyride will continually upgrade to new motor options as aviation electric motors continue are improved and optimised in the future.

Table 46 Electric motor comparison[83], [84]**.**

Engine	Power (kW)	Mass (kg)	P/W (kW/kg)	Continuous Torque (Nm)	Efficiency (%)	Dimensions ($mm \times mm \times mm$)
DA36 E-Star	70	13.6	5.22	70	90	-
SP260D	261	50	5.22	1000	95	418×300×300
S270 EM	240	46	5.22	1000	95	400×300×300

Although the designed operation of the powertrain only utilises 90% of the electric motor's power, the power split device allows the electric motor to operate at full capacity in the case of ICE failure to add redundancy to the propulsion system. The 240 kW maximum power output of the electric motor will be more than sufficient to allow the aircraft to safely manoeuvre to the ground in an engine-out case.

2.6.4. Electric propulsion noise reduction

Results from a survey conducted by Project SkyRide show that, on average, the general public consider noise from aircraft as more disruptive than motorway and road traffic noise, and almost as disruptive as railway noise. It is likely that the public will be opposed to the idea of a drastic increase in air traffic noise from local airports that do not usually accommodate large volumes of traffic. In addition, internal noise reduction will be very important to potential passengers of the S270 aircraft. Therefore, noise reduction will be especially vital during flight phases where the aircraft will be close to the ground (and when engine noise is greatest), i.e. take-off, climb, descent and landing.

This noise reduction can be achieved, in part, by maximising electric motor contribution in these phases of flight. Studies have been undertaken to determine the noise reduction available by utilising electric motors over ICE engines, outlined in [85], [86]. Experiments were carried out on a stock Cirrus SR20 and a noise reduction of 12dB was achieved using an electric motor compared to using an ICE. More experimental/simulation data is required to determine the exact value of noise reduction achieved by the S270. However, existing simulation techniques are not entirely accurate when predicting hybrid electric propulsion noise due to the requirement for considerable simplification of physics and geometry [87]. This is an area of future development that will be conducted to reduce the noise emissions of the S270 aircraft.

2.6.5. Powertrain Operation

The power split device is a vital component in the HEP system of the S270 aircraft, this component allows both power inputs (the ICE and motor generator) to drive a common output shaft. When operating together, the sum of torques are added together through a double-planetary gearset within the power split device housing, which are connected to a common drive gear. When operating separately, the inactive driver can be disconnected from the power split device to preventing undue stress on the components, thus prolonging engine/motor life [21]–[24]. The problem of matching rotational speeds is mitigated by the fact that the design speed of both the ICE and MG is approximately 2700 rpm, therefore neither driver will be forced to undergo off-design rotational loads during tandem operation. If the design speeds were different, a propeller speed reduction unit (PSRU) could be implemented to reduce the higher speed of the electric motor; however, this extra component is not required in the S270, thus reducing weight and complexity. An added benefit of this series-parallel configuration is that the motor can be used as a generator to recharge the batteries during flight. This “generator mode” operation occurs during the cruise phase where the ICE is generating all of the propulsive power. The motor operates at a negative speed (against the direction of torque) and generates power which is fed back into the batteries [21].

2.6.6. Engine sizing

One of the problems with the development of piston engines is the low power to weight ratio compared to engines that have a gas turbine [88]. The rate of development of piston engines is shown in Fig. 49 [82][65][67]; using this data, the S270's ICE will aim to achieve a power to weight ratio of 1.5 kW/kg. It is also worth noting that the piston engine specific fuel consumption (SFC) decreases as technology develops; it is expected that the S270's ICE will achieve an SFC of 0.25 kg/kW/hr by the time of certification.

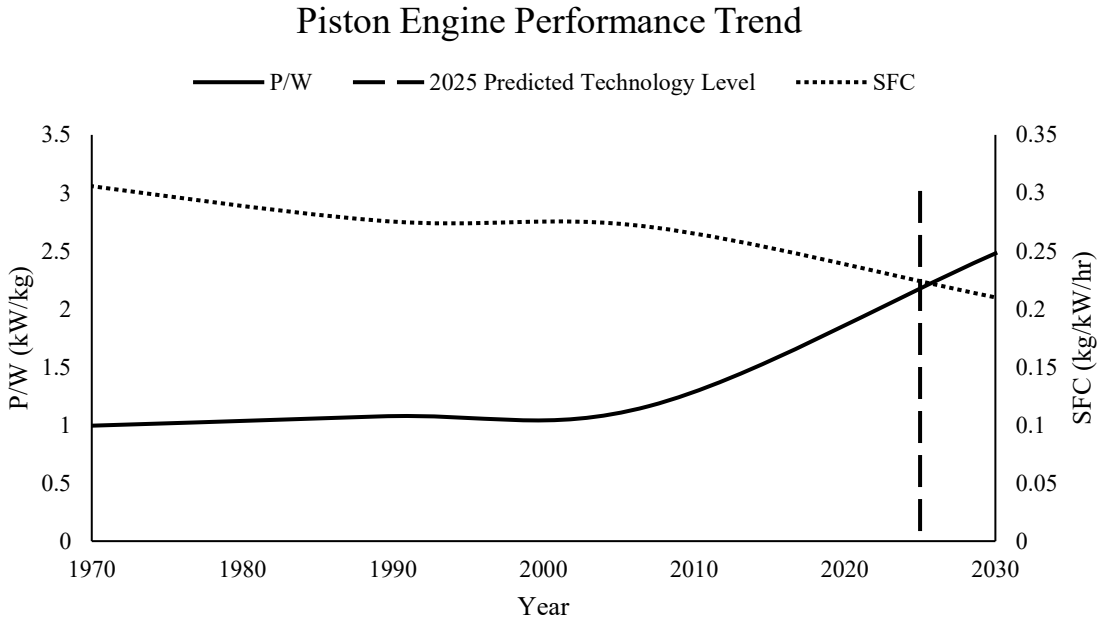

Figure 49 Piston Engine Performance Trend

2.6.7. Propeller Noise Reduction

The aim of the propeller design is to provide relatively quiet propulsion with high propulsive efficiency. It is said that a 2-blade propeller provides a better cruise performance where as a multi-blade propeller provides advantages such as greater ground clearance, better climb performance and reduction in engine noise [89] .The S270 propeller is designed with a three-blade propeller as this can utilise a smaller propeller diameter to produce the same amount of power compared to a 2-blade propeller. One of the problems to encounter in thin-haul operations is the amount of noise complaints received from the nearby residential area. A three-blade propeller is said to provide less noise as the diameter of the propeller is smaller, the blade tip speed is smaller under the same revolution speed.

Metzger has investigated various propeller configurations on a Beechcraft 35 Debonair and has generalised the test results on 19 different propeller configurations [90]. The investigation broke the propeller configurations down into few major categories. This includes the number of blades, the angle of sweep of the blade, the blade tip shape, diameter as well as the blade tip thickness. The investigation compares the sound pressure level, the cost and the total weight of the aircraft while

providing the same maximum continuous power. According to the research, a three-blade configuration with a nominal design, a thin rounded tip that has a swept tip, produces the least sound pressure level at 1000 feet flyover. A 2-blade configuration that has an elliptical and non-swept tip produces an extra 6 dBA sound pressure level at 1000 ft flyover but is also cheaper to manufacture and 10 lbs (4.5 kg) lighter. The S270 propeller will be using the 3-blade configuration with round, thin and swept back blade tips despite the increased manufacturing cost and propeller weight. This is because the mass portion of the propeller is insignificant compare to the mass of the aircraft, thus the mass of the propeller is not a consideration. The cost estimation of the 3-blade propeller configuration is expected to be 1000 USD more expensive than the 2-blade propeller configuration at the time the investigation has been conducted. However, the extra cost of the propeller blade only takes account to less than 1% of the overall cost of the aircraft and with advancing technology, it is believed that propeller blades with a sweptback configuration is easier to manufacture and maintain.

2.6.8. Propeller Sizing

The pitch of the propeller changes the angle of attack of the blades. The S270 will adapt a fix pitch propeller but with 3 pitch settings in order to optimise the aircraft performance in different stages of climb. The S270 pitch settings include a 15, 20 and 25 degree pitch settings depending on the airspeed of the aircraft based on the performance maps described by McCormick[91] . A detailed table of the recommended pitch settings and its relative propulsive efficiency is listed in the Table 47 below.

Table 47 S270 pitch settings

Airspeed (m/s)	Pitch Angle (Degrees)	Propulsive Efficiency
0 – 51	15	0.72
51 – 79	20	0.825
79 – 93	25	0.85

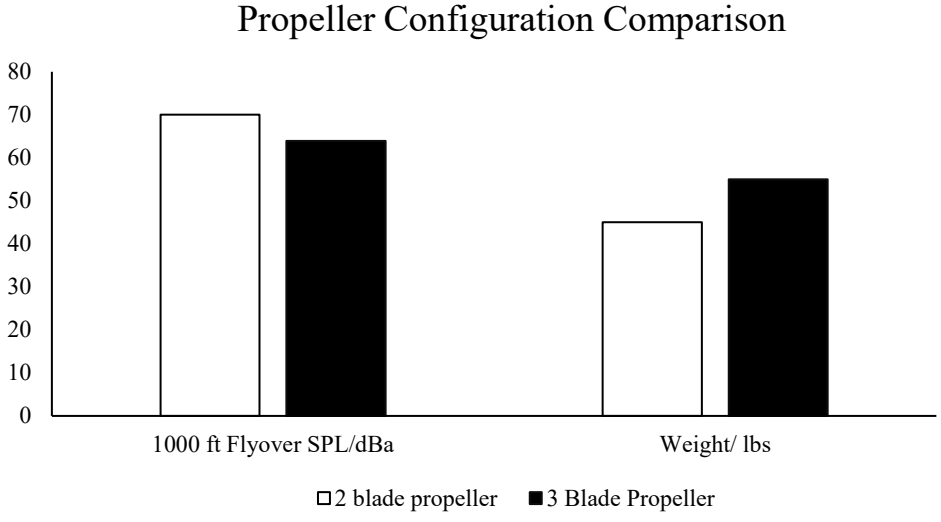

Figure 50 Results from Metzger's Investigation

A variable pitch is unfavourable as a fixed pitch propeller has a simpler configuration and the maintenance cost is lower.

To size the propeller, the advance ratio of each flight phase in being considered. Using the simplified method mentioned by Tulapurkara [91], the approximate propeller diameter required of a two-blade configuration propeller can be mapped on the performance map investigated by McCormick [92]. Initially the propulsive efficiency at cruise is set to be 0.8. Using the available data from the flight conditions and the revolution speed of the propeller, the speed power coefficient C_s can be obtained. By selecting the maximum propulsive efficiency with the relative C_s, the optimum advance ratio and the pitch angle can be returned. Once the advance ratio is returned, the diameter of the propeller can be calculated using the equation below.

$$d = \frac{V}{nJ} \tag{21}$$

where v is the airspeed in m/s, J is the advance ratio and n is the rotational speed of the propeller in revolutions per second.

Using this technique, the advance ratio returned is 1.0 with a speed power coefficient of 1.8 and a pitch angle of 25 degrees at cruise. The diameter for a 2-blade configuration propeller is 2.07m in order to achieve the performances of the S270.

In order to find the diameter of a 3-blade propeller that has a similar performance of a 2-blade propeller, a conversion is needed as a 3-blade propeller has a shorter diameter. A simplified approach proposed by Hepperle uses the power relationship between the ratio of the number of blades and the blade diameter to approximate the equivalent diameter of a multiblade propeller[93] .

$$\frac{D_1}{D_2} = \left(\frac{N_2}{N_1}\right)^{\frac{1}{4}} \tag{22}$$

Using the equation above, it is estimated that the diameter of the propeller blade in a three- blade configuration is around 90.4% the diameter of a two-blade propeller configuration. Hence the finalised propeller blade diameter in the S270 is 1.87m with a blade tip speed of 0.71 Mach at sea level conditions.

2.6.9. Propulsion Installation

The powertrain is located in the front of the aircraft, shown in Fig. 51. The electric motor and ICE are configured one in front of the other to reduce the overall frontal area of the aircraft and thus reduce drag. By having the engine in the front of the aircraft, minimal mechanical losses occur between the shaft and the propeller and maintenance is simplified due to ease of access.

Fig. 51 Engine location in S270 engine bay.

2.6.10. Summary

In summary, the series-parallel HEP architecture used in the S270 allows for reduced fuel burn and noise. Added redundancy is incorporated into the design because the power split device enables engine only or motor only propulsion in the case of one propulsion unit becoming unavailable. As battery technology improves in the future, the contribution of the electric motor can be increased across all flight phases. The series-parallel configuration means that a complete overhaul is not required to increase the contribution of the motor in the future, the ICE will be simply be required to operate at lower power until it is only required as a redundancy in a motor-out situation. A propeller design has been carried out to reduce the noise and increase its efficiency.

2.7. Batteries

The batteries provide the essential propulsive power needed for take-off; therefore, it is important to accurately calculate the number of cells needed. However, it is just as important to keep this value to a minimum. This is because the gravimetric energy densities of batteries are approximately 100 times lower than of AVGAS. The study begins with a comparison of Li-S with Li-Ion cells, taking into account the discharge nature of each. It then moves onto an optimisation stage to minimise the total battery mass. Finally, the pack arrangement is considered along with the necessary systems needed for optimal performance.

2.7.1. Trade-off Study

A trade-off study was performed to compare the projected Li-S cell against current Li-Ion cells more commonly used in electric vehicles. Table 48 displays these results. The figure to especially notice is the number of cells in parallel, which is usually calculated by satisfying the total energy required

for a given flight mission. However, it is also important to consider the cells' ability to safely provide full power at take-off. This is determined by the maximum discharge c-rating of the cell, which according to OXIS Energy's specification sheet is 6C [31]. Compared to Li-Ion's value of 1.5C, Li-S can provide the required power at take-off with significantly less connections in parallel; thus, reducing the total battery mass by 85.4%. This is further reinforced by the 89.8% increase in pack specific energy.[31].

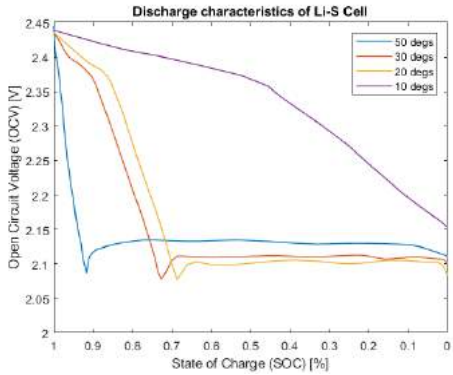

Fig. 52 Discharge characteristics of Li-S cell.

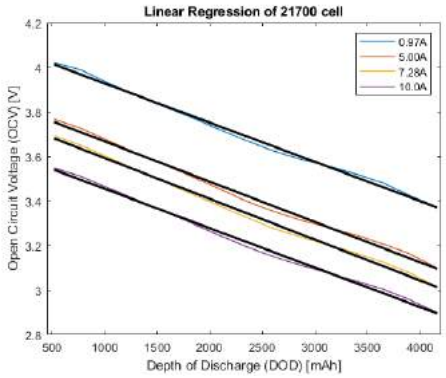

Fig. 53 Linear regression of Li-Ion cell.

Table 48 Trade-off study between Li-S and Li-Ion batteries.

	OXIS Energy (Li-S)	LG INR21700 (Li-Ion)
Number of cells in series (Ns)	277	160
*Number of cells in parallel (Np)	4	57
Total number of cells (Nt)	1108	9120
Total battery pack mass [kg]	159.2	1069.24
Total battery pack volume [L]	149.47	279.63
Pack specific energy [Wh/kg]	285	154.81
Pack energy density [Wh/L]	303.56	591.95

**Number of cells in parallel given 580V in series*

At this stage the nature of the discharge curve of each type of cell was also included as a factor in the calculations. Figure 52 illustrates the discharge curve of a typical Li-S cell. It begins with a high-plateau region which then transitions to a low-plateau region; this allows for a more reliable prediction of the Open Circuit Voltage (OCV) after the transition point, which can be seen to occur earlier at higher temperatures. Previous studies have shown that operating at higher temperatures can reveal an increase in capacity by approximately 10% [94]. This can be favourable as a less sophisticated cooling system would suffice. Figure 53 captures the voltage dynamics of the Li-Ion cell by means of local linearization; this involves the use of linear regression in the quasi-linear region of the curve where studies have shown the error to be less than 5% [95].

2.7.2. Optimisation

The battery pack was sized to be directly compatible with the nominal voltage (580V) of the electric motor and hence neither a step-up or step-down transformer will be required, thus reducing losses. However, electric motors are quite often fully functional within an operating voltage range; this range is 530-680 V for the S270. Therefore, by manipulating this voltage and sizing the pack accordingly, a fluctuation in battery mass can be observed over a large voltage range as seen in Figure 54. A general increase in battery mass is revealed with increasing voltage; this is due to the greater number of cells required in series. However, with increasing voltage, the number of cells required in parallel is reduced. As this value must be an integer, a dip is noticed where this number decreases from 5 to 4. As a result, the battery pack was tailored to 530V with the final configuration shown in Table 49.

Table 49 Final battery parameters.

Cell formation	253s4p
Battery capacity (kWh)	41.4
Total number of cells (Nt)	1012
Total battery pack mass (kg)	146
Total battery pack volume (L)	137

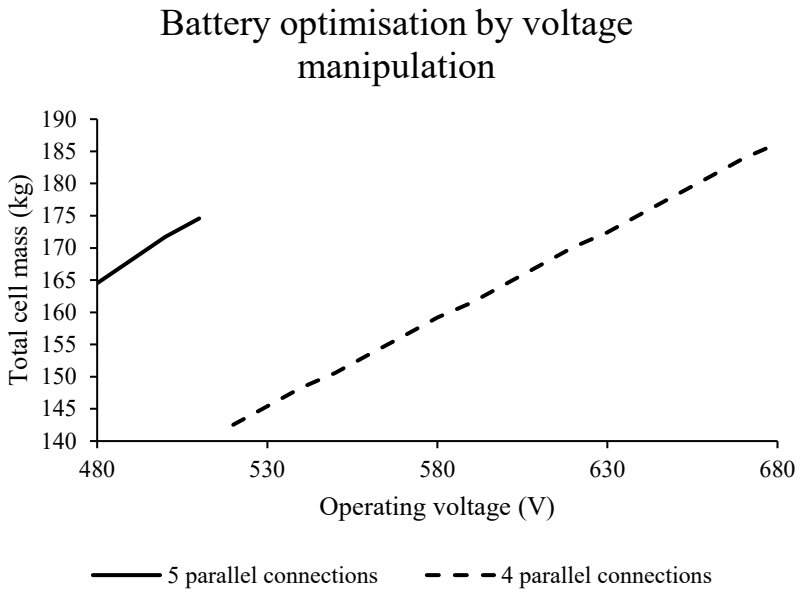

Fig. 54 Battery optimisation.

2.7.3. Pack Arrangement

Figure 55 illustrates a schematic of the battery pack. The arrangement consists of 253 cells in series and 4 of those series connections in parallel. The pack is divided into 4 modules, each of which

contain cells only connected in series in a 23 by 11 formation; this was done to maintain a parallel connection between modules and reduce the complexity involved with connecting modules in series. The outer ring casing is used as a ground bus, whilst also having a cross shaped live bus in the centre; this simplifies the wiring required between each module.

As mentioned earlier, a complex cooling system will not be required, thus a liquid cooling system is implemented with a water/glycol mixture. Although air cooling is simpler in nature, it is not used as this method is heavily dependent on the outside ambient temperature. The cells are under most stress during take-off, therefore they are at the highest temperature at this stage. Airflow is also very limited at this point and will not be sufficient to cool the battery pack. A water/glycol mixture is used because previous research has shown this to be more effective than oil or air cooling. A 5.71% and 10.81% reduction in average temperature was observed in comparison to oil and air, respectively [96]. It is ideal for aviation use due to its low freezing temperature and high specific heat capacity; thus, the operating temperature of the heat transfer fluid can be minimised. This also encourages temperature uniformity in each cell [97].

The cycle starts with the coolant in the reservoir and is pumped into each of the four modules through aluminium tubes. These pass through each row to maximise the surface contact with the copper pads on each cell. This is known as an indirect cooling method and provides a more cost-effective and versatile solution than direct cooling [98]. The fluid then exits the modules through the ‘COOLING OUT’ channels and delivered to the radiator. The temperature of the fluid is significantly reduced at this stage by means of a secondary cooling loop. This is a separate loop which uses refrigerant from the air conditioning system to remove heat from the radiator. Finally, the fluid is returned to the reservoir and the cycle is restarted.[98].

Fail-safe mechanisms are also integrated into the system through various methods. The low number of modules reduces potential points of failure as there are fewer terminal contacts between each module. Each cell is also connected to a busbar with a fuse, which connects them all in series; therefore, in the event of a cell failure, that particular cell will be isolated from the remaining cells in the module. The Module Control Unit (MCU) will have monitored the reduction in voltage and would relay that information to the Battery Management System (BMS). The BMS uses this information to balance the cells in each module in the event of a discrepancy [99]. The shunt sensors on the ground terminal of each module aids in this by providing current data.

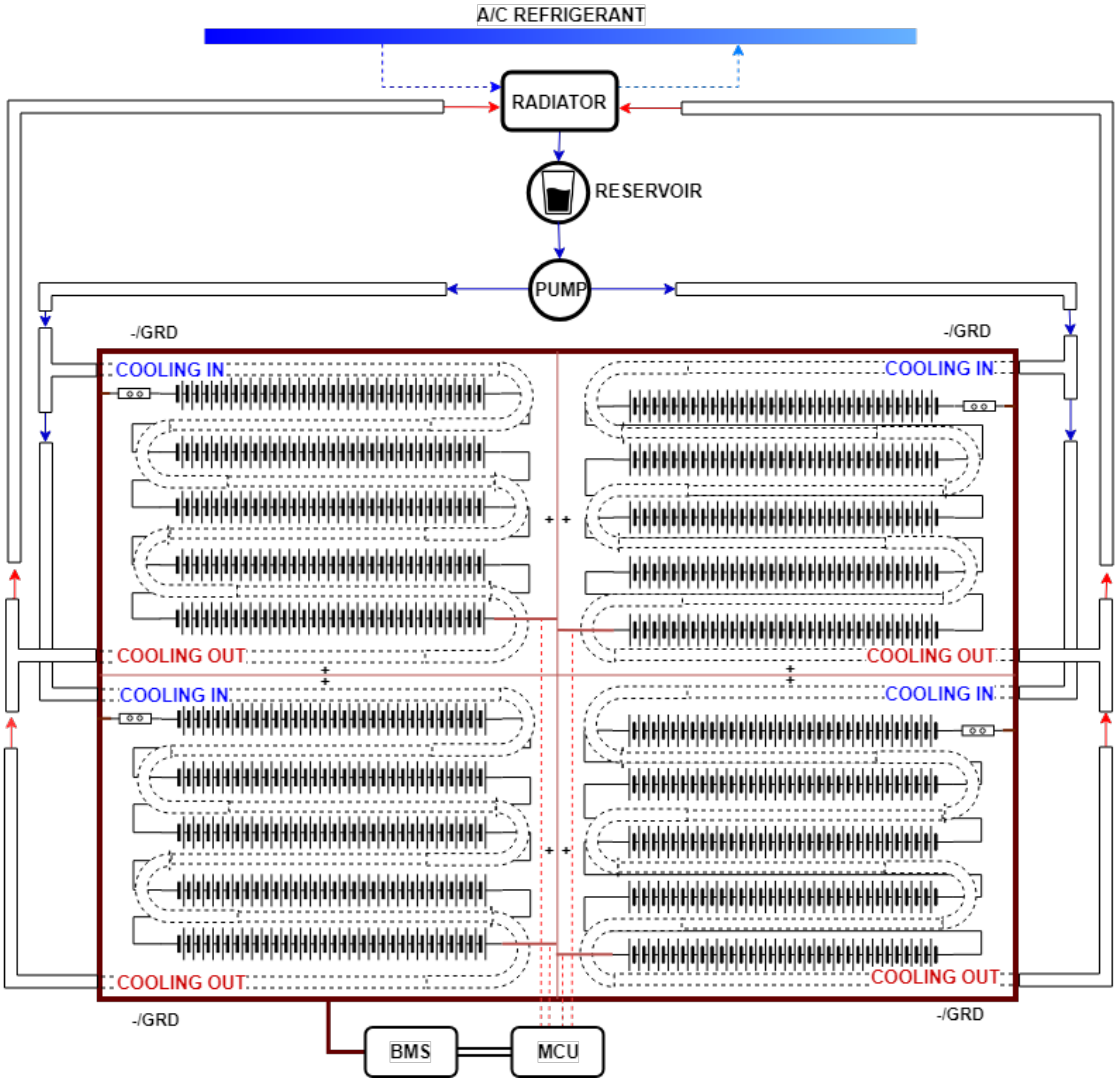

Fig. 55 Battery pack arrangement.

2.8. Structures

The structure of the aircraft has multiple functions, the most important being to maintain structural integrity at limit loads. It also needs to provide protection for passengers and payload, whilst being lightweight, durable and easy to maintain. The design process starts with determination of maximum loading conditions experienced by the structure throughout the flight envelope. For these conditions, shear force and bending moments are calculated, which are then used to determine stresses experienced by the structure. The materials will then be assigned, ensuring they are capable of maintaining structural integrity under loading conditions. Finite Element Analysis (FEA) will be performed for the wing to verify initial calculations for various structural components.

2.8.1. Wing Loading Conditions

An estimation of maximum load factor experienced by aircraft during its operations can be determined from the flight envelope. These limits are established by legal requirements for various

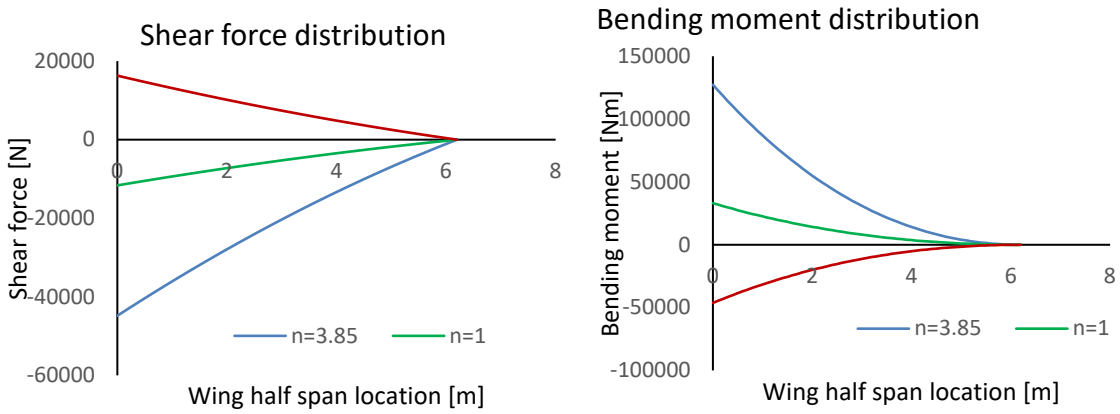

Fig. 56 Shear force and bending moment distribution.

aircraft categories. Using the n-V diagram (discussed in 2.4.1), the maximum load factor has been calculated to be 3.85.

In order to find net shear force and bending moment distribution for the wing, it is first necessary to consider net wing loadings in flight conditions. Wing loading is resultant of aerodynamic, gravity and inertial loading, as shown in Fig. 57.

Shear force and bending moment distributions have been calculated using the approach undertaken in [100] for a tapered wing. These are primary loadings which the structure must withstand, hence they determine the overall wing design [101]. Two factors are applied to the shear force and bending moment values; 1.05 to account for the force generated by the tail and a safety factor of 1.5 to obtain the ultimate load factor, which ensures that the failure does not occur at limit load. Shear force and bending moment distribution for the wing are presented in Fig. 56. This shear force and bending moment distribution have been used for subsequent stress analysis.

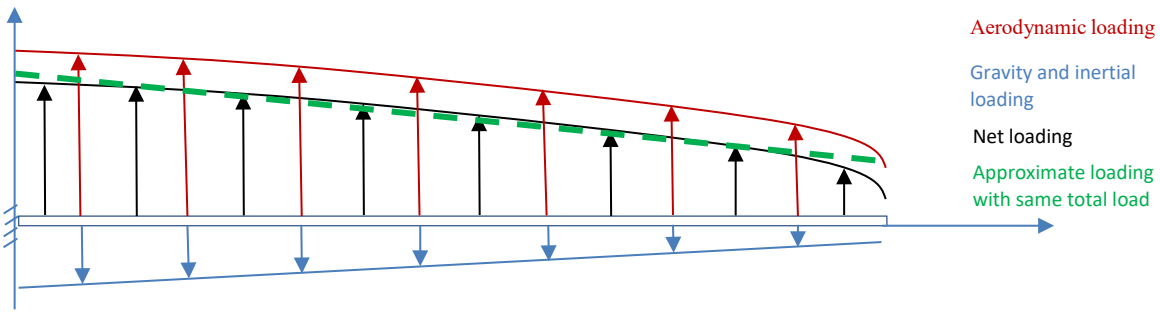

Fig. 57 Wing loading diagram.

2.8.2. Design Criteria

The structural layout of the aircraft is primarily governed by the choice of materials. The design rules for traditional aluminium structures significantly differ from those for modern composite structures. Composite materials are widely used in general aviation; many of the main competitors of the S270,

including the Cirrus SR-22, use a large amount of composite structures in their design. Composite materials provide a number of advantages when compared to traditional materials; high strength to weight and stiffness to weight ratios, excellent fatigue stress limit and good corrosion resistance. In addition, advanced composite manufacturing techniques allow for a higher level of integration; according to [102], it is possible to achieve 55% fewer parts, 57% fewer fasteners and a 21% weight reduction when using composites as opposed to using an aluminium structure. For example, a composite wing spar is manufactured as a single piece as opposed to assembling spar caps, webs and stiffeners with rivets for aluminium spar. Composite materials can be used to reinforce various structural components, which further reduces the part count; for example, reducing the total number of ribs required. [103] Composites also enable the forming of a highly aerodynamic shape, which is vital to drag reduction and hence operating cost reduction. Although they are usually more expensive, the overwhelming number of benefits mean that composite materials are the obvious choice for the S270.

2.8.3. Wing Structural Layout

Dimensioning the wing planform area was followed by wing structural design. Preliminary design of structural layout consisted of spars and ribs sizing and placement, followed by materials assignment. An FEM simulation was used to ascertain design feasibility.

Spar webs and caps, ribs and skins were the main structural elements. The function of spar webs is to carry vertical shear forces coming from wing aerodynamic loading. Spar caps consisting of upper and lower flanges attached to the web carry bending stresses generated in flight. This causes the upper flange to be in compression and lower in tension. Ribs are designed to maintain aerodynamic profile of the wing and support skins from buckling. Finally, skin gives aerodynamic shape to the wing and is responsible for transmitting in-plane loads into surrounding structure. Stringers usually support skin against buckling and carry axial loads from wing bending. An initial decision was made not to use stringers to reduce structural mass; this was supported by the FEM results (see section 2.8.5), ascertaining that structural integrity is maintained in most severe flight loading conditions.

Although some general aviation aircraft, for example Mooney Ovation, use a single main spar, it is generally known that statically indeterminate structures are significantly safer, hence the S270 wing uses two spars, making the structure fail safe; in case of structural failure of one spar, the loads can be carried by the remaining spar. This approach has also been undertaken by Rockwell 114 and 115 general aviation aircraft. The wing structure consists of two C-beam spars; this shape was chosen for its weight efficiency, as well as ease of manufacture compared to an I-beam. The front spar is located at 23% of the wing chord, which minimises level arm for lift forces, that usually act at quarter chord[101], [104]. The rear spar is located at 55% of the wing chord, which maximising the spar depth and allows sufficient space for flaps and ailerons. Spars have been sized to so that the wing

box takes maximum advantage of the available structural height within aerofoil contours; this also allows to optimise structural weight [104]. The spanwise variation of bending moment and wing taper mean the spars have been tapered towards the wing tip to increase structural efficiency. [101], [104]. The rear spar is located at 55% of the wing chord, which maximising the spar depth and allows sufficient space for flaps and ailerons. Spars have been sized to so that the wing box takes maximum advantage of the available structural height within aerofoil contours; this also allows to optimise structural weight [104]. The spanwise variation of bending moment and wing taper mean the spars have been tapered towards the wing tip to increase structural efficiency.

Using a classical design approach as outlined in [104], the ribs should be placed at some predefined intervals. However, for modern composite aircraft it is common to minimise the number of ribs and reinforce the skin instead. The S270's wing consists of two ribs at the root and tip and flanges to enable bonding to the skin. Although it is a common to cut out holes in the ribs to reduce the mass, this approach is only valid for homogeneous materials; for composite ribs this poses a significant challenge in terms of material removal and induces unnecessary stress concentrations. Detailed FEM analysis (see section 2.8.4) proved that stringers were not necessary to maintain structural integrity and have not therefore been implemented in the structure. Final wing structural layout can be seen in Fig. 58.

Fig. 58 Wing internal structure layout (skins not shown for clarity).

2.8.4. Wing Finite Element Method (FEM) analysis

The model was built and postprocessing was completed using Patran V9; the solver used was Nastran 2004. Due to time constraints and simplicity, the finite element model only accounts for structural parts of the wing, omitting structurally non-essential parts such as control systems and electrical installations, although these are implemented in the final design. Predefined simulation modes

defined as ‘cards’ were used which are outlined throughout. The model layout with mesh is shown in Fig. 59.

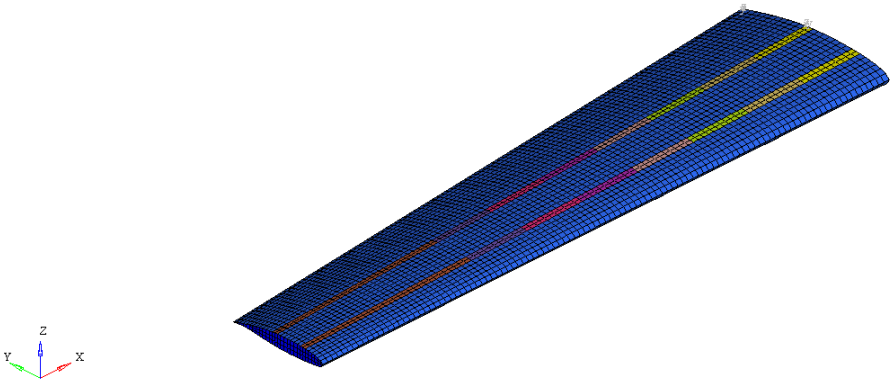

Fig. 139 Wing model layout with mesh.

As previously mentioned, the wing consists of two C-beam spars, two root ribs and wing skins. Spars consist of web and caps; with varying thickness along the span. The skin-removed wing model is shown in Fig. 58. Differing properties of each cap are marked by different colour.

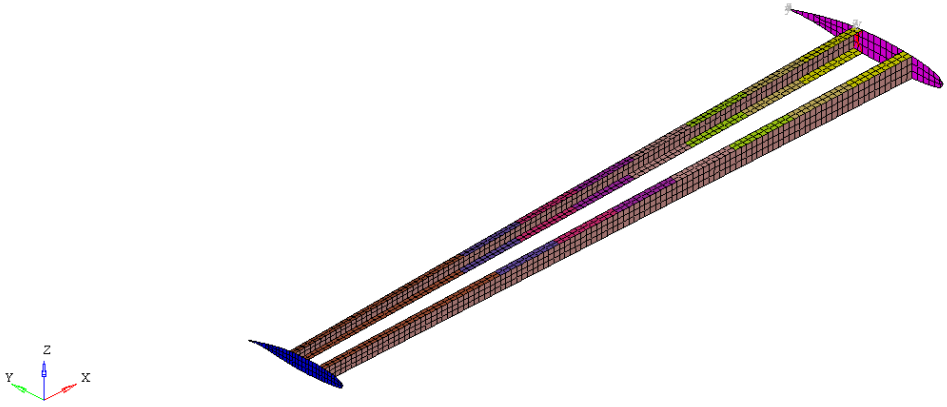

Fig. 60 Wing model layout with mesh without skins shown.

Structural parts of the wing have been modelled using CQUAD4 and CTRIA3 types elements. Those are first order shell elements (2D); examples of these are shown in Fig. 60. [105].

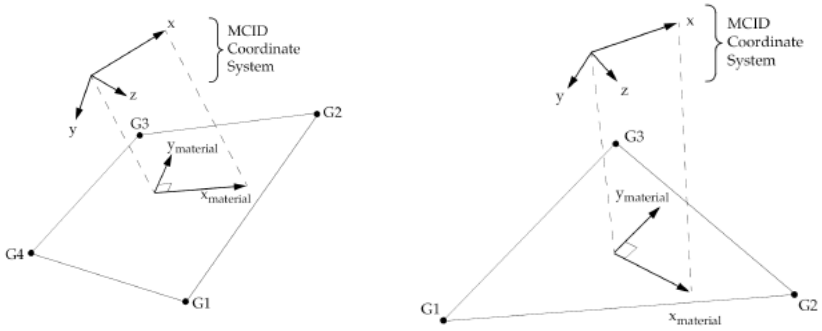

Fig. 61 First order two-dimensional shell elements used for meshing [Nastran QRG]

After analysing the wing structure, the decision has been made that neither solid nor 1D elements were necessary. In addition to 2D elements, RBE2 type elements have been used close to supporting points to apply constrains; RBE2 is ideally stiff element. [105] The model consists of 7182 CQUAD4 and 12 CTRIA3 elements, alongside two RBE2 type elements, giving 6978 nodes in total.[105] The model consists of 7182 CQUAD4 and 12 CTRIA3 elements, alongside two RBE2 type elements, giving 6978 nodes in total.

Few different types of materials have been used. UD CST150 was chosen as unidirectional carbon tape, Interglass 98140 as carbon fabric, Interglass 92125 as glass fabric and Divinycell H60 as foam. Orthotropic materials are listed and described in Table 50; orthotropic materials used card MAT8.

Table 50 Orthotropic material properties used in FEM analysis.

Type	Modullii (GPa)			v_{12}	ρ (kg/m$^{3)}$	Allowable Stress (MPa)		
	E_1	E_2	G_{12}			Compression Tension [1]	Compression Tension [2]	Shear
Carbon tape, UD (CF-UD)	100	3	2.9	0.28	1450	560	40	23
Carbon fabric (CF)	55	55	4	0.048	1400	340	340	196
Glass fabric (GF)	23	23	2.9	0.048	1700	170	170	98

Isotropic materials have also been used in the model; these are listed and described in Table 51. For isotropic material card MAT1 has been used.

Table 51 Isotropic material properties used in FEM analysis.

Name	Young's Modulus E (GPa)	Poisson ratio, v	Density ρ (kg/m$^{3)}$
Foam	0.080	0.40	80
Resin	6	0.35	1500

Table 52 Card properties used for all element except spar caps.

Skin			Spar web			Outer tip rib			Inner root rib		
M*	O**	T***	M	O	T	M	O	T	M	O	T
GF	±45	0.1	CF	±45	0.5	CF	±45	0.25	CF	±45	0.25
CF	±45	0.5	CF	±45	0.5	CF	0/90	0.25	CF	0/90	0.25
Foam	-	8	Foam	-	8	CF	0/90	0.25	CF	0/90	0.25
CF	±45	0.5	CF	±45	0.5	CF	±45	0.25	CF	±45	0.25
			CF	±45	0.5				CF	±45	0.25
*M-material,**O-orientation [deg], ***T-thickness [mm] (refers to individual layer thickness, i.e. for 0/90 or ±45 it is doubled)									CF	0/90	0.25
									CF	0/90	0.25

All composite elements have been made using PCOMPG properties; RBE type elements do not need properties card. The properties of cards used for all elements except spars (which were varying along the span) are shown in Table 52. The properties for spar caps are shown in Table 53.

Table 53 Card properties used for spar caps.

Spar cap	**M**	GF	CF	CF	Resin	CF	CF	CF-UD	CF	CF
	O	±45	±45	±45	---	±45	±45	0/90	±45	±45
	T	0.1	0.5	0.5	2	0.5	0.5	13/9/6.5/4.5/3/2/1/0.5*	0.5	0.5

* - thickness depending from properties

Wing skin consists of 4 layers; the top layer, made from glass fibre at 45°, is not the main element to carry flight loads due to low strength, but it provides good impact resistance which can be of particular importance if something is dropped on aircraft wing during maintenance action for example. There are also two carbon fibre layers of 0.5mm thickness oriented at 45°, designed to carry flight loads such as shear and torsion. Finally, 8mm foam incorporated in between carbon fibre layers provide local stiffness; as a result, stringers are not necessary as the skins structure is already reinforced and does not need any additional support. This was also confirmed by FEM results.

Root ribs have been built using both 0°/90° and +/-45° layers, as it substantially improves the damage tolerance of layered composites, especially as ribs are not redundant elements. This design also limits the area of delamination. No direction is prioritised, so delamination has approximately circular shape.

The main loads applied to the wing are bending and shear, they have been applied so as to achieve proper distribution of shear load. In this circumstance, the applied bending load was higher than required to give conservative results. Loads has been applied as a pressure on lower shell and lower cap. The card used was PLOAD4.

Two RBE2 elements connected to spar webs and spar caps have been used as a support in the model in centroids. Rear point was fully constrained in translations and additionally rotation around X has been also locked. Front point was supported in similar way except lack of locking translation in X direction. RBE2 with supports is shown in Fig. 62.

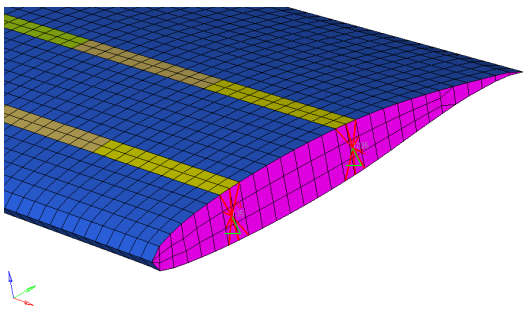

Fig. 62 RBE2 element with supports.

First analysis was concerned with wing displacement under maximum load factor. The maximum displacement was found to be 473 mm, as shown in Fig. 63.

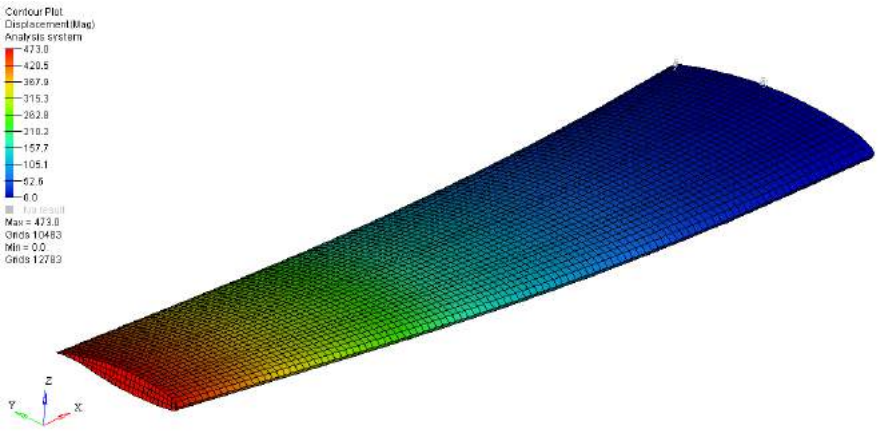

Fig. 63 Displacement distribution.

Stress postprocessing is divided into section describing structure without UD tapes and spar caps.

First stress analysis was done for fabric type structure, the maximum stress was 188.7 MPa, giving reserve factor of 1.8. It is shown in Fig. 64.

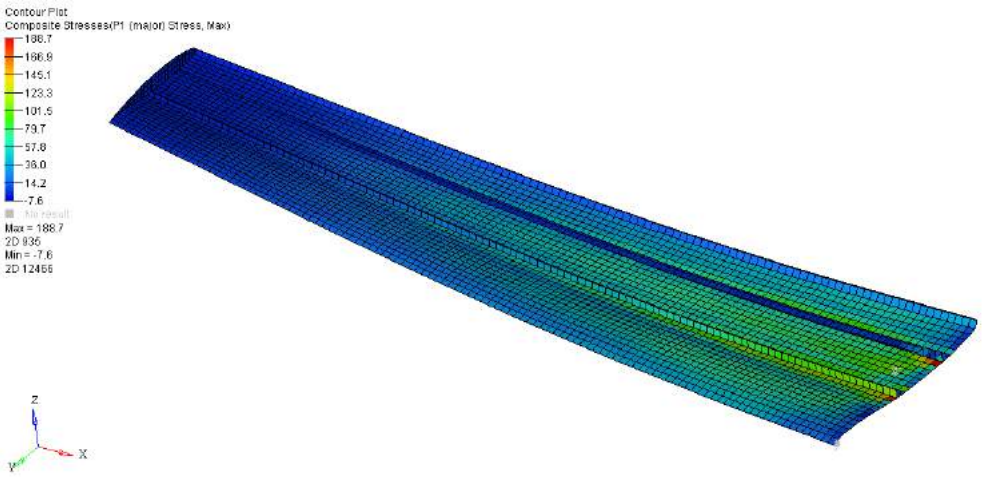

Fig. 64 Maximum stress distribution for fabric structure.

The subsequent analysis was concerned with minimum stress on fabric type structure. From FEM analysis it was found to be 170.5 MPa, which gives a reserve factor of 1.99. Minimum stress distribution is found in Fig. 65.

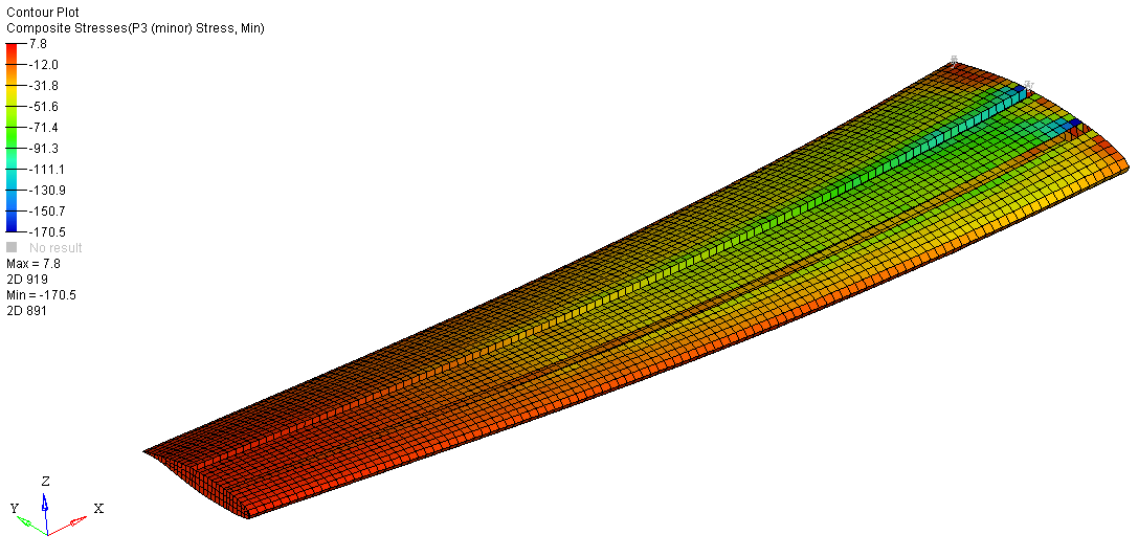

Fig. 65 Minimum stress distribution for fabric structure.

Finally, maximum shear stress on fabric type structure was analysed, found to be is 124.9 MPa for fabric structure and reserve factor of 1.56.

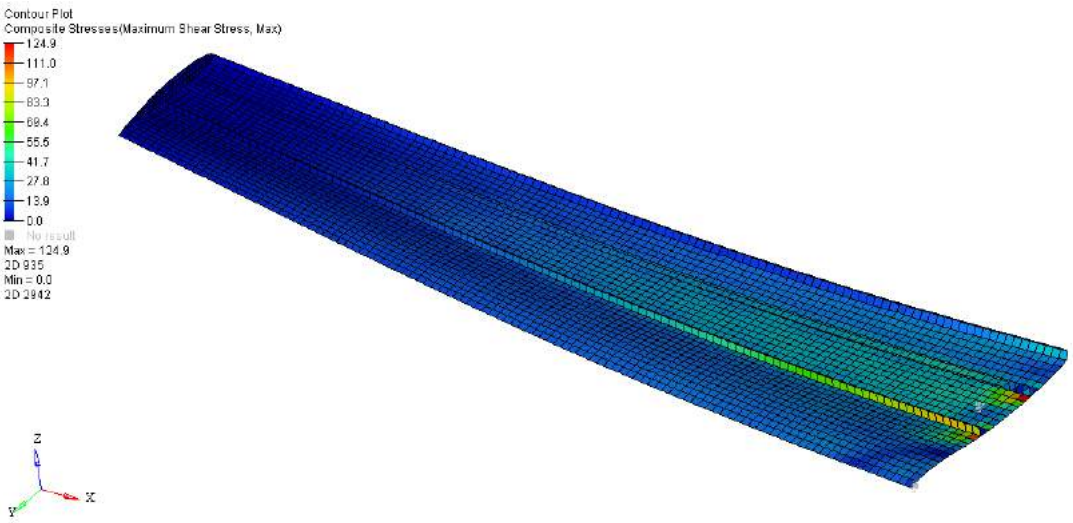

Fig. 66 Maximum shear stress distribution for fabric structure.

In addition, stresses in spar caps have been considered separately, as they differ from other parts due to spanwise thickness variation. As can be seen in Fig. 67, the maximum stress in spar caps is 330.2 MPa, which gives a reserve factor of 1.69.

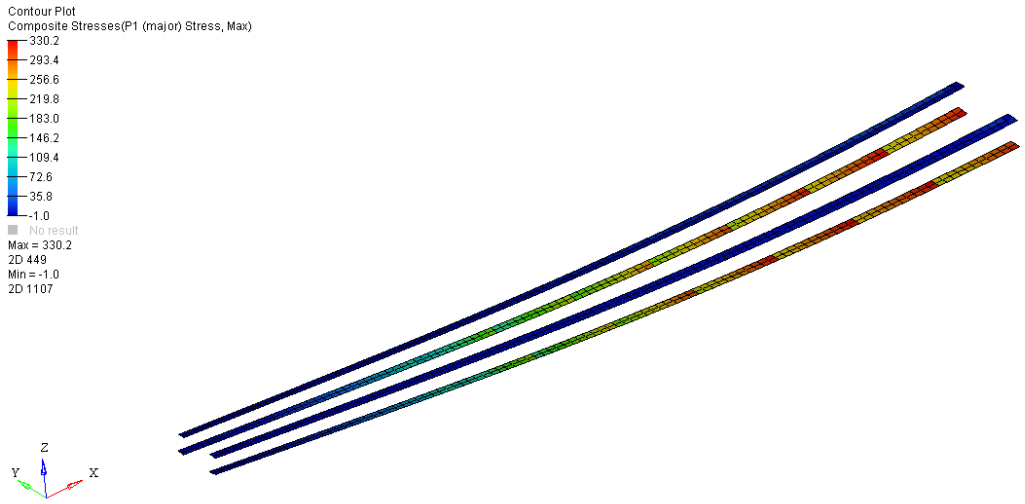

Fig. 67 Maximum stress distribution for spar caps.

Similarly, analysis was done for minimum stress in spar caps. As can be seen in Fig. 68, it reached 337.8 MPa which corresponds to reserve factor of 1.65.

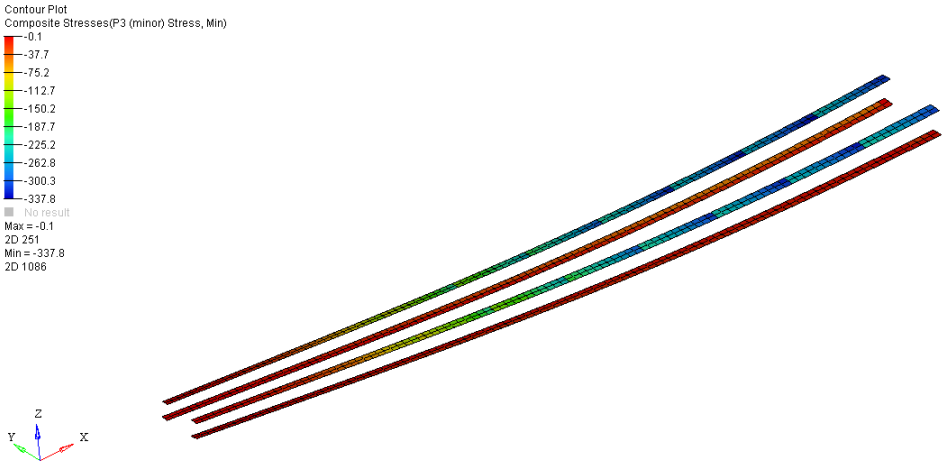

Fig. 68 Minimum stress distribution for spar caps.

Multiple criteria exist to analyse composite failure, one of them is Tsai Hill criterion. It allows to combine different stress components, both principal and shear stresses within a single criterion. It has been implemented for the wing structure, giving maximum failure index of 0.44, which corresponds to safety factor of 1.51. The results are shown in Fig. 69.

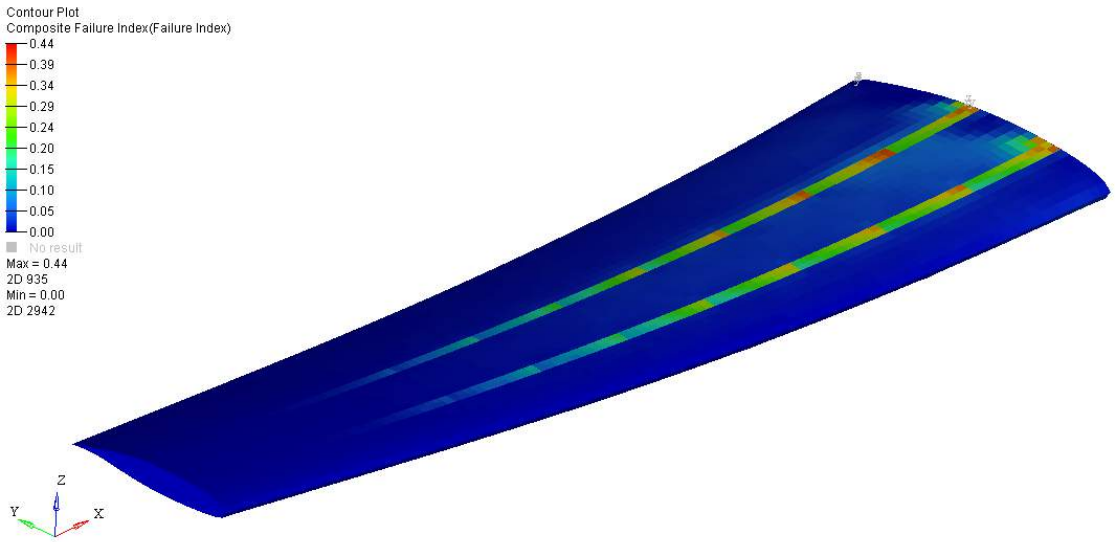

Fig. 69 Tsai-Hill failure criterion.

As in the structure considered sandwich panels replace all internal structure like ribs and stringers, global buckling was considered as a possibility. Lowest reserve factor for global buckling was found to be 1.92, which is considered as a safe value. Buckling analysis results are shown in Fig. 70.

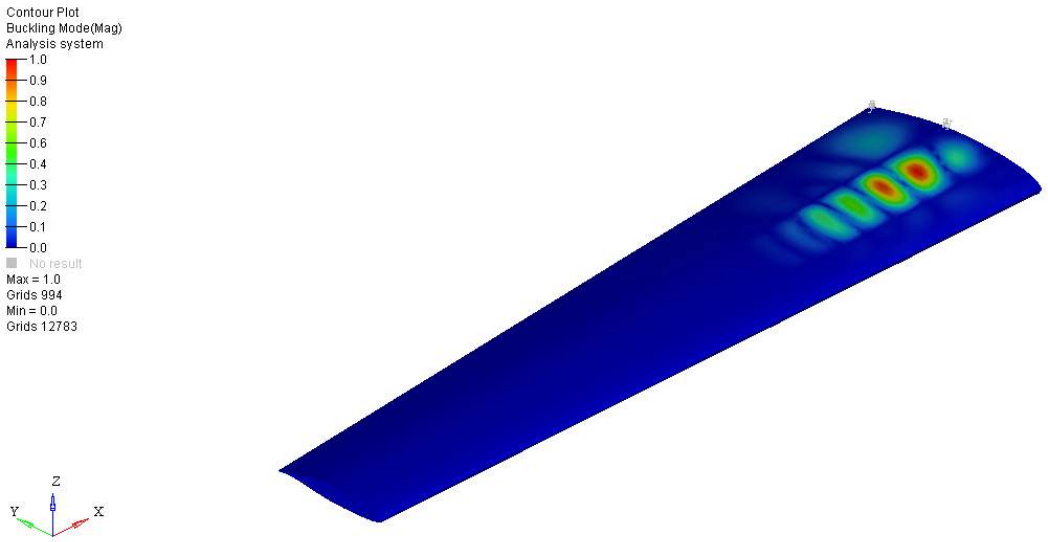

Fig. 70 Global buckling analysis.

2.8.5. FEM Outcomes Summary

Multiple FEM analysis for main structural wing elements proved the structural design feasibility. The wing structure is capable of withstanding loads at maximum load factor with decent reserve factor in all cases. It was also confirmed that having two ribs only as well as lack of stringers will not negatively affect the wing feasibility. Composite failure criteria applied further confirmed that all loads can be carried safely by the wing structure without any failure and with great safety margin.

2.8.6. Fuselage Structural Layout

Two main drivers determined the fuselage materials and structural layout; structural performance at lowest weight and manufacturing costs. Both these drivers are generally higher for composite structures than for their aluminium counterparts.

The S270's fuselage is a semi-monocoque structure which consists of hollow frames in lateral and longitudinal directions, accompanied with fuselage skins reinforced with an aramid fibre honeycomb core. The frames are combined with more structure in areas of increased stress, such as passenger doors and windows; these stress concentrations are then distributed into the skins. The skins' aramid core prevents buckling, dampens skin vibration and provides insulation. This overall fuselage design substantially reduces the required number of frames [103].

Loads from the nose-mounted engine are carried by an engine truss; upper portion truss loads are passed through fittings to hollow frames and via the firewall flange further aft to the rear bulkhead. Similarly, lower portion loads are passed via a flange into fittings to the engine mount reinforcement. The wings are attached to the fuselage using 2-point fuselage tunnel, recommended for a low wing aircraft in [103].

Introducing a parachute as an emergency system requires the implementation of specific structural features. Parachute landing load case requires reinforcement of skins around the passenger seating area, which will be achieved by using unidirectional fibre glass tape, which has better impact resistance than carbon fibre tape. The parachute is mounted to the fuselage with straps incorporated into the skin and are co-cured with fuselage, eliminating the need for bonding.

Due to the large number of Skyride aircraft that will be operating, the risk of lightning strikes is greatly increased. Unlike Aluminium, composite materials suffer from very high electric resistance hence are severely damaged in case of lightning strikes. The nature of this damage is multifaceted and is caused by two mechanisms - thermal effect due to Joule heating and mechanical effect due to shock waves. The temperature within lightning channel may reach up to several thousand Kelvins which damages both carbon fibres and resin. The damage demonstrates itself in the form of resin sublimation, degradation and fibre breakage. Secondary effects also include delamination. Moreover, rapid discharge of energy leads to formation of shock waves which pull the fibres apart and out of plane, the effect called fibre tufting [106],[107]. All these adversely affect strength of structure, hence require costly repairs. In addition, lightning strikes might incur distortions in the functioning of avionic systems, so called indirect effect. For these reasons, lightning strike protection (LSP) will be incorporated into fuselage, wing and tail structure in the form of aluminium mesh embedded into the resin, which evenly distributes the electric charge and hence prevents arising of high temperatures. Although it will increase the weight (hence driving down main lightweight advantage of composite

materials), their incorporation is ineluctable to ensure safe operations in various environmental conditions. Fuselage structure is shown in Fig. 71.

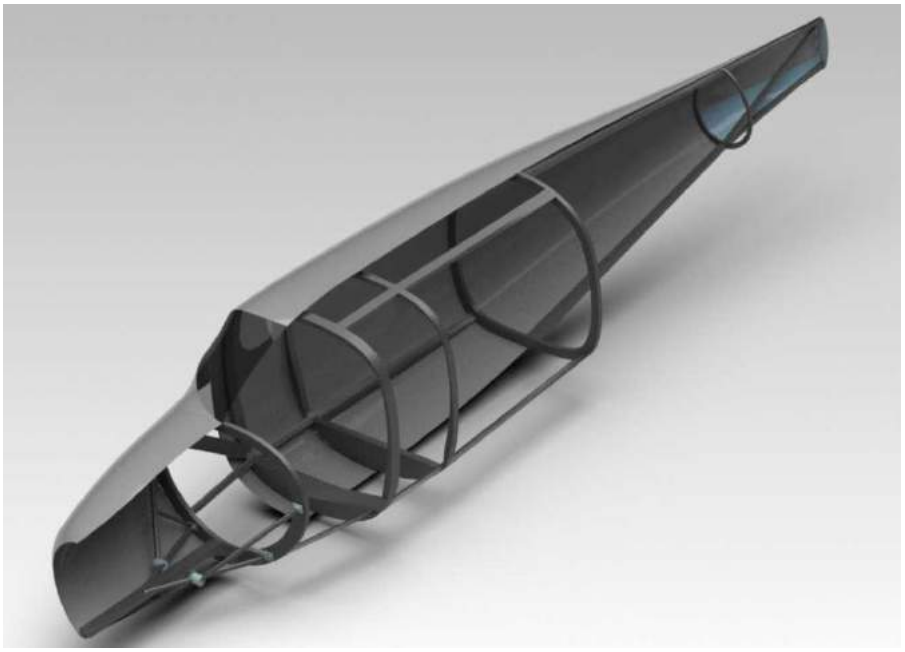

Fig. 71 Fuselage internal structure layout.

2.8.7. Fuselage Manufacturing Process

As previously mentioned, minimising costs is the most important aim of Project SkyRide; therefore, it is a key factor for the fuselage structural design. Three main solutions have been incorporated that helped to achieve this objective. Firstly, structural assembly labour has been minimised by curing the whole fuselage structure as one piece, with all the structural elements incorporated. Secondly, the materials were chosen to be of minimum cost; for that reason, CF/EP prepregs have been excluded at the expense of fibre and resin produced in low cost forms, such as fibre bundle spreading and resin pre-impregnation in-process. This eliminated costs arising from prepregs themselves, the storage requirements and necessity of heat cure. Finally, the use of hollow frames for internal structure provided lightweight and efficient elements with excellent load bearing capability with minimum complexity coming from core material. The core material is added in case reinforcement is necessary at a specific location.

Low cost composite manufacturing approach proposed in [108] has been chosen for S270's fuselage manufacturing process. Carbon fibres are produced from low cost polyacrylonitrile yarn. The bundles are in-line impregnated with epoxy and spread at desired orientation on the fuselage mandrel. This technique, called direct filament winding, allows for very accurate placement of individual fibres, and variation of parameters such as thickness, depending on stress distribution character. Complex shape of fuselage induces need for numerical control of the winding process; head controls will correctly orient fibre bands onto the rotating mandrel surface at even most structurally complex

locations. Most of the loads are carried by hollow frames; they are manufactured using frame mandrels. Any discontinuity within the fuselage structure, such as doors or windows is potentially a weak point. At the point where the doors are latched to the fuselage doorjamb, the frames are not hollow but filled with foam, which provides extra stiffness. The doors are also reinforced with ultra-lightweight aramid honeycomb, which can be formed into curved shapes and has excellent mechanical properties. Hollow frames are placed onto the fuselage structure integrates with doors, bulkhead and engine truss**.** The consolidation and curing are completed with outer mould line mould under pressure applied from within the mandrel, and heat from an industrial oven. Finally, surface finish is obtained by applying full vacuum to the cavity in the mould. Upon completion of curing, mandrel is removed from within the fuselage, as well as hollow frame toolings.

2.8.8. Empennage Structural Design

V-tails require reinforcements in the structures as it can experience high torsional loading when the ruddervators deflect in opposite directions, which is usually necessary to provide good control and stability. These torsional loads are smoothly transmitted to the fuselage frames via tail spars. The spars of the V-tail consist of an extra stub spar, which further reinforces the structure.

The main structural components of tail plane consist of spars and ribs. Adopted process for structural layout followed the rules in [104]. The internal structure of the tail consists of two spars located at 15% and 55% of the chord and 2 ribs positioned at the root and tip, allowing sufficient space for hinges about which the ruddervators are pivoted. Large spacing between the spars will help to improve strength in cross-winds. The ruddervators are attached to the tailplane at 4 points with 2 electro-hydrostatic actuators used at the inner and outer points. The skin of the rudder is made from a composite honeycomb structure to help strengthen the internal structure of the control surface. No holes are incorporated into the ribs to avoid stress concentrations. Internal structural layout of the tail can be seen in Fig. 72.

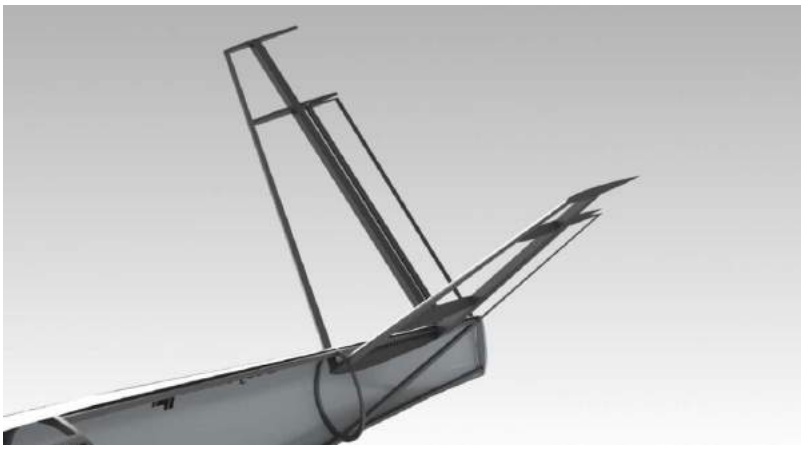

Fig. 72 Tail structural internal layout.

2.8.9. Summary

Composite materials have been chosen to make up whole structure of S270, for multiple reasons, including their omnipresence in general aviation market, excellent properties in comparison to homogeneous materials and development of low-cost manufacturing techniques. Finite Element Analysis using Patran V9 and Nastran 2004 proved that the structure of S270's wing is able to carry the loads under maximum load factor with a good reserve factor, which was further confirmed by analysis with failure criteria.

Fuselage design was aimed at minimising manufacturing costs. It was achieved by using low-cost composite materials and curing the structure as a single piece. As pressurisation is not necessary at cruise altitude, the structural requirements on the fuselage structure are not that severe, which allows for a less conservative approach. This included use of hollow frames as main load-bearing elements alongside skins reinforced with aramid honeycomb. For safety reasons, hollow frames at structurally weakest points have been filled with foam. Although it would be ideal to perform FEM analysis of the fuselage, time constraints of the project did not allow for it; as a future development, FEM analysis should be performed to prove the fuselage structural design feasibility.

Finally, for V-tails which usually carry higher loads than their standard counterparts, a similar approach to the main wing was undertaken leading to two ribs and two spars for each of tail planes. The structure is further reinforced by the stub spar near the leading edge to further counteract torsional loads.

2.9. Mass Estimation and Centre of Gravity

Section 1.9, Table 7 shows the complete mass breakdown of the S270 Aircraft.

As Roskam's books [109] were backdated, composite weight reduction had to be considered. A weight density factor of 0.6 was multiplied to the weight of each structural component to scale them down from aluminium to composites. This factor was calculated by finding the ratio of tensile and modulus strength between Hex Ply and Aluminium [110].

Due to the use of an advanced hybrid propulsion system and Fly-By-Light technology, the weights for the powertrain and electrical components are set higher than normal. However, factors were also included to suggest those component weights would be slightly less by the set release year of 2025. The battery weight was calculated in Section 2.7 and the fuel weight was estimated in Section 2.6.

Centre of Gravity was used to calculate where the wing should be placed on the aircraft. By splitting the aircraft into two groups; wing and body, moments could be taken to find the Leading-Edge MAC number. This method is visually shown with equations below [111] :

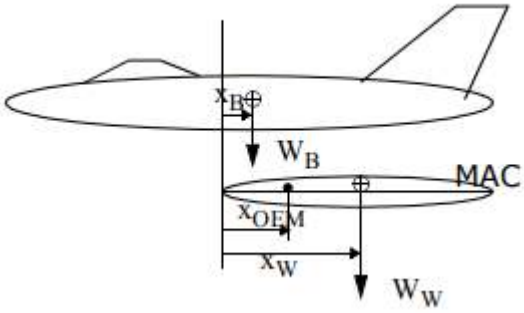

Fig. 73 Wing placement diagram.

$$(W_B + W_W)X_{OEM} = W_B X_B + W_W X_W \tag{23}$$

$$X_B = X_{OEM} + \left(\frac{W_W}{W_B}\right)(X_{OEM} - X_W) \tag{24}$$

$$X_{LE} = CG - X_B \tag{25}$$

Table 54 Wing placement values.

Symbol	Meaning	Value
$\boldsymbol{W_B}$	Weight of fuselage including nose landing gear	1507kg
$\boldsymbol{W_W}$	Weight of wing including main landing gear	164kg
$\boldsymbol{X_B}$	Distance from datum line to Fuselage CG	0.215m
$\boldsymbol{X_W}$	Distance from datum line to Wing CG	0.566m
$\boldsymbol{X_{OEM}}$	Operational empty centre of gravity	0.25CG
$\boldsymbol{CG}$	Fuselage centre of gravity	4.06m
$\boldsymbol{X_{LE}}$	Distance from nose to LE of wing	3.84m

2.9.1. Centre of Gravity Envelope

The centre of gravity of the aircraft changes throughout the flight mission. This change primarily comes from the fuel burn; the aircraft Centre of Gravity (CG) moves further away from the CG of the fuel as the mission progresses. The aircraft has the furthest forward CG during landing, where there is only 38kg of fuel remaining. Therefore, the full landing the weight of the aircraft is 1634kg and the CG is located 3.82m aft the nose. The aircraft has the furthest back CG during take-off, where max weight is 1671kg and CG is located at 4.06m aft the nose. This case is similar for both ferry and full missions.

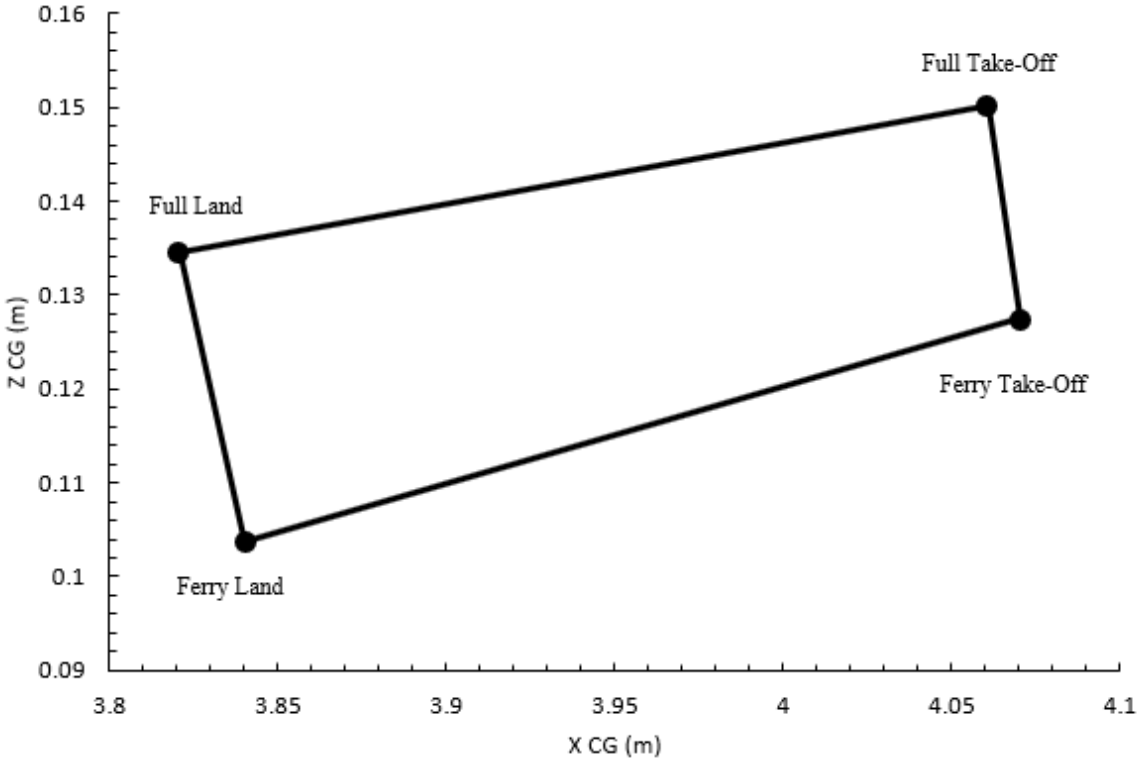

Fig. 74 Centre of gravity envelope.

2.10. Cabin Sizing / Internal Layout

The cabin has been designed to accommodate the needs of the general public, along with the high frequency flights that this aircraft will operate. Boarding and departure is achieved by utilising an external ramp that will be available at the airports. The cabin has a width of 1.5m and a height of 1.67m.

2.10.1. Seating

The cabin will have four passenger seats, constructed of Ambla synthetic leather for endurance, stain resistance, ease of maintenance and comfort. As shown in Fig. 75, the seats are organised in a 2-by-2 configuration with a 0.35m gap in between the front pair of seats, allowing easy access to the back seats. There will be a small amount of space allocated beneath passenger seats to accommodate for the standard luggage allowance. The seats are designed to give adequate space for passengers, with a seat width of 0.47m and a pitch of 0.87m.

2.10.2. Appeal

The cabin has also been designed to be appealing to increase the satisfaction from passengers. LED lights have been added to allow the pilot to change the ambient lighting to whatever could be deemed necessary, for example blue lighting has been found to make passengers feel more relaxed.

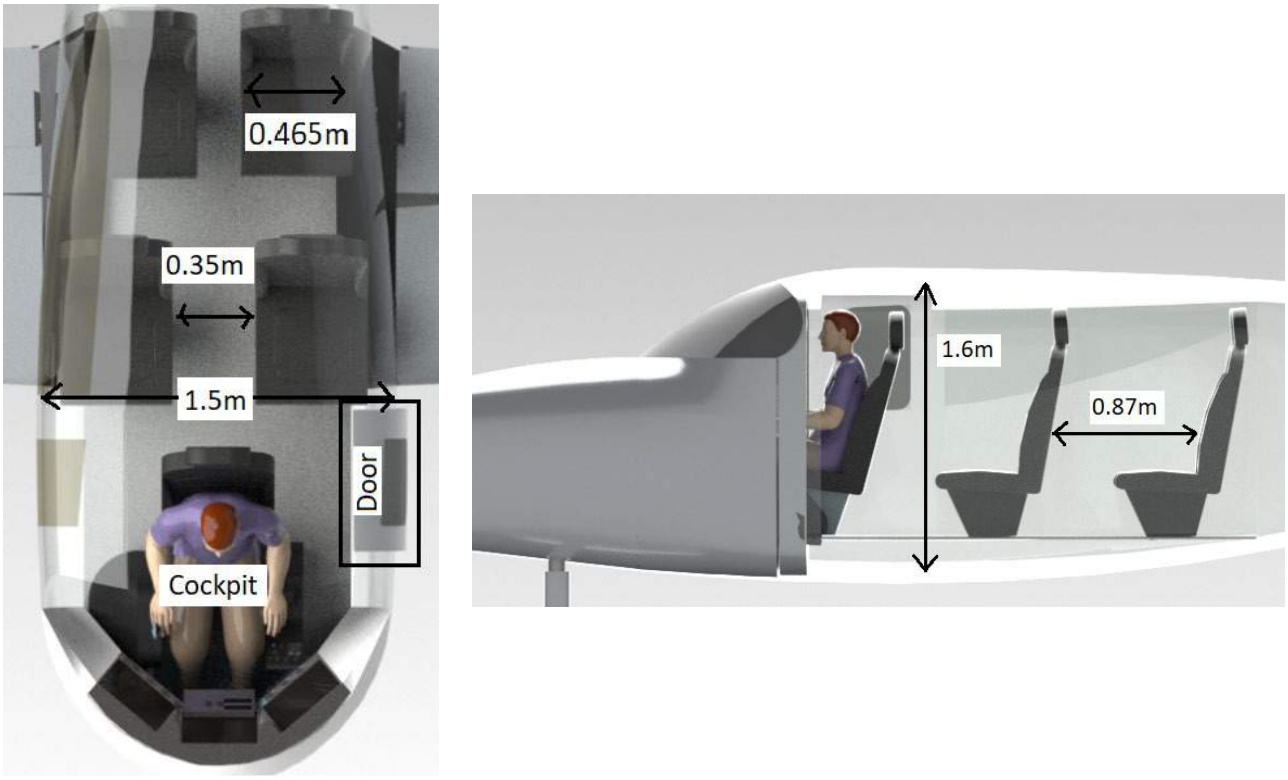

Fig. 75 Dimensioned internal layout.

2.11. Parachute System

When Cirrus designed the parachute system CAPS (Cirrus Aircraft Parachute System), they listed certain attributes that had to be fulfilled to make it successful. The S270 parachute system was designed along the same characteristics:

- SMALL AND LIGHT: The parachute cannot be too heavy where it affects centre of gravity restrictions and aircraft efficiency. It must also not be too large and should not affect passenger comfort.
- RELIABLE: It should be viable to use under a range of emergency conditions, such as engine failure and adverse weather conditions. This gives a sense of trust and safety for owners, pilots and passengers.
- SIMPLE AND FAST: Parachute deployment may be needed near the ground therefore it is important that it is easy and fast to deploy, as every second counts in an emergency.

Parachute deployment scenarios:

- ENGINE FAILURE: In any case of complete propulsion system failure (ICE and power augmentation) where there is no runway nearby, the parachute system must be activated immediately. This includes forced/emergency landing on any surface terrain. In a case where

there is a possibility to glide to a nearby runway the pilot may continue without deploying the parachute.

- AIR COLLISION: Most mid-air collisions with wildlife or other aircraft will cause external damage to the aircraft. This may include complications to primary and secondary flight controls, as well as structural damage to landing gear and main body. In any case of collision, parachute deployment is highly recommended.
- LOSS OF CONTROL: If the pilot loses control of the aircraft due to system failure, turbulence or any other unforeseen circumstances, parachute deployment should be immediate.
- PILOT INCAPABILITY: If a pilot becomes medically incapable of flying the aircraft, the passengers should immediately deploy the parachute.

The deployment of the S270's parachute sequence will be set up as follow:

(1) Activation:

To activate the parachute system, the pilot or passenger (in circumstances when pilot becomes unfit to fly), removes the safety cover and pulls on the handle located in the ceiling. The safety cover is in place to ensure accidental deployment does not occur.

(2) Parachute Extraction:

As soon as the handle is pulled, the cable attached to the handle engages the rocket to ignite. The rocket then extracts the parachute bag from the aircraft fuselage. The bag then opens at full extension, ensuring the parachute can open in free air and away from any dangers of entanglement with aircraft.

(3) Parachute expansion and extension:

The cable of the parachute is embedded under the fuselage skin at four symmetrical points. The arrester cable that travels from the rear of the aircraft to the front during deployment, allows the aircraft to be supported evenly rather than just at one point to the rear of the aircraft. As the parachute opens, it stretches the harness cables to release from under the skin and fully extend. The parachute then fills with air, allowing the aircraft to naturally pitch up which then leads to a natural decrease in airspeed, known as aerodynamic braking.

(4) Altitude decline and touchdown:

Under full parachute conditions, the aircraft will descend to the ground between 1600-1700 feet per minute. The ground impact on touchdown is calculated by CAPS [32] to be equivalent to dropping the aircraft from a height of 4 meters. The level of loads on impact can be absorbed by the reinforced landing gear, airframe and cabin.

Figure 76 shows the parachute sequence visually [112].

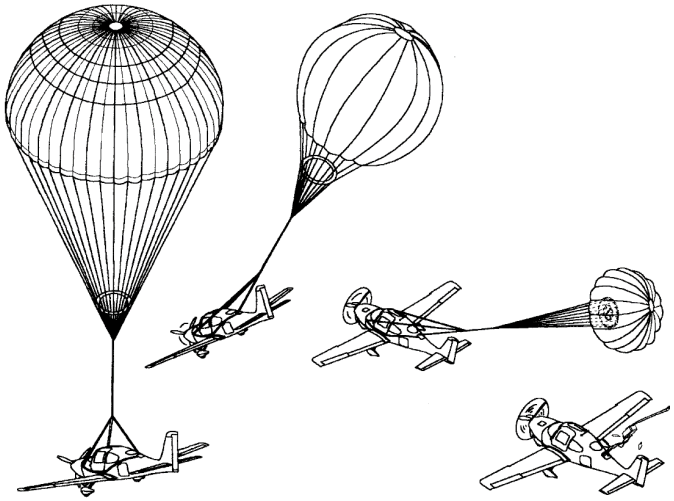

Fig. 76 Parachute deployment sequence.

The parachute system for the S270 weighs 49kg and is placed in an enclosed section at the back of the cabin, 5m aft the nose. The parachute when fully deployed has a diameter of 20.5m. Figure 8 presented in Section 1.10 shows the parachute in full deployment with the S270 Aircraft.

2.12. Landing Gear

The S270 has a fixed tricycle landing gear configuration. This was a critical design choice as it affected both mass and drag calculations, as fixed and retractable configurations give a variety in values. An in-depth preliminary analysis of both landing gears was undertaken, with the advantages and disadvantages compared. One of the major factors that led to the selection of fixed landing gear was the cost implications of a retractable gear. On average for a small general aviation aircraft, a retractable landing gear adds $30,000 onto the selling price. Along with this, the costs increase further when including the extra 50% on insurance costs and 20% on maintenance costs when compared to fixed gear. A downside to fixed gear is the drag penalty during climb and cruise phases, however due to modern technology and the use of wheel fairings, drag on fixed gears can be reduced by up to 50% [113]. An in-depth aerodynamic study was undertaken to compare landing gears with and without fairings; results can be seen in Section 2.3.10. Taking into consideration the substantial savings in cost and possibilities in reducing drag significantly, the fixed landing gear is the most suitable configuration.

As the S270 is a single engine aircraft, it is a requirement that it must have a parachute as a redundancy measure. Cirrus SR22, a competitor aircraft, has the feature with a fixed landing gear. This design choice is focused primarily on emergency scenarios: if the engine has failed and the parachute deploys, the fixed landing gear will take all the loads on impact. However, if the engine

failed on a retractable landing gear aircraft, the impact would be taken solely by the fuselage, thus enhancing any dangers on the passengers and pilot along will excess repair costs.

2.12.1. Design Approach

The landing gear was designed using the methods and constraints described by Roskam [114]. The main constraints are as follow:

(1) FAR 23.925 states that there must be a gap of 7 inches or more between the ground and propeller; this was used to design the landing gear strut length.
(2) The nose gear must support between 5%-20% of the aircraft weight. This is important as it allows for smooth manoeuvrability on the ground.
(3) Tip back angle must be greater than 16^{o} but no greater than the rotation angle of the aircraft.
(4) The angle between the main gear and CG must be between 10^{o} and 25^{0} [115].

2.12.2. Final Design

Table 55 Landing gear parameters.

Parameter	Description	Parameter	Description
Nose Gear location	1.42m aft Nose	Main gear tire width	0.13m
Main Gear location	4.5m aft Nose	Tip back angle	21o
Nose gear tire diameter	0.5m	Nose gear loading	2874N (17.5%)
Nose gear tire width	0.17m	Main gear loading	13518N (82.5%)
Main gear tire diameter	0.35m	Strut length	0.903m

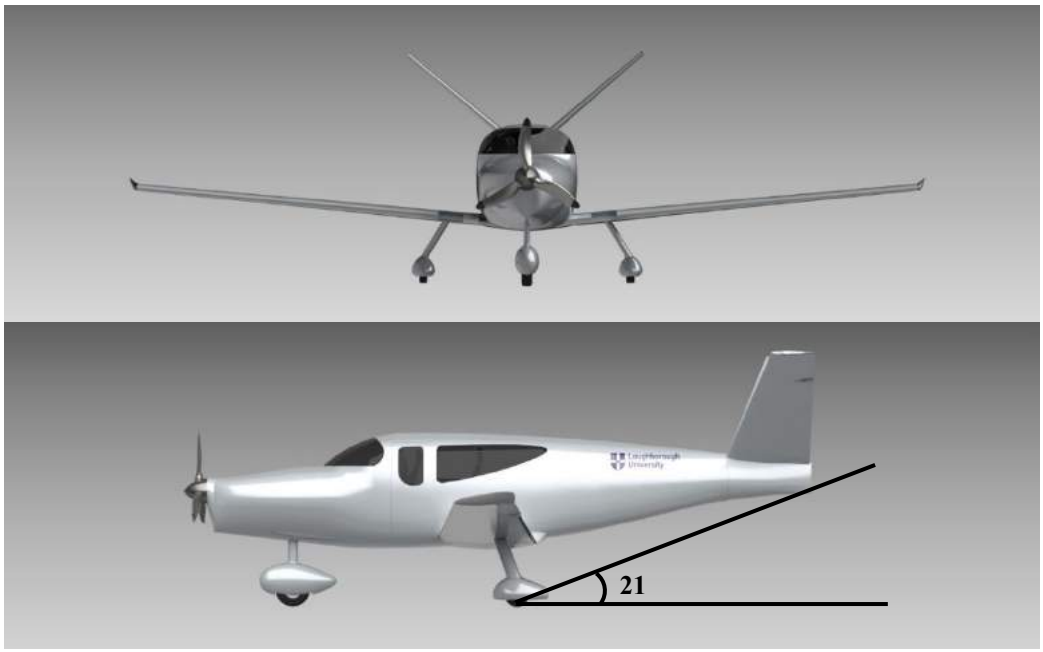

Figure 77 Landing gear configuration with tip back angle

The nose and main landing gears were designed according to the location which gives the optimal value on the loads carried. Constraint 2 states that the nose gear must support between 5%-20% of the aircraft weight during take-off and landing. This allows the plane to be balanced during take-off and ensures that the nose wheel has enough traction for steering during taxi. For the S270, the nose gear is placed 1.42m aft the nose, giving 17.5% of the aircraft ground loads. This percentage is within the required range of 5% to 20%, hence is acceptable under Roskam's conditions. The main gear is placed 4.5m aft the nose, supporting 82.5% of the ground loads. The full list of landing gear dimensions can be seen on Table 55 and visual representation can be seen in Fig. 77 and 78.

Fig. 78 Landing gear attachment views.

2.13. Systems

This section introduces the sub-systems integrated into the aircraft. It comprises of the layout of each and discusses the operation of the components within. In addition, some include potential parts for the S270, whilst others demonstrate the feasibility of the technology to be used

2.13.1. Cockpit Design

The Cockpit has been designed to have 3 large touch screens, along with 6 flight indicators, emergency controls and a radio control panel. The 3 large screens display the most important information to the pilot, this includes a synthetic vision display, virtual map and mission/aircraft information and control. The primary control stick is placed to the right of the pilot's seat and the secondary flight controls (such as thrust and flap control), are placed on the left of the pilot seat. The cockpit also features an emergency override button that disables autopilot functions and returns the aircraft back into the pilot's control (for the unlikely event that autopilot malfunctions). The

emergency override also unlocks the parachute deployment lever that is locked by defaults to prevent accidental deployment.

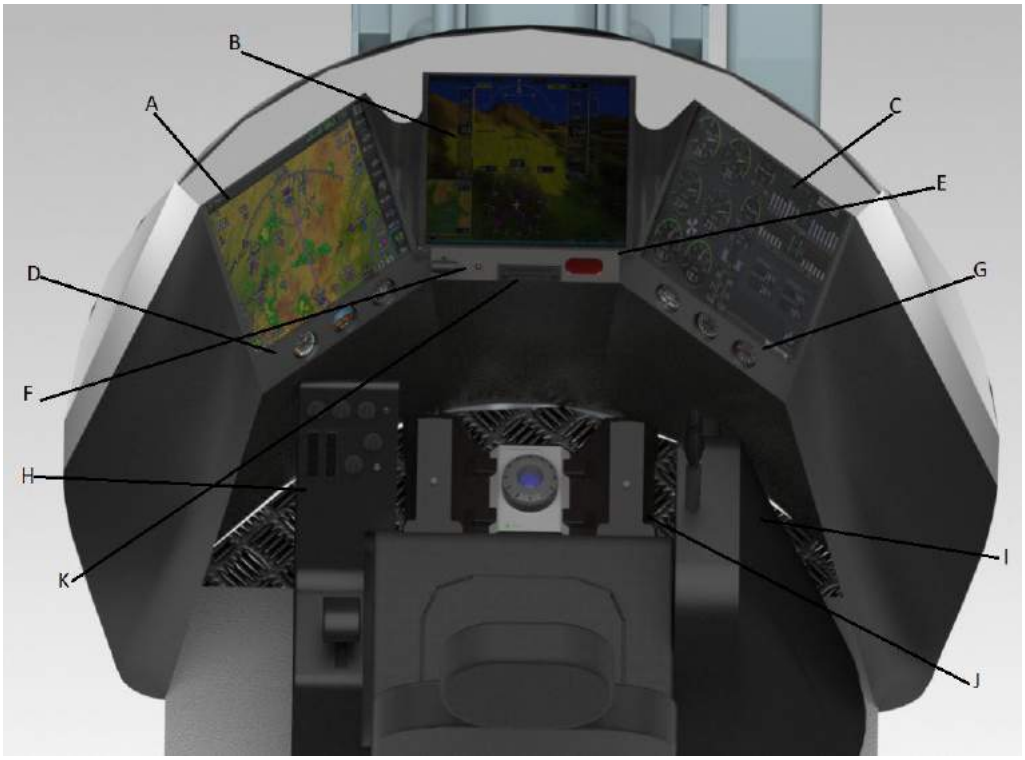

Fig. 79 Labelled cockpit configuration. A – Virtual map display. B – Synthetic vision display. C – Aircraft/mission status and information. D - Airspeed, attitude and altitude indicators. E - Emergency override. F - Parachute release switch. G - Turn co-ordinator, compass and climb rate indicator. H - Secondary Flight Controls. I - Flight Control Stick. J - Rudder Pedals. K - Radio Control Panel

2.13.2. Flight Control Systems

The flight control system of the S270 considerably promotes the move towards more electric aircraft (MEA) [116][117]. A mechanical cable-pulley system is common amongst light aircraft; however, the S270 will be equipped with a more modern, FBL (Fly-By-Light) system. In order to implement this technology, the control surfaces of the aircraft must be operated by actuators. Thus, a combination of Electro-Hydrostatic (EHA) and Electro-Mechanical Actuators (EMA) were chosen. Figure 80 in Section 2.13.8 shows a schematic of this system.

Jamming is a major challenge with EMA, which results in a locked or 'hard-over' state; therefore, this type would be unsuitable for flight critical controls. As a result, EMA will be assigned to secondary control surfaces, i.e. flaps and spoilers. The primary control surfaces will be actuated with EHA in combination with the Flight Control Computer (FCC). This allows for more precise operation of the aircraft via the transducer along with reduced pilot effort [118]. These actuators are also efficient as they draw little to no power when they are not in use, due to a Power-by-Wire setup [119]. In comparison to a fully hydraulic system, the total mass of the actuators is drastically reduced as the need for extra components such as reservoirs is eliminated.

However, to test the feasibility of such actuation, research was conducted on the implementation of EMA and EHA in light aircraft. In 2003, an in-flight test was conducted on the PZL-110 “Koliber”, which is of comparable size to the S270. The test analysed the deflection of the aileron and elevator to the desired input. It concluded that the aircraft successfully performed all the required manoeuvres with minimal differences in the deflection angle. Further laboratory tests in 2005 revealed that EMA could successfully position control surfaces to 0.1 degrees [119]. A more elaborate experiment was performed on an F-18 installed with EHA and EMA; this aircraft was instructed to fly relatively aggressively at various Mach numbers. Despite the success of this test, a problem to arise was the thermal performance of the EMA [120]. However, as the S270 would neither fly in this manner or be used for control surfaces that would experience such high loads, this is not of major concern. Considering the technology has been investigated for the past fourteen years alongside with two years-time of development in the future, it is reasonable to assume it will have matured by 2025.

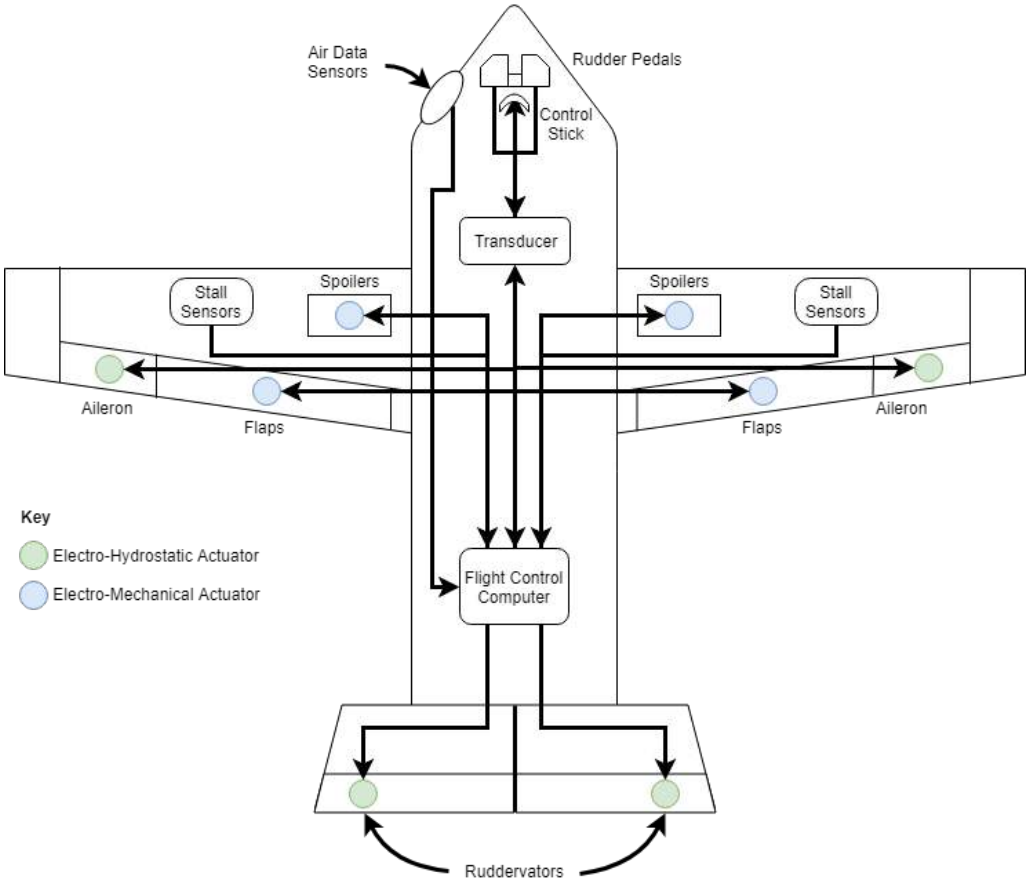

Fig. 80 Flight Control Systems

2.13.3. Avionic Systems

The use of actuators for control will inevitably increase the mass compared to a standard cable-pulley system. To compensate for this increased mass, an FBL system has been implemented; this allows the transmission of higher bandwidth signals, along with reduced mass for wiring and greater resistance to electromagnetic interference [121].

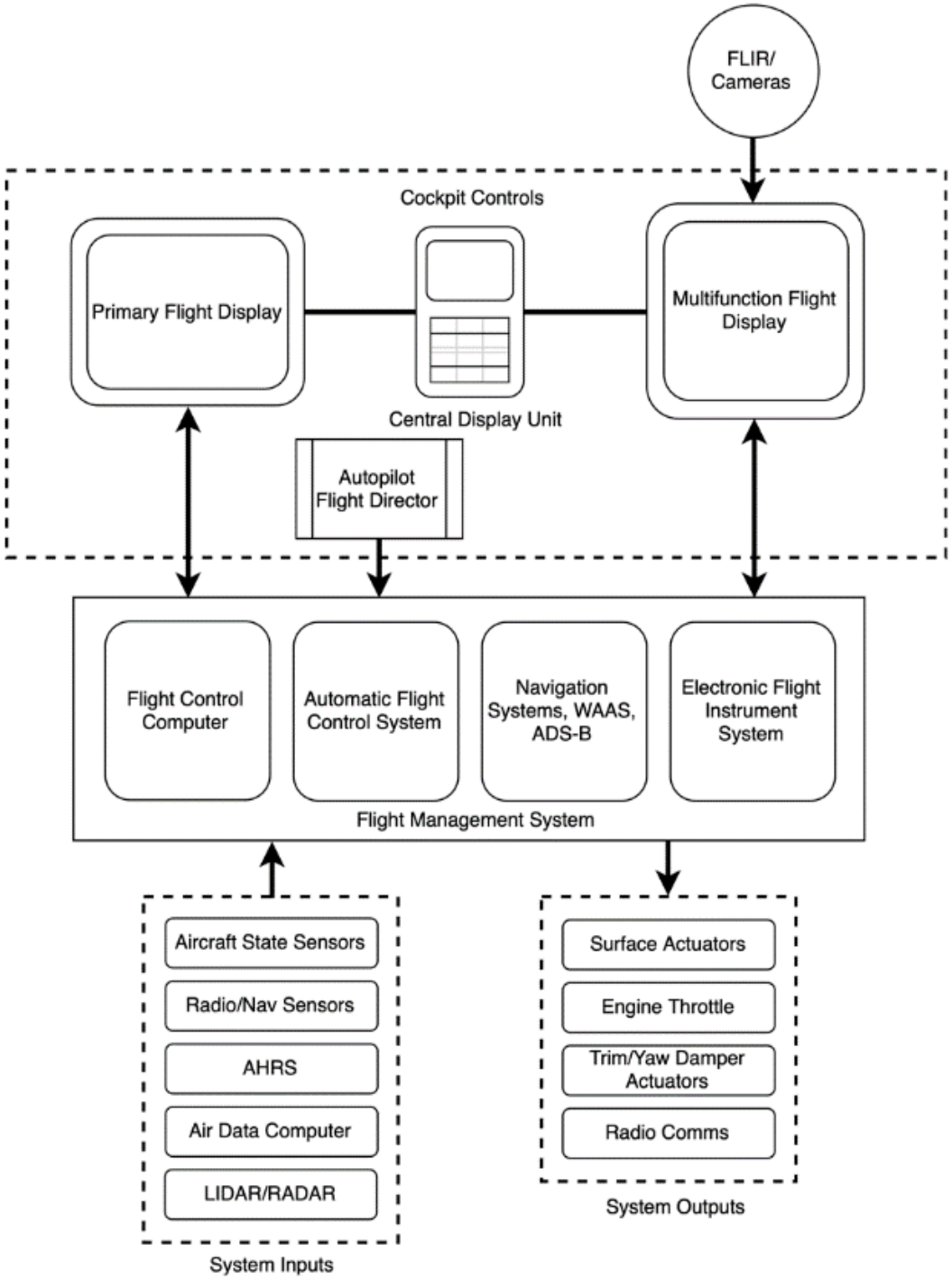

Fig. 81 Avionic Systems

Figure 81 illustrates a schematic of the avionic systems in the aircraft. The contents in the dotted box contain all the interactable displays. These units are connected to the FMS which includes all the inertial, navigation and communication sensors/receivers [122]. The systems prevent excessive inputs from the pilot ultimately reducing control surface loads and prolonging the lifespan of the aircraft [123]. In conjunction with standby displays, the Electronic Flight Instrument System (EFIS) will serve the purpose of keeping the pilot informed of the state of the aircraft.

As per the FAA regulation, all aircraft must be equipped with ADS-B OUT by 1st January 2020 [124]. Therefore, the aircraft includes the Garmin GNX 375 which meets the requirements of ADS-B OUT and also encompasses the benefits of ADS-B IN [125]. This transmits the aircraft's current position and state, as well as receive and interpret other participating aircraft's ADS-B Out data. Additionally, the subscription-free weather information can be taken advantage of [126].

The aircraft also incorporates some level of autonomy on the ground. On-board cameras including RADAR, LIDAR and FLIR will be used to autonomously taxi around the airport and is especially useful at locations with little infrastructure and lighting; this can be made possible by airport maps such as Garmin SafeTaxi where taxi routes, other aircraft and ground equipment are all shown on the navigation display to keep the pilot well informed [127].

A glass cockpit type interface with minimal dials will be used as they provide additional information and functionality. A previous study had investigated traditional mechanical dials; a hybrid option, which combines mechanical instruments with a GPS navigation system and a Technologically Advanced Aircraft (TAA) equipped with full glass cockpit displays. The study evaluated the ease of use for each with an evaluation matrix [128] which ranked accessibility based on the number of physical actions and the importance of the information required. It concluded the TAA system produced higher scores as these avionics provided more information to the pilot, especially for navigation use. However, limited physical dials also meant some communication functions were buried under menus, thus took longer to access; this can be resolved with independent switches or a remap of the GUI [129].

Garmin provide certified displays for single-engine piston aircraft along with a reliable service. The new Garmin G3X Touch satisfies the needs of the S270 [130]. Table 56 displays the list of avionics to be used in the cockpit which allow seamless compatibility across all systems.

Table 56 Individual avionic systems.

Systems	Parts	Systems	Parts
PFD/MFD	Garmin G3X Touch	ADS-B/Weather	Garmin GNX 375
Standby/Back up Flight Instrument	Garmin G5	Autopilot	Garmin GFC 500
Navigation/Communication	Garmin GTN 750	Audio Panel	Garmin GMA 345

2.13.4. Fuel and Power System

The fuel system within the aircraft is largely conventional in nature as a complex fuel system is not required due to the small amount of fuel carried. The battery power will be the main concern in terms of weight and requirement. Figure 82 shows the fuel and power delivery system. The fuel is stored in the wings where collector tanks are used to draw the amounts as and when required. Fuel is stored in the wings as it is easily accessible for refuelling. It also saves cabin space for passengers and other systems. The cross-feed valve is implemented as a backup in the event that a fuel line or tank becomes damaged. A fuel filter ensures the supply is free of any impurities before progressing to the Fuel Control Valve which regulates the amount of fuel based on the demand from the throttle input from the FMS. Finally, the engine driven fuel pump directs the fuel to the manifold where it is distributed to the fuel injectors as required. The battery pack is positioned in the empennage section of the fuselage; this was chosen to compensate for the centre of gravity off-set due to the engine weight. Additionally, battery replacements can be done seamlessly alongside passenger boarding. The parallel hybrid system employs redundancy as the power supplied from the batteries is delivered directly to the transformer; therefore, the fuel and the electrical system are kept separate.

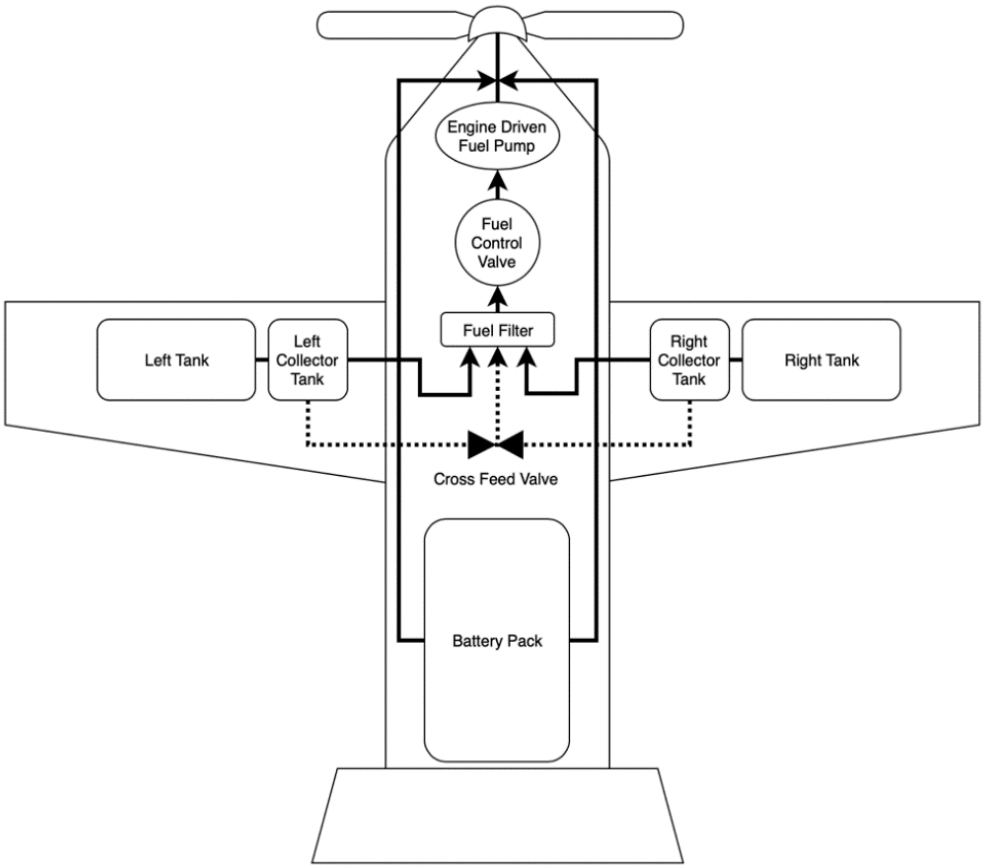

Fig. 82 Fuel/Power Systems

2.13.5. Environmental Control System

Figure 83 illustrates the network of the Environmental Control System (ECS). At 12,000 ft, it is not required to have a pressurisation system in place, thus the S270 does not employ this [131]. The ECS accounts for 75% of the non-propulsive power, therefore efficiency is a primary factor. As the aircraft is classified as an MEA, a completely bleed-less system has been adopted in the interest of improving fuel consumption [132]. Similar to the Boeing 787, the electric compressor would replace the conventional system and feed temperature-controlled air into the heat exchanger. The ram air inlet is also responsible for providing breathable conditions in the cabin alongside the evaporator which maintains humidity levels around 15-20% [133]. Smoke detectors in the cabin serve the purpose of releasing the emergency oxygen masks from overhead. Release catches on these masks ensure oxygen is not wasted on unoccupied seats.

As mentioned in Section 2.7.3, the batteries require independent cooling. The radiator in this liquid cooling system must be temperature-controlled in order to keep the batteries within operating temperature; this is maintained by the aircraft's air conditioning system. ThermaCool provides an electric air conditioning system suitable for the S270. It is run on a 28V DC system, thus seamlessly integrates with existing electrical system. It is also efficient as it requires less than 45 A at peak load. In order to activate the system, the pilot is only required to set the temperature on a digital display [134].

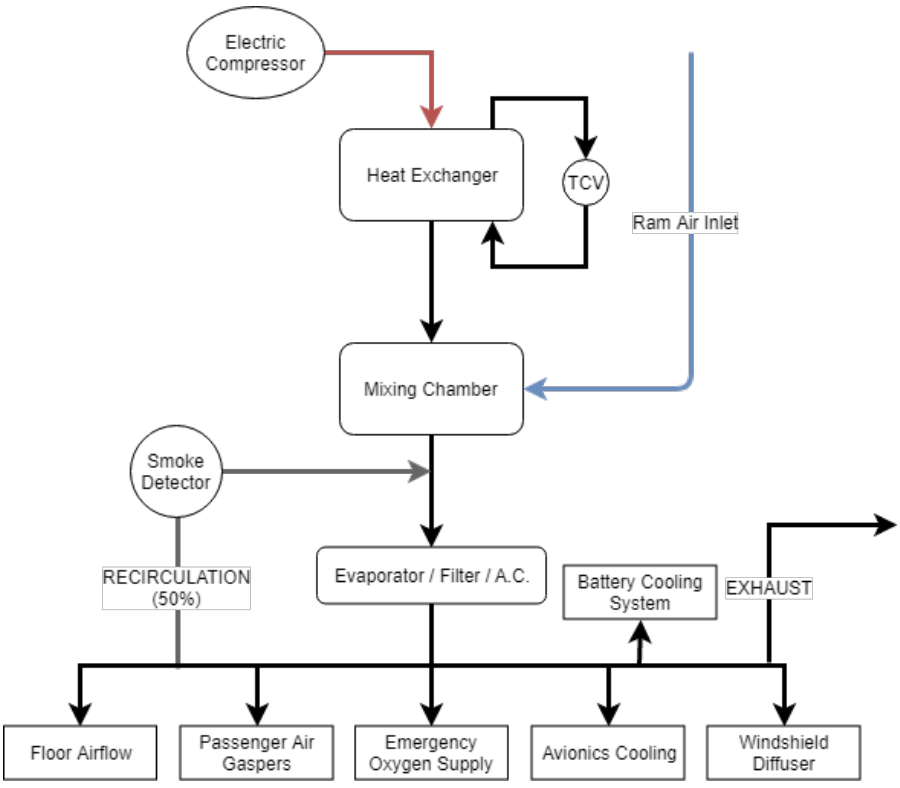

Fig. 83 Environmental Control System

2.13.6. Electrical Systems

The electrical system consists of two separate busses: Main Distribution Bus and the Essential Bus., as shown in Fig. 84. A 115V bus is not required as most of the components are powered by 28V DC. The power is supplied from two alternators which internally rectify the voltage automatically, eliminating the need for additional transformers. They also act as a redundancy in case one was to fail and monitored with the Control Protection Unit (CPU); however, additional voltage regulators and fuses are also installed. In the event of a catastrophic failure, stand-by batteries can supply power to these busses for a limited amount of time. Both batteries are rated at a lower 24V to ensure the alternators can provide sufficient current to tackle the battery's internal resistance. Further assurances allow the use of propulsive batteries to run the aircraft systems; this was made possible with the use of a relay system, which would activate in the event of a power loss on BAT 1. The main distribution bus is split further to three other busses; this provides isolation between the systems as a safety measure. The essential bus carries all the necessary and vital equipment the aircraft would require in case of an engine failure; therefore, this bus must take priority of the power supply. This is done through the implementation of a diode in the system.

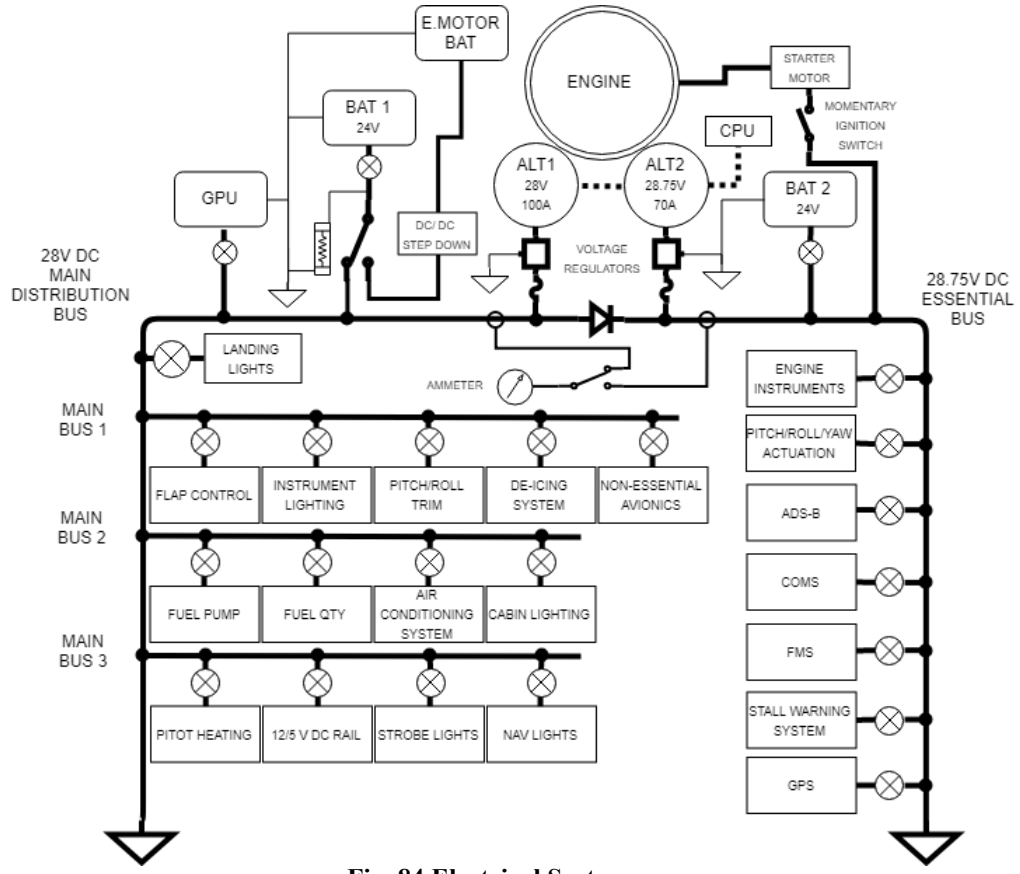

Fig. 84 Electrical System

2.13.7. Ice Protection System

A de-icing system exists on the S270 and serves the purpose of removing ice after accumulating on the surface. The detection of ice is done through icing sensors, which are placed on the aerofoil surface. It is constructed of a copper electrode pattern, which is embedded in a polyimide laminate. On the initial onset of ice, the electric field on the surface detects a change in the field characteristics. The pilot is then alerted when critical levels are reached. IceSight provides a flush mount, low-power solution with alerts at 0.12 cm and 0.64 cm of ice. Coupled with this sensor, an Electro-Mechanical Expulsion De-icing System (EMEDS) will be implemented. This system functions by the transmission of a high current electrical pulse to the actuator coil on the leading edge of the wing; this causes the actuator to rapidly flex at a high frequency, de-bonding the ice from the surface. This method has many advantageous to other traditional pneumatic systems. The flush installation allows little to no increase in drag, along with the ability to de-ice sheets as thin as 0.12 cm. Additionally, with the move towards MEA, it allows for a completely bleed-less system. COX & COMPANY provide a FAR Part 23 & 25 certified solution, which easily integrates into the aircraft's main distribution bus consuming only 0.7 kW.

2.14. Risk and Reliability

The risk assessment given by Table 59 shows identified risks divided into four categories: Pilot, Aircraft, Environment and External. In addition to showing the risks associated, the risk assessment also outlines safety measures implemented within the aircraft; a guide as to how to reduce the effects of the failure that could occur. The risks were assessed by coupling probability and severity. The final risk rating is given by the definitions and matrix presented in Table 57 and Table 58. Definitions were taken from a Risk Management Guide [135].

Table 57 Rating assessment definitions.

Probability		Severity		
Ranking	**Description**	**Ranking**	**Aircraft**	**Persons**
Probable (1)	This event will definitely happen more than once.	Catastrophic (1)	Damage is unfixable, causing loss of whole aircraft.	Results in fatalities of one or more persons.
Occasional (2)	This event is likely to happen over the aircraft's lifetime.	Critical (2)	Major damage to the aircraft, with expensive repairs to be made.	Major injury inflicted to one or more persons e.g. permanent disability.
Remote (3)	This event may occur but is not likely to.	Marginal (3)	Minor damage to the aircraft, with less expensive repairs.	Minor injury inflicted to one or more people e.g. broken arm or leg
Improbable (4)	The likelihood of this event is almost negligible.	Negligible (4)	Very little or no repair needed.	Less than a minor injury or no injury e.g., cuts, bruises or sprains

Table 58 Risk assessment matrix.

Probability		**Severity**			
		Catastrophic (1)	Critical (2)	Marginal (3)	Negligible (4)
Probable	(1)	High	High	Serious	Medium
Occasional	(2)	High	Serious	Medium	Low
Remote	(3)	Serious	Medium	Medium	Low
Improbable	(4)	Medium	Medium	Medium	Low

Risks rated in red in Table 59 are prioritised for immediate action that must take place as soon as possible. Risks rated in orange highlight a risk that needs serious consideration. Yellow rated risks are medium risks. This is when the aircraft is safe to fly, as long as there has been some consideration and safety measures taken. Green shows low risks where the aircraft is safe to fly under normal procedures.

Table 59 Risk assessment: Pilot, Aircraft, Environment and External.

		Name	Description	Probability	Severity	Rating	Safety measures	Final rating
Pilot	1	Medical	The pilot is unfit to control the aircraft to the best ability. For example, if they feel unwell or extreme lack of sleep.	1	1		Enough pilots would be available so in the case where a pilot feels like it is not wise to fly, there is a reserve pilot to take their place.	
	2	Qualification	To fly safely, a pilot needs to have the correct qualifications.	4	1		All qualifications would be checked before being allowed to fly.	
Aircraft	3	Battery failure – failure with connection	During flight, if any electrical connection is lost, no power from the source can be used. The aircraft is optimised with battery power for take-off and landing. A connection failure would also affect other systems, for example, FMS and FBL.	3	2		The aircraft is able to fly just using fuel, without any battery power. The systems that would be affected are not flight critical, and the pilot can manually fly the aircraft. Correct maintenance will reduce the probability of this failure.	
	4	Battery failure – failure to charge	This means that the aircraft cannot use this source of power for take-off and landing as designed.	3	4		The aircraft is able to fly only on fuel, without subsidiary power from the batteries.	
	5	Engine failure	If the engine failed, there will be no power being sourced to the engine or the aircraft.	3	1		To be certified, the engine will go through extensive testing. This is to make sure the engine is fully capable. An emergency parachute is also incorporated into the aircraft. Correct maintenance will reduce the probability of this failure.	
	6	Fuel system control valve fail closed	If the fuel systems control valve failed, then there would be no fuel being fed into the engine.	3	2		A cross feed valve is implemented in the case of this failure. If this fails, then can glide to a new location or use batteries to land the aircraft safely. Correct maintenance will reduce the probability of this failure.	
	7	Battery cooling system failure	Oil cooling is used for the battery system. If this was to fail, it would be critical as	2	1		There is a vent at the front of the aircraft that can be opened to let in colder outside air. The batteries can also be disconnected. Correct	

		the batteries can quickly heat up to a very high temperature.				maintenance will reduce the probability of this failure.	
8	Engine alternator failure	The alternator failing will reduce power available to the electrical systems. There is also a fan, which in the case of failure, the component will get very overheated.	3	2		Some of the battery power can be redirected to the actuator in case of a failure. A vent can be made in the case of the fan failure, using cooler outside air to cool down the component. Correct maintenance will reduce the probability of this failure.	
9	Aircraft icing – Environmental Protection System (EPS) failure	Build-up of ice on the aircraft increases drag and affects the weight distribution, decreasing the aircraft performance. The freezing of the propellers would be critical as there would be no propulsion. However, the aircraft is not at high altitudes, so a build-up is unlikely to occur.	3	2		The pilot can fly to warmer air at a lower altitude. Correct maintenance will reduce the probability of this failure.	
10	Propeller failure – in air	This would stop any thrust to the aircraft, which is a critical state.	3	1		An emergency parachute is to be used in these critical situations. Correct maintenance will reduce the probability of this failure.	
11	Propeller failure – take-off and landing	This would stop thrust to the aircraft, which is a critical state.	3	2		Pilots are trained for emergencies during take-off and landing, although within cities it may be difficult to find open space. Correct maintenance will reduce the probability of this failure.	
12	Landing gear failure	A physical, mechanical break of the struts or components of the landing gear would greatly increase the risk of damage to the aircraft and people inside.	4	2		Correct maintenance will reduce the probability of this failure. This includes looking at the wear and state of the landing gear.	
13	Flight control system (FCS) failure – FBL AND FMS	These systems would also fail if all electrical power was lost. However, these are not flight critical systems and the pilot can fly the aircraft with manual inputs.	2	4		FML and FMS both have a high redundancy. They are both independent so will not affect anything else on the aircraft. They are not flight critical systems and the pilot can fly the aircraft without them. It is possible to use power from batteries originally for the engine.	

						Correct maintenance will reduce the probability of this failure.	
	14	Control surfaces – Electro mechanical actuation	Electro mechanical actuation is used for the flaps and spoilers. The biggest risk to these is jamming. However, each flap and spoiler are independent, and the pilot can still fly with a jammed actuator.	1	3	Correct maintenance will reduce the probability of this failure. In emergencies, a parachute is available to engage the parachute.	
	15	Control surfaces – Electro hydraulic actuation	Electro hydraulic actuation is used for ailerons and ruddervators. As this is a hydraulic system, there is a risk of a leak of hydraulic fluid. This would greatly reduce the pressure, affecting the actuation capability.	1	3	Correct maintenance will reduce the probability of this failure. In emergencies, a parachute is available to engage the parachute.	
	16	Environmental control system (ECS) failure	If the compressor failed within the heat exchanger, cold air from outside the aircraft will enter the cabin. This is not flight critical but will affect the comfort of the passengers onboard.	3	4	To reduce this effect during flight, the pilot can fly at a lower altitude where there is warmer outside air.	
	17	Improper refuelling	Without sufficient fuel required for the flight, this can cause an emergency situation. Fuel is also extremely flammable and improperly stored fuel is a danger to anybody around.	3	1	Pilots will be trained properly and check the fuel before starting a flight. If fuel runs out during flight, and emergency parachute is provided. Signs will be put up about the proper regulations of fuel storage.	
	18	Parachute failure	The parachute is for emergency situations where the pilot needs to land safely.	4	1	Correct maintenance and standards will be followed installing and inspecting the device. This is a ‘last resort’ mechanism, there is nothing else to fall back on if failure occurs.	
Environment	19	Weather – turbulence, icing, lightening, wind	Changes to weather conditions during the flight can lead to rougher conditions than expected. In extreme cases, this can cause the aircraft to land sooner than expected, or cause damage to the aircraft.	1	3	Before flying, weather will be checked. The pilot is trained for varying conditions. The structure incorporates lightning strike protection (LSP) to reduce the damage cause by lightning strike.	

	20	Airport terrain	Small, low-use airports can increase the chance of rougher surfaces for take-off and landing. This can also include short runway distances.	2	4		Airports are chosen which are well within the capability to take-off and land from. The pilots are aware of the different surfaces and properties at each airport.	
	21	Night flying	Night flying decreases the visual ability of the pilot during flight.	2	4		Forward looking infrared and radar systems are implemented for the pilot to continue to fly the aircraft safely. The pilot is trained for these conditions.	
	22	Airport problems - closure	In the event of an airport or area closure, the pilot must find somewhere else to land the aircraft.	4	4		This is accounted for the in the fuel and battery calculation. There will also be a number of airports close nearby.	
External	23	Business or personal pressures	The pilot may be under stress. For example, a strict schedule to keep up with. This can cause a rush in checking the aircraft and a misjudgement under pressure.	2	2		Schedules will be made with enough time to safely and efficiently check over the aircraft and fly to another destination.	
	24	Safety for crew and passengers	Flying with a quick turnaround from small airports does not leave room for any long safety check procedures, as sound in large scale airports.	3	1		The amount of luggage that can be taken on board is limited. Quick bag checks can be made by the pilot before flying. Suggestions can be made to carry a portable metal detector if implementing this service.	
	25	Increase pollution	Pollution will be increased in these areas from the fuel. This can affect long term health of surrounding people and the environment.	1	3		Consideration was given to the increase in pollution by incorporating batteries for take-off and landing.	
	26	Increase noise pollution	Noise will increase in areas where frequent flights are made.	1	4		Using batteries for take-off and landing reduces the noise levels of the aircraft.	

2.15. Certification

The aircraft will be certified to FAA 14 CFR Part 23 regulations under the category of "Normal Aircraft". The S270 aircraft falls under classification level 2 which states the aircraft must have between two and six passengers. Our aircraft is within the limits of the low speed limit by having a maximum operating speed of 92.6 ms^{-1} and normal operating speed of 128ms^{-1} [136].

2.15.1. Hybrid Electric Propulsion

The S270, being an innovative aircraft, features unprecedented technology such as the Hybrid Electric Propulsion system outlined in Section 1.7. This thereby requires special consideration with regards to certification due to the cost and time implications of certifying the aircraft under a brand-new concept. The aircraft can be fully powered by only using the ICE, meaning the use of batteries for propulsion can be defined as power augmentation. This definition, implemented with an Engine Control Unit (ECU), complies with existing certifiable regulations.

With regards to safety, the engine will be tested under numerous conditions. This includes testing the failure of either part of the propulsion system. For example, a failure of the power augmentation battery system will automatically result in full use of the ICE for the remainder of the flight. Failure of the ICE will result in full use of the power augmentation system, to give the pilot time and extra control to guide the aircraft to a suitable landing destination. Proving this will result in a certifiable engine, without the costly and time demanding process under the regulations stated in 14 CFR Part 23.

2.16. Cost and Business Case

Costings of the S270 were analysed using The Eastlake Model [34]. Several factors such as CFR certification, unpressurized fuselage, percentage of composite materials used, plain flaps, tapered wing, and one prototype had to be taken into consideration within this analysis. Despite offering sound justifications in costing the aircraft, the model presents values under the 2012 Consumer Price Index (CPI). Amendments were made to accommodate the 2019 CPI by multiplication of a CPI ratio factor, 1.12 [137]. In addition, any cost values obtained in terms of GBP (£) were converted to US Dollars (US$) [138].

2.16.1. Sales Predictions

To work out the aircraft costing, an investigation into future sale predictions is exercised. Firstly, a study was undertaken to compare the previous worldwide shipments of general aviation aircraft. Figure 85. summarises the results of this study, with specific figures found from the General Aviation Manufacturers Association 2018 Annual Report [139].

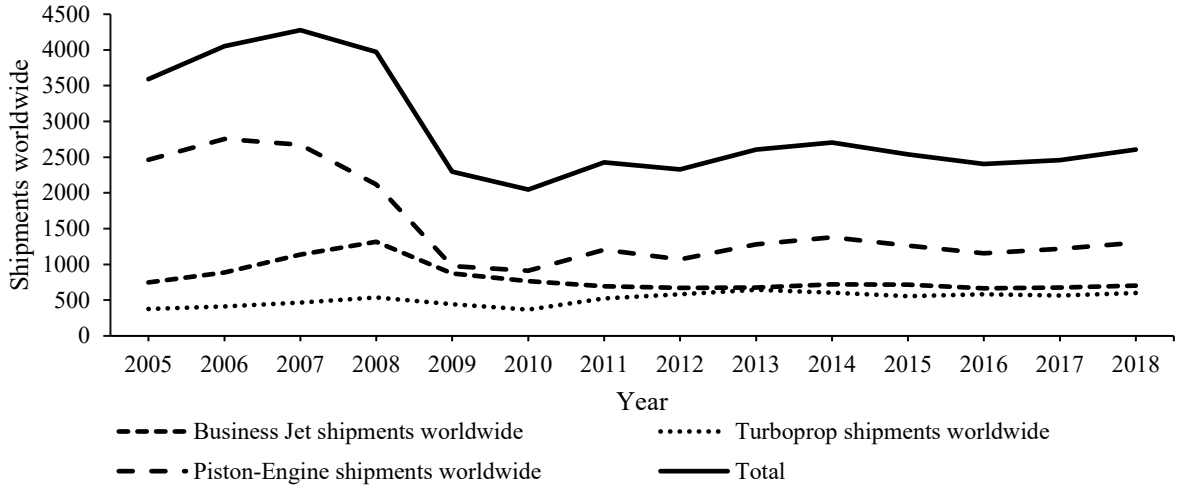

Figure 85 Worldwide shipments for general aviation aircraft.

Figure 85 demonstrates that the sales of each segment of general aviation has levelled out, with no sharp trend fluctuations. A report made by the FAA in 2018 predicted that the forecast for general aviation aircraft will remain steady until 2038 [140]. This means that predictions for sales can be made for the near future with moderate accuracy.

The average value for the total general aviation worldwide shipments over the last three years amount to 2489 aircraft per year. This average was for a total of 34 companies that shipped at least one aircraft in that timeframe. Looking at the total general aviation aircraft shipments of the top five competitor aircraft, the average percentage share was 3.38%. As the S270 is new aircraft, for the first five years of production, it is unrealistic to assume that it would have a higher share than this.

Table 60 Percentage share of the average total value of general aviation worldwide shipments.

Percentage share	Aircraft per year	Aircraft per month
1%	26	2
2%	52	4
3%	78	6

From these values, it was decided that a conservative 3 aircraft per month (1.5% share) would be realistic for the first two years. In year three, as the aircraft has become more established, it is predicted that an average target sale of 6 aircraft per month (3% share) will be reached. The average value of shipments made per month for all 34 companies was just over 6 per month. This justifies the sales forecast.

2.16.2. Avionics Cost

The equipment in the avionics suite are from Garmin [141] to accommodate new technologies. The avionics cost is given below in Table 61.

Table 61 Avionics cost.

Avionics Component	Model	Unit Cost ($)
ADS-B Transponder	GNX 375	7995
Navigation/Communication	GTN 750	17495
Audio Panel	GMA 345	1895
Touchscreen Flight Displays	G3X Touch	14865
Digital Autopilot	GFC 500	6995
Back up Display	G5	2249
Total Avionics Cost per aircraft		**51494**

2.16.3. Quantity Discount Factor

Equipment costs are conditional to a Quantity Discount Factor (QDF), which details the number of units produced and the development of manufacturing and labour experience. The value for QDF is found according to Equation 26 where F_{EXP} represents the increasing labour experience and N being the number of units produced.

$$QDF = (F_{EXP})^{1.4427 \ln N} \tag{26}$$

2.16.4. Wrap rates and Inflation

The wrap rates were provided by the Eastlake model [34] and have been adjusted by CPI ratio as stated in Section 2.

Table 62 Wrap rates.

Wrap Rates	2012 ($)	2019 ($)
Engineering	92	103.04
Tooling	61	68.32
Manufacturing	53	59.36
Technician	16	17.92

2.16.5. Total Production Cost & Minimum Selling Price

The table below shows the total production cost and minimum selling price found using the Eastlake Model [34]. Skyride's initial estimate of number of units to produce in five years is 288 and the RFP requires production cost per unit at 500, 1000, and 2000 units, hence all four units have been presented below. The selling price for the S270 with 15% profit is given below. Price per unit has been calculated based on assumption of 288 units produces in 5 years.

Table 63 Total cost and minimum selling price.

`	Man Hours	Rate, $/hr	Total Cost	Cost Per Unit	
Engineering	61,543.82	103.04	30,717,083.70	106,656.54	
Development Support	-	-	913,673.68	3,172.48	
Flight test operations	-	-	19,919.51	69.16	
Tooling	49,464.22	68.32	16,369,247.32	56,837.66	
Certification Cost	-	-	48,019,924.22	-	
Manufacturing Labour	392,667.42	59.36	112,903,774.57	392,027.00	
Quality Control	-	-	29,354,981.39	101,927.02	
Materials/equipment	-	-	6,179,928.01	21,458.08	
units produced in 5 years	-	-	-	-	288.00
Quantity Discount Factor	-	-	-	-	0.16
	-	-	-	**Without QDF**	**With QDF**
Fixed Landing Gear Discount	-	-	-	-8,400.00	-1,356.84
Engine(s)	-	-	-	102,051.90	16,484.31
Propellers	-	-	-	30,886.47	4,989.05
Avionics	-	-	-	51,494.00	8,317.76
TOTAL COST TO PRODUCE	-	-	-	**858,180.32**	710,582.23
Manufacturer's Liability insurance	-	-	-	-	16,128.00
MINIMUM SELLING PRICE	-	-	-	-	**726,710.23**

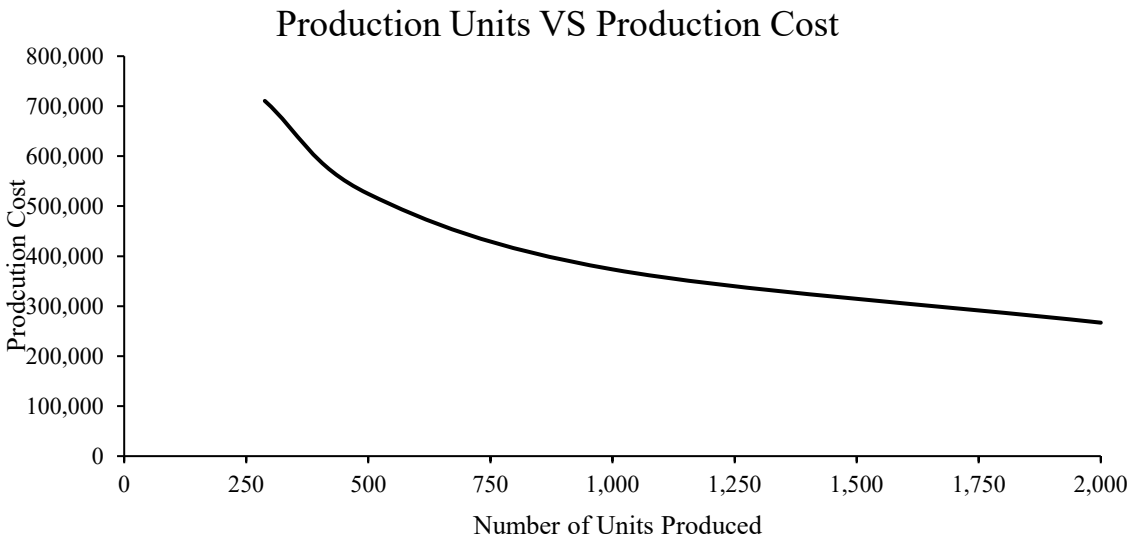

Figure 86 Production units vs production cost.

Table 64 Total cost and minimum selling price of different units.

Units produced in 5 years	288.00	500.00	1,000.00	2,000.00
Quantity Discount Factor	0.16	0.14	0.11	0.09
Total Certification Cost	48,019,924.22	52,971,698.30	59,938,515.08	67,838,225.21
		Cost Per Unit ($)		
Engineering	106,656.54	61,434.17	38,575.46	21,896.25
Development Support	3,172.48	1,827.35	913.67	456.84
Flight test operations	69.16	39.84	19.92	9.96
Tooling	56,837.66	36,116.32	20,429.46	11,556.07
Manufacturing Labour	392,027.00	301,492.89	216,763.82	155,846.31
Quality Control	101,927.02	78,388.15	56,358.59	40,520.04
Materials/equipment	21,458.08	21,458.08	21,458.08	21,458.08
Fixed Landing Gear Discount	-1,356.84	-1,136.06	-908.85	-727.08
Engine(s)	16,484.31	13,802.06	11,041.64	8,833.30
Propellers	4,989.05	4,177.26	3,341.80	2,673.44
Avionics	8,317.76	6,964.33	5,571.46	4,457.16
TOTAL COST TO PRODUCE	710,582.23	524,564.38	373,565.06	266,980.37
Manufacturer's Liability insurance	16,128.00	56500	56,000.00	112,000.00
MINIMUM SELLING PRICE	726,710.23	581,064.38	429,565.06	378,980.37
Selling Price with 15% profit	835,716.76	668,224.04	493,999.82	435,827.43

2.16.6. Operating Costs

Table 65 Breakdown of operating costs.

Maintenance Cost ($/Year)	15,295.80	Annual inspection cost ($/Year)	1,205
Maintenance to flight hour ratio	0.37	Engine Overhaul fund ($/Year)	3,900
Storage cost ($/Year)	3,360	Monthly loan payment ($)	9,291
Annual Fuel/Battery Cost ($/Year)	78,427.80	Annual Loan payment ($/Year)	111,492
Annual Insurance cost ($/Year)	1,205	Annual Crew Cost ($/Year)	58,500
Total yearly cost ($)		161,248.60	
Cost per flight hour ($)		206.73	

The initial operational cost is the addition of cost of fuel, maintenance, storage, insurance, inspections, engine overhaul, battery recharge. The costs are calculated using the Eastlake model [34]. The crew cost was compared with the current competitors of S270 and finalised a value of 75 $/hour [142]. Dividing Cost per flight among the 4 Passengers and allocating 15% profit gives the allocated journey ticket price for an hour.

Table 66 Example of ticket prices.

Cost per flight hour ($)	206.73
Price Per Person (without profit) ($/hour)	51.68
Price Per Person (with 15% profit) ($/hour)	59.43

2.16.7. Flyaway Cost

Table 67 gives the total flyaway cost which is the addition of cost of manufacturing labour, materials, avionics, and the propulsion system.

Table 67 Breakdown of flyaway cost.

	Man Hours	**Rate, $/hr**	**Total Cost**	**Cost Per Unit ($)**	
Manufacturing Labour	392,667.42	59.36	112,903,774.57	392,027.00	
Materials/equipment	-	-	6,179,928.01	21,458.08	
	-	-	-	**Without QDF**	**With QDF**
Propellers	-	-	-	30,886.47	4,989
Engine(s)	-	-	-	102,051.90	16,484
Avionics	-	-	-	51,494.00	8,318
Total Flyaway cost	-	-	-	597,917.45	405,495

2.16.8. Breakeven Analysis

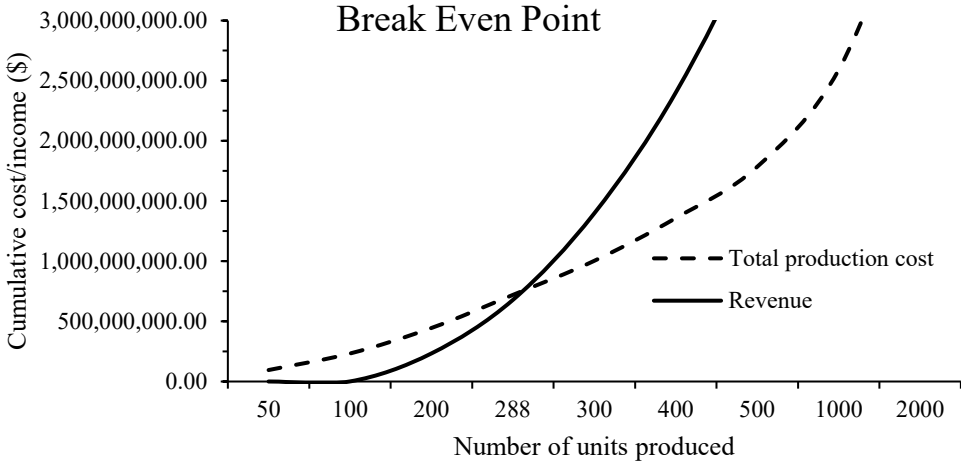

Fig. 87 Break-even point

The break-even point graph is given in Fig. 87. The break-even point for the S270 is at 288 units, in 5 years' time. This is what Project Skyride has predicted to sell due as described above in Section 2.16.1. 5 years' time is an acceptable breakeven point, which can quickly increase with more sales.

2.17. Business Case and Infrastructure

The S270 was designed for the use of frequent flights operating out of small regional airports. Whilst such an aircraft can facilitate the general aviation market in a leisure context, the S270 has been tailored for a wider transport model via new ventures into the concept of "air-taxi"; comprising high-frequency scheduled or on demand flights. This therefore requires a more extensive infrastructure for operating companies to utilise the S270 aircraft in this context. The following segment provides an initial outline of how companies could operate such a business taking into consideration target areas for business set up, customer booking procedure and necessary staff.

2.17.1. Business Consideration

Initially, the business will run only from scheduled flights. Small airports located near major airport hubs are a key target area. This will provide customers with quicker and more time efficient travel options in those regions. In addition to this, there lies scope to target airports in more remote locations thus providing a selling point for companies serving customers based in rural areas. Local small-scale businesses that require high amounts of travel are likely to have an interest in this service, making industrial areas a key target area of operation.

As the demand increases and the air-taxi market grows, there is an option to run on-demand flights on top of the scheduled flights. This is where a customer can book a flight from their desired location from as little as 15 minutes before take-off. Whilst a relatively new concept within general aviation travel, the technology infrastructure behind privatised on-demand travel is already well established. Future integration plans also include creating a system whereby customers also receive a car taxi service from the departure residence, to the airport, to the final destination, thus essentially making the service "door-to-door".

2.17.2. Staff

The aircraft is designed with only one pilot required to fly. The use of small airports means no external security is required, however a government wide program named 'Airport watch' allows pilots to assume security authority for their passengers [106]. This includes the search of bags and persons as well as the right to cancel flights if a security threat is identified. Other staff not directly associated with the flight operation such as customer service teams are easily employable and function trivially with respect to current travel apps.

2.17.3. Charging

At each airport, batteries will be left to charge connected to the general 120V U.S. mains, which is a standard voltage connection to the grid. Charging at higher voltages requires substantial infrastructure costs, which may not be viable at early stages of the business. Although charging

through the mains will take a longer period of time, this will be countered by having a surplus of batteries on site. In the unlikely case of the batteries not carrying enough charge on arrival of the aircraft, the aircraft has the capability to run from only fuel. Therefore, batteries can be left charging and it will not cause delay to the aircrafts schedule.

In the future, new charging methods can be investigated, for example, using solar panels. At present, these methods are not efficient and cheap enough to be viable, including the infrastructure it would require. However, as technology progresses, this may change, providing charging with more of a consideration to the environment.

2.18. Conclusion

This report has provided both an overview and an in-depth breakdown of the design of the S270 aircraft. Elements comprising the hybrid engine layout, system breakdown, structural analysis, aerodynamics optimisation and battery configuration have been presented with technical specification alongside comparison with existing competitor aircraft.

2.18.1. Design Evaluation

The main aim of the S270 aircraft is to reduce congestion on the US roads by providing a low cost, fast alternative for commuters. The S270 has been shown to reduce operating costs by up to 43% compared to competitors and a unit cost reduction of up to 37%. In addition, by utilising electric propulsion during take-off and climb, the fuel burn of a standard mission is greatly reduced compared to competitors, and hence the environmental impact of the S270 is much lower. Advanced battery technologies, battery system optimisation, composite materials and innovative manufacturing techniques have minimised the overall mass of the S270, which reduces the power requirements and consequently further reduces the operating costs of the aircraft. The S270 has been shown to be laterally and longitudinally stable without the need for any control system augmentation to assist pilot inputs.

2.18.2. Future Work

Further efforts will extend to carrying out more extensive computational analysis. Particular focus will be invested in FEM analysis of the fuselage and tail structures which have currently not been achieved due to time constraints of the project. Continued CFD analysis will be carried out to further maximise drag reduction. Skyride also recommend the construction of a prototype which will not only permit wind tunnel testing to optimise specific components, but also provides the first step in achieving certification. At present, this aircraft is designed to be flown by one pilot. Developments can be made to progress the autonomy of the aircraft. Currently the aircraft has been shown to be naturally stable; however, a future consideration could include a stability augmentation system to tackle the coupling experienced at the tail due to yaw and roll movements. The move towards MEA

is evident in the design from the use of hybrid electric propulsion and systems such as Fly-by-Light along with EHA/EMA. A liquid battery cooling system is also used at this stage with a consideration for a future fully electric concept; this will allow for seamless integration with the current architecture as higher energy densities become possible.

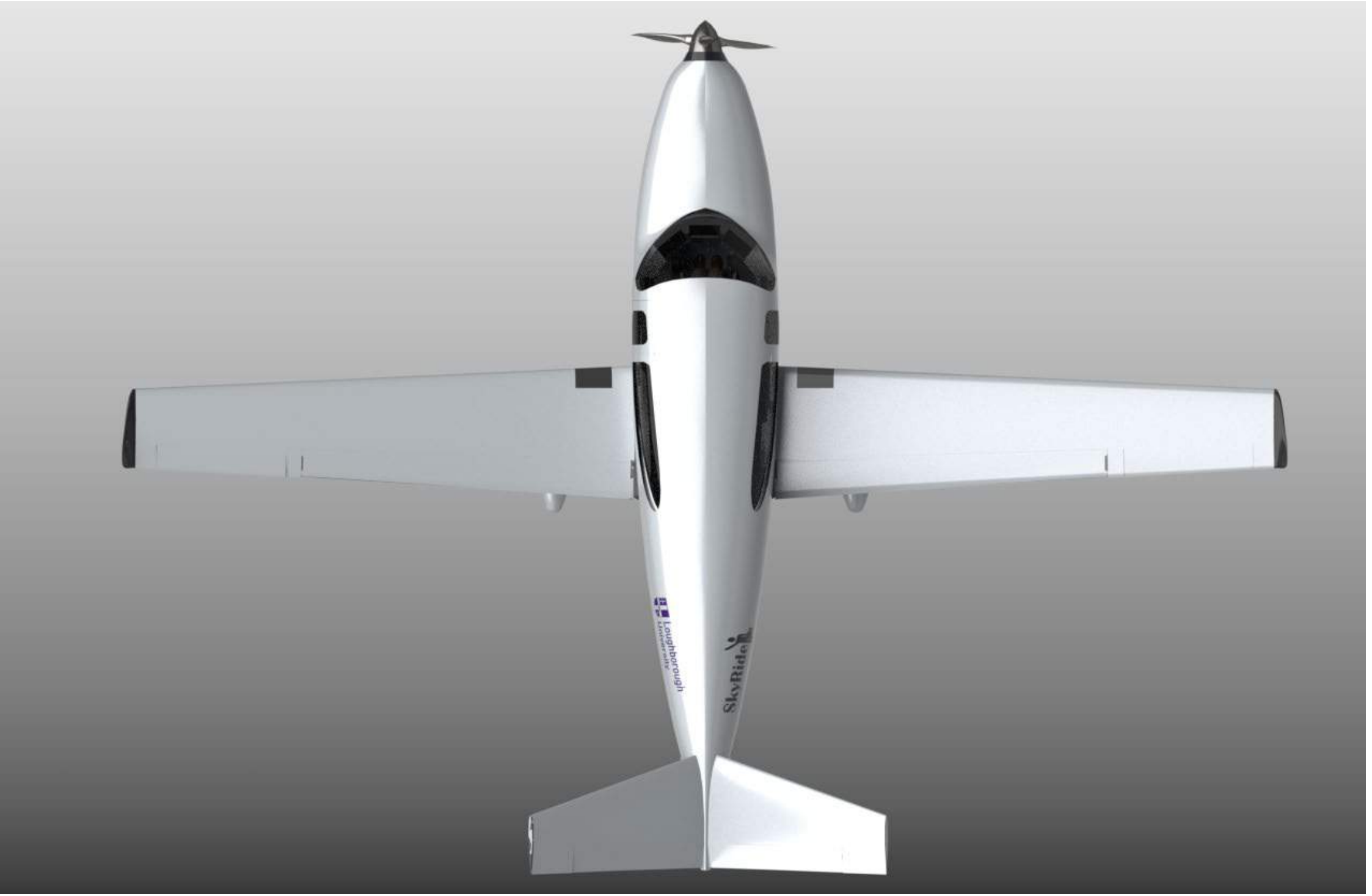
Loughborough University
SkyRider

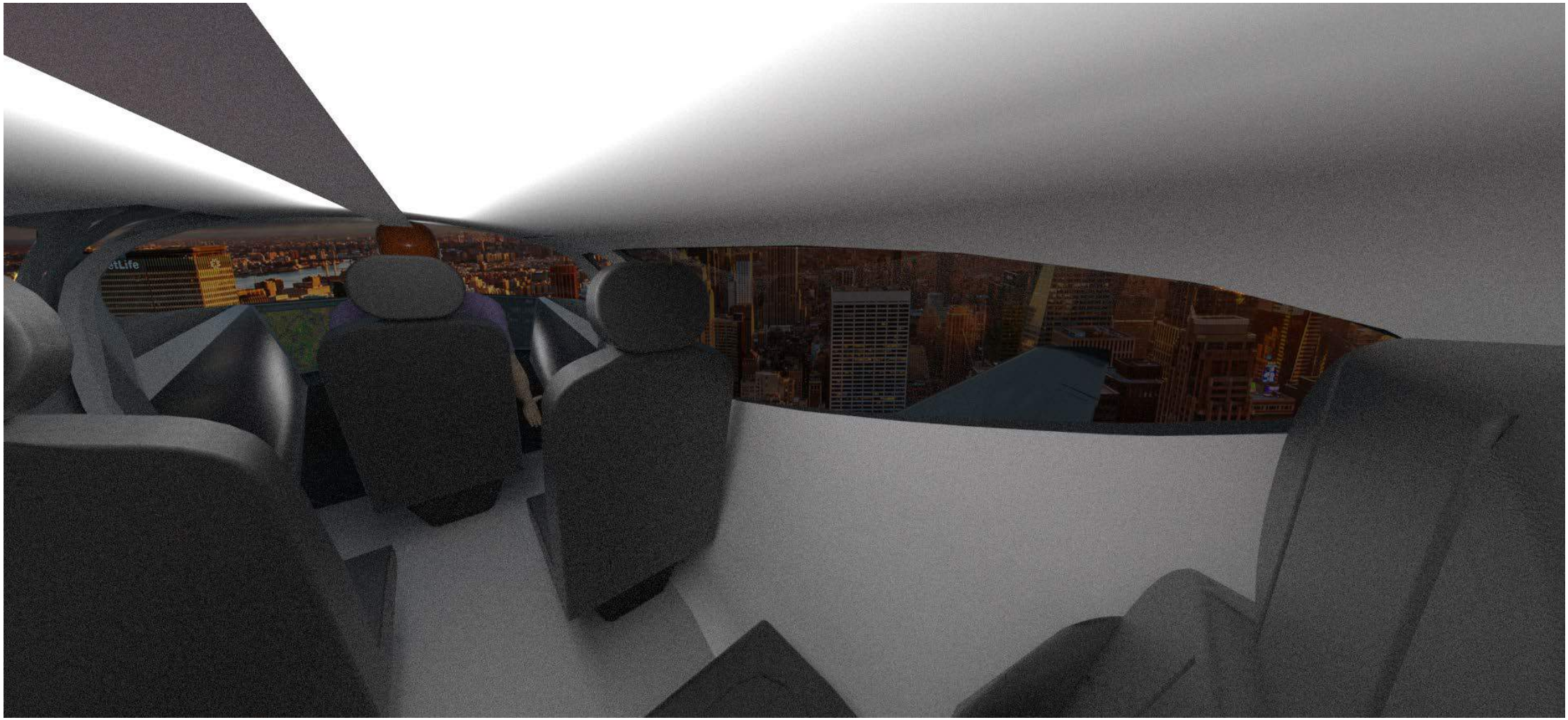


4W 880

References

[1] "Why don't Americans ride trains?," *The Economist*, 2013.

[2] M. Yglesias, "Amtrak turns 45 today. Here's why American passenger trains are so bad.," 2016. [Online]. Available: https://www.vox.com/2016/5/1/11539966/amtrak-45-anniversary.

[3] G. Budig and A. Heaps, "Traffic congestion will be with us for a while," *The Charleston Post and Courier*, 2019.

[4] A. Downs, "Traffic: Why It's Getting Worse, What Government Can Do," *Brookings*, 2004.

[5] R. Wall, A. Sider, and Wall Street Journal, "U.S. Airlines Report Delays Caused by System Fault," 01-Apr-2019.

[6] P. Bedard, "Trump to cut $4 billion in domestic programs, elimination of Legal Services Corporation," *Washington Examiner*, Mar-2019.

[7] A. Harish *et al.*, "Economics of Advanced Thin-Haul Concepts and Operations," no. June, 2016.

[8] P. SkyRide, "Design Freeze Report - 18TTD009 Group Design Project."

[9] "Reducing emissions from aviation," *European Comission*. .

[10] NEWS TEAM, "Airbus abandons E-Fan as electric tech moves on," *Flyer*, 2017.

[11] N. Rossi, "Conceptual Design of Hybrid-Electric Aircraft," 2017.

[12] "NASA/LANGLEY LS(1)-0413 (GA(W)-2) AIRFOIL (ls413-il)." [Online]. Available: http://airfoiltools.com/airfoil/details?airfoil=ls413-il. [Accessed: 29-Apr-2019].

[13] G. Cinar and D. Mavris, "Sizing, Integration and Performance Evaluation of Hybrid Electric Propulsion Subsystem Architectures," 2017.

[14] T. J. Wall and R. Meyer, "A Survey of Hybrid Electric Propulsion for Aircraft," *53rd AIAA/SAE/ASEE Jt. Propuls. Conf.*, no. July, pp. 1–15, 2017.

[15] C. Friedrich and P. A. Robertson, "Hybrid-Electric Propulsion for Aircraft," *J. Aircr.*, vol. 52, no. 1, pp. 176–189, 2015.

[16] C. Pornet and A. T. Isikveren, "Conceptual design of hybrid-electric transport aircraft," *Prog. Aerosp. Sci.*, vol. 79, pp. 114–135, 2015.

[17] C. E. D. Riboldi, "An optimal approach to the preliminary design of small hybrid-electric aircraft," *Aerosp. Sci. Technol.*, vol. 81, pp. 14–31, 2018.

[18] K. P. Duffy, "Electric Motors for Non-Cryogenic Hybrid Electric Propulsion," *51st*

AIAA/SAE/ASEE Jt. Propuls. Conf., pp. 1–10, 2015.

[19] B. J. Brelje and J. R. R. A. Martins, "Electric, hybrid, and turboelectric fixed-wing aircraft: A review of concepts, models, and design approaches," *Prog. Aerosp. Sci.*, vol. 104, no. March 2018, pp. 1–19, 2018.

[20] J. Liu and H. Peng, "Jinming Liu_Modeling and control of a power-split hybrid vehicle_IEEE trans. Control Syst. Technol._Nov 2008.pdf," vol. 16, no. 6, pp. 1242–1251, 2008.

[21] M. Ehsani, Y. Gao, and J. M. Miller, "Hybrid electric vehicles: Architecture and motor drives," *Proc. IEEE*, vol. 95, no. 4, pp. 719–728, 2007.

[22] J. M. Miller, M. Ehsani, and G. Yimin, "Understanding power flows in HEV eCVT's with ultracapacitor boosting," *2005 IEEE Veh. Power Propuls. Conf. VPPC*, vol. 2005, pp. 742–746, 2005.

[23] M. Ehsani, Y. Gao, and A. Emadi, *Modern Electric, Hybrid Electric, and Fuel Cell Vehicles: Fundamentals, Theory, and Design*, First. CRC Press LLC, 2005.

[24] J. M. Miller, "Architectures of the e-CVT Type," *IEEE Trans. Power Electron.*, vol. 21, no. 3, pp. 756–767, 2006.

[25] G. E. Blomgren, "The Development and Future of Lithium Ion Batteries," *J. Electrochem. Soc.*, vol. 164, no. 1, pp. A5019–A5025, 2016.

[26] M. M. Thackeray, C. Wolverton, and E. D. Isaacs, "Electrical energy storage for transportation - Approaching the limits of, and going beyond, lithium-ion batteries," *Energy Environ. Sci.*, vol. 5, no. 7, pp. 7854–7863, 2012.

[27] T. Mai, "Technology Readiness Level," 2015.

[28] T. Mai, "Technology Readiness Level," 2015.

[29] J. Kopera, "Sion Power's Lithium-Sulfur Batteries Power High Altitude Pseudo-Satellite Flight," *Airbus Def. Sp.*, p. 1, 2014.

[30] X. Q. Zhang, C. Z. Zhao, J. Q. Huang, and Q. Zhang, "Recent Advances in Energy Chemical Engineering of Next-Generation Lithium Batteries," *Engineering*, vol. 4, no. 6, pp. 831–847, 2018.

[31] OXIS ENERGY, "Ultra Light Lithium Sulfur Pouch Cell," 2018.

[32] D. Klapmeier, "Guide to the Cirrus Airframe Parachute System," pp. 1–16, 2013.

[33] M. V. Cook, *Flight Dynamics Principles, Second Edition: A Linear Systems Approach to Aircraft Stability and Control*, vol. 53, no. 9. 2007.

[34] Snorri Gudmundsson, *General Aviation Aircraft Design : Applied Methods*. 2013.

[35] “Cirrus SR22T GTS for Sale.” [Online]. Available: https://www.globalair.com/aircraft-for-sale/Cirrus-SR22T-GTS.

[36] “AIRCRAFT SPOTLIGHT THE CIRRUS SR22: SPEED, COMFORT, AND TECHNOLOGY…FOR A PRICE October 18, 2015.” [Online]. Available: https://www.aopa.org/community/flying-clubs/flying-club-newsletter/2015/october/18/aircraft-spotlight.

[37] “DA42 New Generation - Pricelist.” [Online]. Available: http://www.greatlakesdiamond.com/Docs/DA42NG Euro Pricing.pdf.

[38] “Aircraft Cost Evaluator-Cessna.” [Online]. Available: https://www.conklindd.com/CDALibrary/ACCostSummary.aspx?seoctl00_ContentPlaceHolder1_grid=page6.

[39] “Piper PA-34 Seneca.” [Online]. Available: https://en.wikipedia.org/wiki/Piper_PA-34_Seneca.

[40] “Aircraft Cost Evaluator-Piper.” [Online]. Available: https://www.conklindd.com/CDALibrary/ACCostSummary.aspx?seoctl00_ContentPlaceHolder1_grid=page10.

[41] “Beechcraft Bonanza.” [Online]. Available: https://en.wikipedia.org/wiki/Beechcraft_Bonanza.

[42] “PILOT BRIEFING: BUDGET BUY FAMILY HAULER.” [Online]. Available: https://www.aopa.org/news-and-media/all-news/2015/january/pilot/briefing_budget.

[43] R. Jaggi, “US air taxi pioneer comes to end of the road,” *Financial Times*, 2008.

[44] NASA, “Distributed Electric Propulsion (DEP) Aircraft.” .

[45] “8 High Lift Systems and Maximum Lift Coefficients,” p. 1–219E8pO6qc.

[46] J. Roskam, *Airplane Design Part VI: Preliminary Calculation of Aerodynamic Thrust and Power Characteristics*. 1987.

[47] J. Roskam and C.-T. E. Lan, “Airplane Aerodynamics and Performance.” 2003.

[48] J. Roskam, *Airplane Design: Part VI: Preliminary Calculation of Aerodynamic, Thrust and Power Characteristics*. Lawrence, Kansas [USA]: DAR Corporation.

[49] E. Clemmitt, A. Cepeda, L. Brodhead, Z. Dong, and J. Lullo, “FINAL DESIGN REPORT Team Hotel,” 2018.

[50] D. C. Wilcox, “Turbulence Modeling for CFD,” *Japanese Journal of Applied Physics*. 1999.

[51] “FAA 14 CFR Part 23,” vol. 23, no. c, 2011.

[52] P. Render, “Take-off and Landing Performances.” pp. 1–12, 2011.

[53] J. Roskam, *Aircraft Design Part 1*. .

[54] “Cirrus SR22 G2 GTS Specifications and Performance.” [Online]. Available: www.cirrusaircraft.com.

[55] “Cirrus SR22.” [Online]. Available: https://cirrusaircraft.com/aircraft/sr22/.

[56] E. Verification, “REPORT No. 823,” no. 823, 2019.

[57] “9 Empennage General Design.” [Online]. Available: http://www.fzt.haw-hamburg.de/pers/Scholz/HOOU/AircraftDesign_9_EmpennageGeneralDesign.pdf. [Accessed: 20-Feb-2019].

[58] M. Scherrer, “About stability analysis using XFLR5,” no. November, p. 70, 2010.

[59] J. D. Anderson, *Aircraft Performance and Design*. McGraw-Hill, 1999.

[60] D. R. (NACA) Chapman, “for Aeronautics,” no. November 1951, pp. 1–19, 1952.

[61] Federal Aviation Regulations, “FAR Part 23, Rate of Roll.”

[62] P. F. Ailerons and F. Ailerons, “ProAdvice 3 : AILERON SIZING,” pp. 1–12, 2011.

[63] J. Y. Hung and L. F. Gonzalez, “On parallel hybrid-electric propulsion system for unmanned aerial vehicles,” *Prog. Aerosp. Sci.*, vol. 51, pp. 1–17, 2012.

[64] I. Kim and H. Kim, “Configuration Analysis of Plug-in Hybrid Systems using Global Optimization,” vol. 6, pp. 391–404, 2013.

[65] EASA, “Continental IO-550 Data Sheet,” 2017. .

[66] “IO-550 Price.” [Online]. Available: http://blog.overhaulbids.com/continental-overhaul-cost/continental-550-overhaul-cost/.

[67] EASA, “Lycoming IO-580 Data Sheet,” 2017. [Online]. Available: https://www.easa.europa.eu/sites/default/files/dfu/EASA-TCDS-E.027_%28IM%29_Lycoming_IO--580--B1A_series_engines-02-06052008.pdf.

[68] “IO-580 Price.” [Online]. Available: http://www.airpowerinc.com/productcart/pc/TLEngineDetail.asp?catID=33&prodID=476100.

[69] Lycoming, “Lycoming DEL-120 Data Sheet.” [Online]. Available: https://www.lycoming.com/engines/del-120.

[70] EASA, “Thielert Centurion 4.0 Data Sheet,” 2015. [Online]. Available: https://www.easa.europa.eu/sites/default/files/dfu/EASA E.014 TCDS Technify Motors

GmbH_ Centurion 4.0_issue 06_2015.18.09_1.0.pdf.

[71] “Centurion 4.0 Price.” [Online]. Available: https://ipfs.io/ipfs/QmXoypizjW3WknFiJnKLwHCnL72vedxjQkDDP1mXWo6uco/wiki/Thielert_Centurion.html.

[72] EASA, “Red A03-102 Data Sheet,” 2018. [Online]. Available: https://www.easa.europa.eu/sites/default/files/dfu/EASA_E_150_TCDS_REDA03_issue 02_20180827.pdf.

[73] “RED A03 Price.” [Online]. Available: http://flash.avweb.com/avwebflash/news/V12_Diesel_Engine_207130-1.html.

[74] FAA, “Arrius Data Sheet,” 2007. .

[75] “Arrius 1A Price.” [Online]. Available: https://aeroval.com/ref/1883518/ARRIUS+1A/.

[76] EASA, “Pratt & Whitney Canada PT6 Data Sheet,” 2007. .

[77] “PT6A-52 Price.” [Online]. Available: http://blog.overhaulbids.com/pratt-whitney-pt6a-overhaul-cost/.

[78] EASA, “Lycoming LTS101 Data Sheet,” 2010.

[79] “LTS101-600 Price.” [Online]. Available: https://www.pprune.org/rotorheads/310195-honeywell-lts101-700d-2-engine.html.

[80] Rolls Royce, “Rolls Royce Model 250 Data Sheet.” [Online]. Available: https://www.rolls-royce.com/~/media/Files/R/Rolls-Royce/documents/customers/defence-aerospace/vcomb-1958-m250-c47e-engine-for-heli-expo-ver-3-final-tcm92-55498.pdf.

[81] “Rolls Royce M250 Price.” [Online]. Available: http://www.fi-powerweb.com/Engine/Rolls-Royce-M250.html.

[82] SMA, “SMA HPDE.” [Online]. Available: https://www.smaengines.com/our-product/hpde.

[83] M. Filipenko, “HTS-Technology for hybrid electric aircraft,” 2017.

[84] K. Petermaier, “Electric propulsion components with high power densities for aviation,” 2015.

[85] D. L. Huff, B. S. Henderson, and E. Envia, “Motor Noise for Electric Powered Aircraft,” pp. 1–12, 2016.

[86] J. J. Berton and D. M. Nark, “Low-Noise Operating Mode for Propeller-Driven Electric Airplanes,” 2018.

[87] Aerospace Technology Institue, “Insight - Aircraft Propulsion Technology Watch,” 2016.

[88] M. Asselin, *An Introduction to Aircraft Performance*. 1997.

[89] D. Miljković, J. Ivošević, and T. Bucak, “TWO VS. THREE BLADE PROPELLER - COCKPIT NOISE COMPARISON.”

[90] F. B. Metzger, “An Assessment Noise Reduction of Propeller Technology Aircraft,” *Order A J. Theory Ordered Sets Its Appl.*, 1995.

[91] E. G. Tulapurkara, “Flight Dynamics,” vol. 14, pp. 1–10.

[92] I. Waltz, “Unified Propulsion Quiz,” vol. 1, pp. 10–11, 2001.

[93] M. Hepperle, “Selection of Multiblade Propellers.” [Online]. Available: https://www.mh-aerotools.de/airfoils/propuls2.htm.

[94] F. Tudron, J. Akridge, and V. Puglisi, “Lithium-Sulfur Rechargeable Batteries: Characteristics, State of Development, and Applicability to Powering Portable Electronics,” *Sion Power*, no. January 2004, pp. 1–4, 2004.

[95] G.-S. Chen, B.-C., & Chuang, “State of charge estimation for lithium-ion batteries using extended kalman filter with local linearization,” *SAE Int.*, 2017.

[96] D. Chen, J. Jiang, G. H. Kim, C. Yang, and A. Pesaran, “Comparison of different cooling methods for lithium ion battery cells,” *Appl. Therm. Eng.*, vol. 94, pp. 846–854, 2016.

[97] S. Stanton and X. Hu, “Battery Thermal Management and Design,” vol. 1, pp. 1–61, 2010.

[98] L. S. Wickramaratne, “BATTERY THERMAL MANAGEMENT SYSTEM,” no. December, 2017.

[99] K. Liu, K. Li, Q. Peng, and C. Zhang, “A brief review on key technologies in the battery management system of electric vehicles,” *Front. Mech. Eng.*, vol. 14, no. 1, pp. 47–64, 2019.

[100] “Wing bending calculation,” *M.I.T.* .

[101] “Introduction to wing structural design,” *Aerotoolbox*. .

[102] K. A. Y. Toi, A. Harada, S. Tanaka, “Development of affordable composite wing structure,” *Adv. Compos. Mater.*, vol. 12, no. 4, pp. 321–329, 2004.

[103] S. Gudmundsson, *General Aviation Aircraft Design, Applied Methods and Procedures*. Elsevier, 2014.

[104] J. Roskam, *Airplane Design Part III: Layout Design of Cockpit, Fuselage, Wing and Empennage: Cutaways and Inboard Profiles*, 5th ed. Kansas: DARcorporation, 2017.

[105] Siemens, “NX Nastran 9. Quick reference guide.” .

[106] J. Carafano, “Keeping the Skies Friendly: Next Steps for General Aviation Security,” *The Heritage Foundation*, Jul-2007.

[107] G. Zhou, W. Sun, and B. Mahy, “Investigation of Damage in Composite Structures Caused by Simulated Lightening Strikes,” pp. 1–17, 2016.

[108] C. Simpson and A. Anderson, “Low cost manufacturing method for a general aviation aircraft fuselage,” *AIAA/CAS Int. Air Sp. Symp. Expo. Next 100 Years*, 2003.

[109] ROSKAM. J, *Airplane Design: Part V- Component weight estimation*. 1989.

[110] NORRIS.G and WANGER.M, “Boeing 747 Dreamliner,” *Mineap. ZENITH Press*, 2008.

[111] G. J. Page, “Layout II.” .

[112] “Cirrus parachute.” [Online]. Available: https://grabcad.com/library/ballistic-parachute-rocket-igniter-mechanism-1.

[113] “The drag of an airplane, W. Fairings, L. Gear,” *Natl. Advis. Com. Aeronaut.*, vol. 518, 2018.

[114] J. Roskam, *Airplane Design, Part IV:Layout design of landing gear*. 1989.

[115] P. Raj, “AOE 6045: Aircraft Design/Aircraft Configuration,” *Virginia Technol. Univ.*, 2017.

[116] P. Wheeler, “The more electric aircraft: Why aerospace needs power electronics,” *Univ. Nottingham*.

[117] P. Wheeler, “The more electric aircraft: Why aerospace needs power electronics?,” *Univ. Nottingham*, vol. 44, no. 0, 2009.

[118] R. Wilkinson, *Aircraft Structures and Systems*. Mechaero Publishing, 2009.

[119] J. Gruszecki, J. Grzybowski, and P. Rzucidlo, “Electro-mechanical actuators for general aviation fly-by-wire aircraft,” *Aviation*, 2005.

[120] S. C. Jensen *et al.*, “FLIGHT TEST EXPERIENCE WITH AN ELECTROMECHANICAL ACTUATOR ON THE F-18 SYSTEMS RESEARCH AIRCRAFT,” pp. 1–10.

[121] T. Chowdhury, R. Islam Linda, and A. Garg, “Evolution of Flight Control System & Fly-By-Light Control System,” *Int. J. Emerg. Technol. Adv. Eng.*, vol. 3, 2013.

[122] J. Sparks, “An Epic Tale - A Look at an Integrated Avionics System,” 2004.

[123] F. George, “GA Airframe Manufacturers Embrace Fly-By-Wire.”

[124] FAA, “FAA Safety Briefing - January/February 2019.”

[125] “GNX™ 375 | ADS-B Transponder and GPS | GARMIN.” [Online]. Available: https://buy.garmin.com/en-GB/GB/p/577174. [Accessed: 29-Apr-2019].

[126] “Difference Between ADS-B Out and ADS-B In?” [Online]. Available: https://www.thebalancecareers.com/what-s-the-difference-between-ads-b-out-and-ads-b-in-282562. [Accessed: 29-Apr-2019].

[127] J. Bradley, “How Autonomous Vehicles Fit in the Future of Airports,” 2018.

[128] J. Schvaneveldt, R.W., Beringer, D.B. & Lamonica, “Priority and organization of information accessed by pilots in various phases of flight,” *Int. J. Aviat. Psychol.*, vol. 11, no. 3, pp. 253–280, 2001.

[129] C. J. Hamblin, C. Miller, and S. Naidu, “Comparison of Three Avionics Systems Based upon Information Availability, Priorities and Accessibility,” *Proc. Hum. Factors Ergon. Soc. Annu. Meet.*, vol. 50, no. 17, pp. 1825–1828, 2012.

[130] “G3X Touch™ Flight Displays | Experimental Aircraft | GARMIN.” [Online]. Available: https://buy.garmin.com/en-GB/GB/p/166058. [Accessed: 30-Apr-2019].

[131] FAA, “Part 23 –Small Airplane.” 2009.

[132] I. Martinez, “Environmental control system in aircraft,” 2014.

[133] M. D. and C. A. H. Nurcomb, “Aircraft Environmental Control Systems,” *Air Qual. Airpl. Cabins Similar Enclosed Spaces*, 2005.

[134] K. Aerospace, “ThermaCool - Electric Air Conditioning.” [Online]. Available: http://www.kellyaerospace.com/thermacool-aircraft-air-conditioning.html.

[135] NBAA, “Risk management guide for single-pilot light business aircraft,” 2016.

[136] Legal Information Institute, “14 CFR Part 23 - Ceritification of normal category airplanes.”

[137] “U.S. Bureau of Labor Statistics,Databases, Tables & Calculators by Subject.” [Online]. Available: https://www.bls.gov/data/inflation_calculator.htm.

[138] “Currency Converter.” [Online]. Available: https://www.google.com/search?q=pounds+to+dollars&rlz=1C5CHFA_enGB829GB829&oq=pounds+to+doll&aqs=chrome.0.0j69i57j0l4.3986j1j7&sourceid=chrome&ie=UTF-8.

[139] GAMA, “2018 Annual Report, General Aviation Manufacturers Association,” 2019.

[140] FAA, “Forecast Highlights (2018 – 2038),” 2018.

[141] “Garmin Products.” [Online]. Available: https://www.garmin.com/en-US/.

[142] “Fly BlackBird.” [Online]. Available: https://www.flyblackbird.com/.

Part 3. Public Engagement and Outreach Appendix

3.1. Booth Wood Primary School

On Friday 3rd May, 4 members of Project SkyRide visited Booth Wood Primary School, in Loughborough, to teach a class of Year 5/6 children a little bit about aircraft and introduce to them the idea of air taxis. The idea was received very well, and the children had lots of questions about this futuristic idea; they quite liked the idea of flying to school rather than driving!

The children were given an activity to complete where they made paper aeroplanes and fired them out of a launcher, which they thoroughly enjoyed. They also used the "Round the pole" equipment where a small balsa wood aircraft is connected to a power source and flies around a central pole. The children could adjust the voltage and see what effect this had on the flight of the plane, this was also received very well by everyone. Finally, the children were told a little bit about what University is like and hopefully some of them were inspired to pursue careers in engineering in the future.

Fig. 88 Booth Wood Primary School visit.

3.2. Public Perception Survey

Project SkyRide initially gained public exposure by sending out a survey that included questions about the public's perception of air taxis, various related issues. The results were as follows:

- 75.5% of people said that they would fly in a small general aviation aircraft.
- 73.5% of people said that they would use Project Skyride if it became available.
- 47.9% of people said they would be comfortable flying in a fully autonomous aircraft, which increased to 79.6% if the aircraft was partially autonomous, i.e. a pilot was on-hand to take control of the aircraft in emergencies.
- The most important aspects of an air taxi were ranked by all participants and the overall rankings were:
    1. Safety
    2. Cost
    3. Journey duration
    4. Convenience
- Participants were asked to rank different sources of noise by level of disturbance (1 causes most disturbance and 4 causes least disturbance):
    1. Railway noise
    2. Aircraft noise
    3. Motorway noise
    4. General road traffic noise
- Finally, 92% of people said they saw potential in Project SkyRide as a business.

These results were incorporated into the QFD analysis which enabled the design choices for the S270 to accurately reflect what a consumer would want from this air taxi aircraft, which would enable the business to have a greater chance of success in a very unpredictable market.

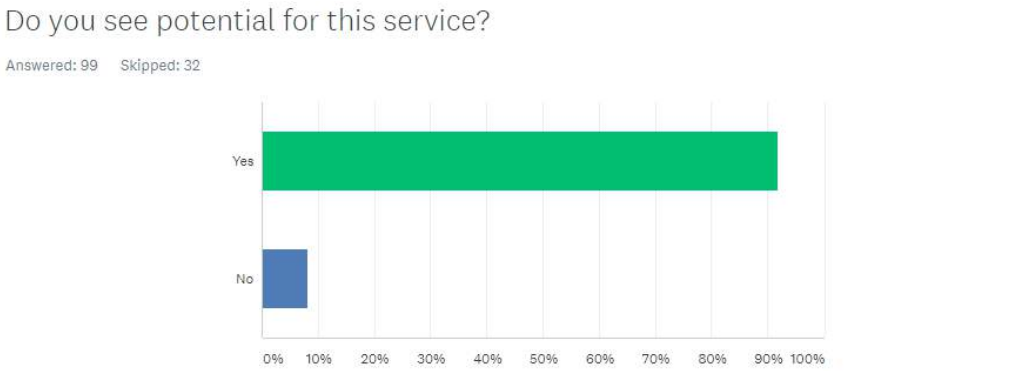

Fig. 89 Survey question results (1).

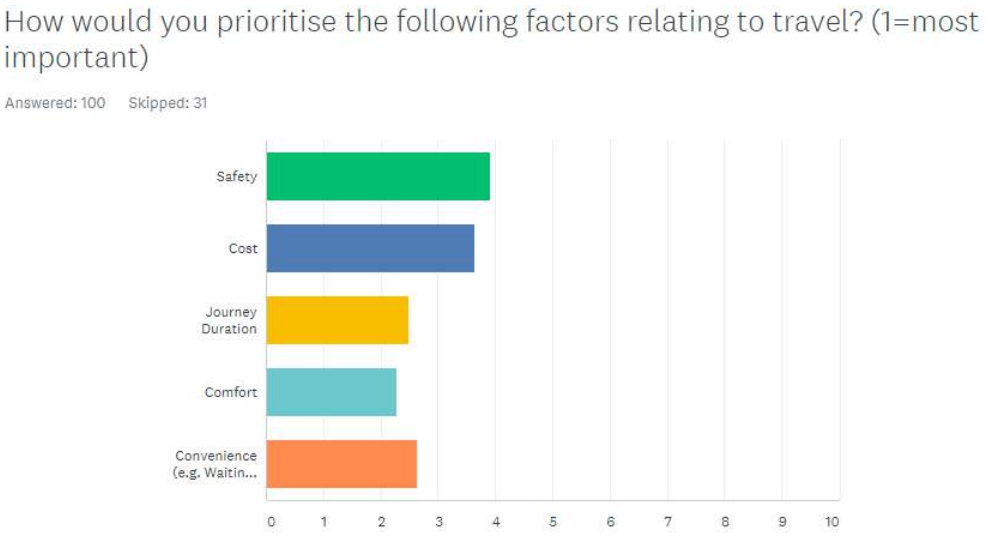

Fig. 90 Survey question results (2).

3.3. Typhoon Squadron Presentation

Loughborough University's engineering departments have excellent links with the military, with many final year projects being conducted alongside various units across all three services; the Royal Navy, the Army and the RAF. Typhoon Squadron is one of these units and is based in Loughborough, consisting of approximately 70 engineering officers and officer cadets across all three services. Project Skyride were able to give a presentation to Typhoon Squadron about the SkyRide S270 aircraft and the thin haul transport model as whole; the breadth of engineering experience within the squadron meant that some interesting questions and discussions followed the presentation.

One question concerned the operation of the parachute, as this is obviously quite an uncommon feature that many of the officers had not heard about before. The main design point that interested people was the arrester cable that travels from the rear of the aircraft to the front during deployment, which allows the aircraft to be supported evenly rather than just at one point to the rear of the aircraft. Another Officer asked about the consideration for airport security due to the large number of aircraft flying out of small airports very frequently, where there is little infrastructure with regards to security. The response from Project SkyRide eluded to the fact that the air taxi business will operate with minimal security, much like Uber, to minimise the door to door time. Obviously, all pilots will be vetted before they are taken on to operate the aircraft. The most interesting discussion came from a question about the feasibility of the project due the large costs involved in operating general aviation aircraft compared to road travel. Many people were initially sceptical of the cost saving of using a hybrid powertrain, however when presented with our cost analysis, they were pleasantly surprised to see operational savings of up to 43% with respect to our most competitors. Furthermore, the added benefit of noise and emissions reduction means that the risk associated with public perception is

minimised. In addition, many people were very impressed with the time savings that can be achieved using Project SkyRide when compared to road travel, which makes up for the higher cost compared to driving.

Overall it was a very interesting experience for both Project SkyRide and Typhoon Squadron, and it allowed the project to gain some exposure to the public. In addition, it has raised awareness about the emission reduction targets within the aeronautical industry and how they will be achieved.

Fig. 91 Presentation to Typhoon Squadron about Project SkyRide.

3.4. Loughborough Campus Radio

Fig. 92 Members of Project SkyRide in the Loughborough Campus Radio recording studio.

Radio broadcasts are an excellent way to engage with the public and spread messages to a wide and varied audience. Several members of Project SkyRide were fortunate enough to be invited onto the Loughborough radio station "LCR" to discuss the project and have the opportunity to answer questions that members of the public may have. The broadcast was very well received because many people, especially students, are very interested in ways that people can reduce their environmental impact, and clearly hybrid propulsion is an excellent way to do this. It was an interesting experience because the radio host had experience in autonomous UAV operation, and this tied in quite well with the autonomy of air taxi businesses of the future; a concept that will be introduced to eliminate pilot-related costs.

3.5. RAeS Hybrid Propulsion Lecture

All members of Project SkyRide attended a lecture from Dr Panos Laskaridis, Head of the Hybrid Electric Propulsion Group at Cranfield University. This lecture covered many of the topics that were very important to the design of the SkyRide S270 aircraft; the most significant of which was regarding existing batteries and the future development of batteries that needs to be carried out in order to achieve large-scale electric air travel. It was very rewarding for all of the team to hear a

world leading expert talk about many of the design considerations in hybrid electric aircraft design, many of which had already been incorporated into the S270.

One topic that was discussed was the incorporation of hybrid propulsion into long haul civil aviation, a concept that Dr Laskaridis assured everyone would not be possible in the next 50 years due to restrictions in battery specific energy density and the associated technological breakthroughs that would be required to make this concept a reality. The issue is twofold, firstly, battery chemistry can only be improved to a certain extent to reduce the mass of batteries for a given power output. Secondly, cooling requirements for massive cell configurations would need to be so complex and heavy, that they would simply not be feasible for long haul flights. This information is massively important to the thin haul industry because many long-haul flights may need to be replaced with numerous shorter flights, facilitated by small aircraft such as the S270.

3.6. Twitter

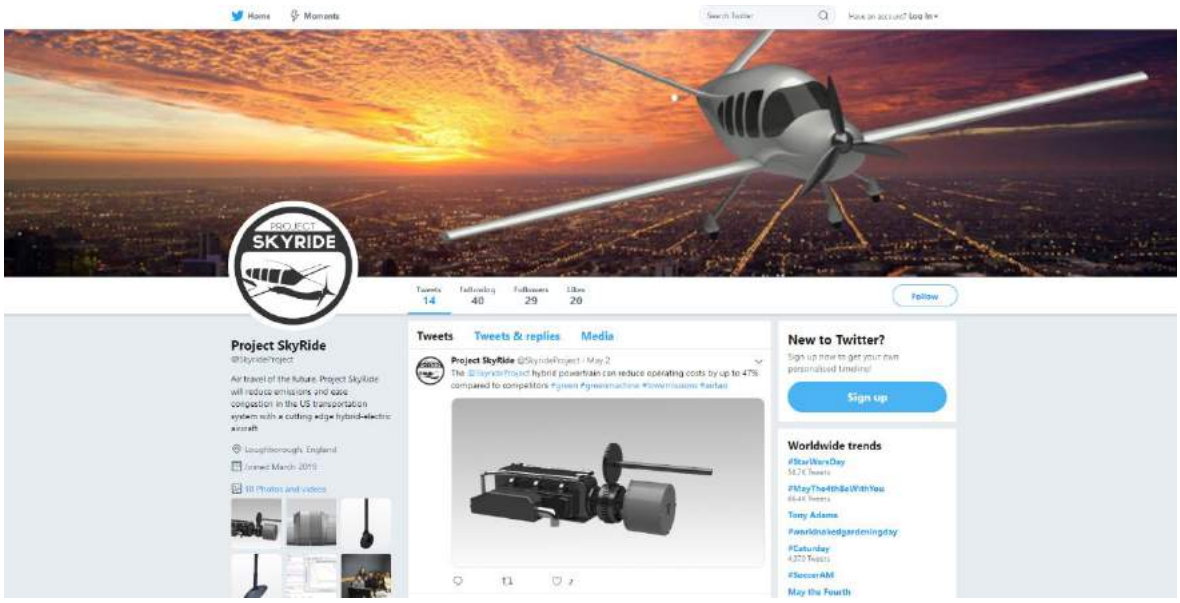

Fig. 93 Project SkyRide Twitter page.

Another way that Project SkyRide engaged with the public was through Twitter. By setting up a Twitter page and sending out periodic updates, networking with other air taxi companies was made possible. The European Air Taxi page took a particular interest in the project and the team there were especially interested in the idea of hybrid propulsion and moving towards fully electric flight. The owner of the page even suggested working alongside Project SkyRide in the future on a collaborative project. The constraints of this project obviously meant that this would not be possible, but it shows that many people are interested in this concept and that significant future development in the thin haul industry will very likely occur in the near future. The Twitter page has also been a good way for people that conducted the initial survey to see the progress of the project and give feedback about how they felt about it after seeing it materialise from an initial concept.